S 4ᴦ

R. K. SCOTT

THERMOCHEMICAL NONEQUILIBRIUM IN ATOMIC HYDROGEN AT ELEVATED TEMPERATURES

Technical Report No. HTGDL-8

December 1972

$\mathcal{I}$

THERMOCHEMICAL NONEQUILIBRIUM IN

ATOMIC HYDROGEN AT

ELEVATED TEMPERATURES

Technical Report HTGDL-8

by

Robert Kenmer Scott

December 1972

High Temperature Gas Dynamics Laboratory

School of Mechanical Engineering

Purdue University

West Lafayette, Indiana

To the loving memory of my father and mother.

ACKNOWLEDGMENTS

TABLE OF CONTENTS

LIST OF TABLES

LIST OF FIGURES

LIST OF SYMBOLS

<u>English</u> <u>Letter</u> <u>Symbols</u>

    A   ambipolar diffusion coefficient

    a   acceleration, see Equation (E-1)

    b   impact parameter, see Equation (C-1)

    c   speed of light, species thermal speed (with overbar),
vector particle velocity

    D   diffusion coefficient

d_{atom} atomic diameter

    E   electric field intensity

    e   electronic charge

    f   thermal flux of particles, general algebraic
function, Maxwellian velocity distribution function

    G   center of mass velocity of two particles

    g   relative velocity of two particles

    h   Planck's constant, specific enthalpy, species
enthalpy

    I   arc current

    I_p ionization potential

    J   current density

    J_w sheath wall current

    K   reaction rate coefficient

    k   Boltzmann's constant, thermal conductivity

m   species particle mass

$\dot{m}$ mass flux

n   species number density

$\dot{n}_e$ electron production rate

P   static pressure, species partial pressure, see
Equations (A-10) and (A-11)

P_I diffusion of ionization energy

P_r energy radiated by accelerating charged particle,
see Equation (E-1)

P_{rad} radiative heat emission

Q   heat transfer rate, total kinetic cross section

q   heat flux

R   tube radius, species gas constant, finite differ-
ence parameter, see Equation (3-2)

r   radial coordinate

S_{ec} elastic collision energy transfer between electrons
and heavy particles

S_{ic}^e inelastic collision energy transfer between elec-
trons and heavy particles

T   temperature

t   time

U   mass average axial velocity

U_d electron drift velocity

U_i species axial diffusion velocity

V   mass average radial velocity

V_i species radial diffusion velocity

x   species mole fraction

z   axial coordinate

Greek Letter Symbols

α general algebraic function

β electron reflection coefficient

Γ flux of particles

γ integral substitution, see Equation D-3

Δ incremental change

θ angular coordinate, azimuthal coordinate

λ mean free path length

μ reduced mass of two particles, charged particle mobility, see Equations (A-6) and (A-7); viscosity

ν particle collision frequency, frequency of light photon

χ ion reflection coefficient, particle collision angle of deflection

π 3.1415926...

ρ total mass density, species mass density

$\dot{\rho}$ species mass production rate

σ electrical conductivity, differential scattering cross section

τ shear stress

ϕ general algebraic function, electrostatic wall sheath potential, see Equation (4-3)

Ω gas kinetic collision integral

ω solid angle

Subscripts

A	species A
amb	ambipolar
B	species B
CL	centerline
CM	center of mass
D	dissociation
e	electron
eq	equilibrium
ex	excitation
H	hydrogen atom
H^+	hydrogen ion
h	indicates summation over heavy particle species
I	ionization
i	species i
n	grid point number
R	radiation
r	r-component
rad	radiation
w	wall
z	z-component

Superscripts

D	diffusion
1	superscript on Q and Ω to denote diffusion
2	superscript on Q and Ω to denote viscosity or thermal conductivity

+ positive charge

- negative charge

Overlines

— average over thermal velocity distribution

→ vector notation

Mathematical Operations

$\frac{\partial}{\partial z}, \frac{\partial}{\partial r}$ partial differential operators

d differential operator

∇ gradient operator

log log base 10

ln natural logarithm

exp exponentiation

| | absolute value

$\sum$ summation

$\int$ integration

ABSTRACT

Scott, Robert Kenmer. Ph.D., Purdue University, December 1972. Thermochemical Nonequilibrium in Atomic Hydrogen at Elevated Temperatures. Major Professor: Frank P. Incropera.

A numerical study of the nonequilibrium flow of atomic hydrogen in a cascade arc was performed to obtain insight into the physics of the hydrogen cascade arc. A rigorous mathematical model of the flow problem was formulated, incorporating the important nonequilibrium transport phenomena and atomic processes which occur in atomic hydrogen. Realistic boundary conditions, including consideration of the wall electrostatic sheath phenomenon, were included in the model. The governing equations of the asymptotic region of the cascade arc were obtained by writing conservation of mass and energy equations for the electron subgas, an energy conservation equation for heavy particles and an equation of state. Finite-difference operators for variable grid spacing were applied to the governing equations and the resulting system of strongly coupled, "stiff" equations were solved numerically by the Newton-Raphson method.

Parametric solutions were obtained with arc current, pressure and tube radius as independent variables. It was observed that nonequipartition of kinetic energy between electrons and heavy particles was a relatively insignificant

effect. However, although chemical equilibrium existed near the centerline of the arc, significant departure from this condition occurred in the wall region. The radial location marking the onset of chemical nonequilibrium shifted toward the centerline as the current and pressure decreased and as tube radius increased.

Heat transfer in the hydrogen cascade arc is mainly due to radiation and the heavy particle conduction mechanism. Heat transfer by electron conduction and diffusion and the diffusion of ionization energy was found to contribute less than 2% to the total for all parametric conditions. Radiation becomes a dominant mode of heat transfer in the high pressure hydrogen arc, with radiative transfer accounting for over 50% of the heat loss for a pressure of 10 atmospheres.

Speculations for the molecular hydrogen arc indicate that, if the molecular species were considered, higher electron number density and temperature and lower heavy particle temperature would be observed in the wall region. However, it is expected that bulk parameters, such as electric field and the total and radiative wall heat flux, would not be substantially different for molecular hydrogen.

1

CHAPTER 1   INTRODUCTION

1.1   The Cascade Arc

In the past, much interest has been shown by researchers
in the phenomena associated with high temperature gases.
This interest centered on astrophysical and geophysical
problems, but more recently attention has been focused on
man-made devices which are capable of heating gases to high
temperatures.   One such device, commonly referred to as the
cascade arc (a gas flowing through an electrical discharge
confined by the cooled wall of a tube), has attracted the
attention of a number of theoreticians and experimentalists
(see Figure 1-1).   This theoretical study is concerned with
the flow of hydrogen in the cascade arc.

For purposes of discussion, the flow field in the arc
constrictor is divided into three general regions (Figure 1-1):
(1) the entrance region, (2) the asymptotic region and (3) the
field free region.   The entrance region is characterized by
significant variation of flow properties in the axial direc-
tion, the asymptotic (fully developed) region by its lack of
such property variation and the field free region by the
absence of an external electric field.

Due to the aforementioned characteristics of the
asymptotic region, the flow properties determined at one
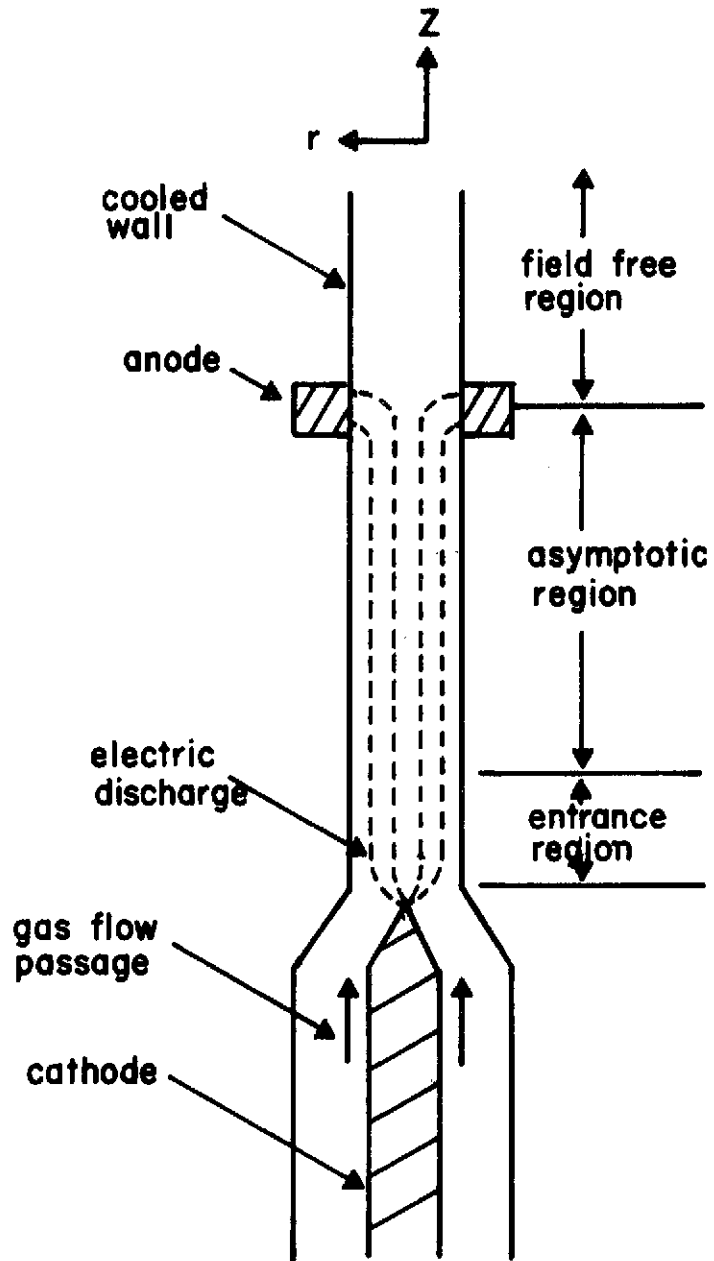
Figure 1-1.   Schematic Diagram of Cascade Arc.

axial location for a given set of operating conditions are applicable to all other axial locations (of the same region) and thus possess a "semi-universal" nature. This implies that the flow properties of the asymptotic region are independent of the cathode and inlet geometry as well as axial location, a fact which makes meaningful comparisons between theory and experiment possible. Also, due to their simplified form, the asymptotic region governing equations can be used in conjunction with experimental measurements of cascade arc flows to experimentally determine high temperature gas transport properties. Therefore, due to the practical importance of this region, the present study of hydrogen flow through the cascade arc has emphasized the determination of conditions in the asymptotic region.

Many previous studies of the cascade arc have incorporated the assumption that the gas flowing through the arc is in local thermodynamic equilibrium (LTE). (The ramifications of this assumption are discussed in the next section.) More recent studies [1, 2] of high temperature gas flows indicate that the LTE assumption is not valid in regions of high temperature and concentration gradients such as might exist near the wall of a cylindrical cascade arc. Therefore, for this particular study, the LTE assumption is not utilized, thus permitting a critical comparison of the equilibrium and nonequilibrium theories of the cascade arc for hydrogen.

1.2 Equilibrium and Nonequilibrium in the Cascade Arc

In order to give the reader a proper perspective, the concept of equilibrium and nonequilibrium in cascade arc flow is discussed in this section. The term "complete thermodynamic equilibrium" (CTE) is used to describe the state of a gaseous system which has been isolated from its environment for a sufficiently long period of time. This period of time must be long enough (theoretically infinite) to insure that the gas is in thermal, mechanical and chemical equilibrium, thus implying the absence of temperature, pressure and concentration gradients, respectively. Therefore, any system in complete thermodynamic equilibrium cannot possibly transfer heat, momentum or mass across the boundaries of that system. Since virtually all gaseous systems of interest do not satisfy the CTE requirement, it would seem impossible to use the concepts of classical thermodynamics (such as pressure, temperature, internal energy, etc.) to solve practical flow problems. For this reason it has become necessary to develop the concept of local thermodynamic equilibrium (LTE) to establish a more reasonable set of criteria for applicability of thermodynamic concepts to flow systems. Therefore, if a system is in LTE, thermodynamic concepts can be used to mathematically describe it.

Before discussing the definition of LTE for this problem it would be beneficial to review some of the microscopic conditions which would exist in a high temperature gas

(T ≈ 10,000°K) in CTE. For the purpose of concreteness, it is assumed that the gas is composed primarily of electrons, atoms, molecules and singly-charged atomic and molecular ions. With the aid of statistical mechanics [3], the following facts can be demonstrated:

1. The particle velocity distribution function of each chemical species is Maxwellian, and the species kinetic temperatures are given in terms of the root mean square speeds of these distributions $\left(\frac{3}{2} kT_i = \frac{m}{2} \overline{c_i^2}\right)$. In CTE, all species kinetic temperatures are equal.

2. The populations of the bound electronic states of each neutral and ionic species are given by the Boltzmann distribution function evaluated at a common excitation temperature, T_{ex}.

3. The electron number density contribution of each atomic and molecular species (due to ionization) is given by the Saha equation for that particular species ionization reaction. The total electron number density is given by the sum of these individual contributions and the Saha equations are evaluated at a common ionization temperature, T_I.

4. The neutral atom number density is given in terms of the neutral molecule number density by the law of mass action applied to the dissociation reaction and evaluated at some dissociation temperature, T_D.

5. The radiation intensity within the gaseous system
    satisfies the Planck function at the radiation tempera-
    ture, T_R.

6. In CTE, there is a unique temperature, T, which
    describes all of the aforementioned phenomena.
    Therefore, in CTE, $T = T_i = T_{ex} = T_I = T_D = T_R$
    throughout the entire system.

For the purposes of this problem, LTE is said to exist
when the first four conditions plus the condition
$T = T_i = T_{ex} = T_I = T_D$ are satisfied at each point in the
flow field. No requirements are placed on the nature of
the radiation field. Therefore, in LTE, the thermodynamic
temperature (and hence all temperature dependent properties)
is allowed to vary throughout the flow field, thus permitting
the molecular phenomena of heat, mass and momentum transfer
to occur.

The conditions necessary for LTE to exist also suggest
several possible modes of nonequilibrium for the gaseous
flow system. Taken individually, these nonequilibrium con-
ditions are:

1. Non-Maxwellian velocity distribution of one or more
    of the different species.

2. Inequality of two or more of the species kinetic
    temperatures (nonequipartition of kinetic energy).

3. Excitation nonequilibrium, or nonequilibrium population of atomic and molecular excited states, and

4. Chemical nonequilibrium, or nonequilibrium number densities of the different chemical species (electrons, atoms, molecules, atomic and molecular ions).

Processes which tend to promote or suppress the above nonequilibrium conditions are discussed below in their respective order.

1. Strong electric fields may cause a "drift" motion of electrons with respect to the mass-averaged gas velocity. If this drift velocity is of the same order of magnitude as the mean electron thermal velocity, then the electron velocity distribution will be non-Maxwellian. Also, ionization and three-body recombination reactions selectively absorb and release energy in the high energy wings of the electron velocity distribution function, thus tending to promote a non-Maxwellian electron velocity distribution. This nonequilibrium tendency is retarded by elastic collisions among the particles of each chemical species.

2. The electric field, by selectively imparting kinetic energy to the electrons, is partially responsible for nonequipartition between electrons and "heavy" particles. In addition, diffusion of the relatively mobile electrons away from the hot central core of the arc contributes to

nonequipartition in the outer periphery near the wall.
Finally, the ionization (three-body recombination) and
collisional excitation (or deexcitation) processes
tend to absorb (or release) electron energy in those
regions where they are dominant. In contrast, the
primary process through which equipartition of energy
is restored is the occurrence of elastic collisions
between the electrons and the heavy particles.

3. For an optically thin gas, the emission of radiant
    energy causes a depopulation of the excited states,
    since the photoexcitation restoration mechanism is not
    present. The collisional excitation process (when
    dominant) will serve to restore excitation equilibrium
    to the heavy particles in the gas.

4. The existence of large concentration and electron
    kinetic temperature gradients in the presence of
    finite ionization, dissociation and recombination
    rates is primarily responsible for chemical nonequilib-
    rium. For example, diffusion of electrons from the
    hot core of the arc toward the cool wall will elevate
    the electron number density in the wall region above
    the equilibrium value for the local electron tempera-
    ture due to finite ionization and three-body recombina-
    tion rates. Therefore, restoration of chemical equi-
    librium can only be realized in the absence of large

concentration and species kinetic temperature gradients or in the presence of very large reaction rates.

Earlier in this section it was stated that, if a gaseous system is in LTE, classical thermodynamic concepts can be used in its mathematical description. However, since the LTE assumption is not utilized in this study, the use of any thermodynamic concepts needs to be justified for this particular nonequilibrium situation.

As mentioned in Section 1.4, nonequipartition and chemical nonequilibrium are treated in this study. However, it is assumed that Maxwellian velocity distributions do exist for the individual species present. The important consequence of this assumption is that species kinetic temperatures can then be uniquely defined. Therefore, thermodynamic properties which are a function of the species kinetic temperatures (such as enthalpy and internal energy) are useful concepts, even in this nonequilibrium situation, and the governing equations can be derived by the same methods that are used to derive the governing equations for LTE flow.

1.3 Previous Studies of Cascade Arc Flow

It is the purpose of this section to familiarize the reader with the type of theoretical and experimental techniques used in the past to obtain the flow characteristics of cascade arcs. This is not intended to be even a cursory

review of the cascade arc literature, but simply an overview of some of the more popular methods of investigating flow phenomena in such devices.

One of the earlier treatments consists of writing an energy balance for the gas in the asymptotic region in terms of an electric field (Ohmic) heating term, a Fourier conduction term and a radiation heat loss term. The basic assumption in the resulting energy equation (Elenbaas-Heller equation) is that the gas is in local thermodynamic equilibrium. Analytical solutions to this equation have involved its simplification through use of a heat flux potential and/or approximated coefficients. Numerical solutions have also been obtained utilizing the equation in its basic form.

Stine and Watson [4] proposed a simplified method of analytically treating flow in the entrance region of a cascade arc. Assumptions used in their theory include LTE, constant mass flux throughout the constrictor, no radiation heat loss and gas properties which are linearly dependent upon enthalpy. Due to the limiting assumptions of the Stine-Watson model, it is capable of yielding only rough estimates of flow properties in the entrance region of the cascade arc.

Although there are a variety of approximate methods used to analytically obtain the flow characteristics of cascade arcs, it is impossible to accurately treat the problem by non-numerical methods. For this reason, Bower [5] elected to derive a rigorous model of arc flow in a tube

and to solve it numerically with a minimum of simplifying assumptions. He used an implicit finite-difference, marching scheme to obtain the LTE flow characteristics for argon. Bower's LTE program has been modified for hydrogen flow by Greene [6] and will be used to compare results obtained in this study.

As mentioned in the first section, Incropera and Viegas [1] investigated the existence and nature of nonequilibrium in an arc by means of a time-scale study and demonstrated the probable existence of thermal and chemical nonequilibrium in argon. They then proposed a non-LTE fluid flow model, similar to those which had been used by other researchers to compute high temperature, non-LTE gas flows in various devices and geometries. For the sake of background information, some of these non-LTE studies are discussed.

Okuno and Park [7] investigated nonequilibrium, stagnation point flow of nitrogen over a hemispherical body. After transforming variables, they obtained a system of coupled, nonlinear ordinary differential equations which were not solvable by the usual finite-difference techniques due to strong coupling of the equations. They, therefore, utilized a "shooting" method in which certain boundary conditions were estimated, a marching solution was then effected from that boundary, and the calculated results were compared with conditions imposed at the other boundary. The method of solution then consisted of a "conversational" iteration with

the computer until convergence upon the correct set of boundary conditions was obtained.

Kruger [8] utilized a flow model similar to that proposed by Incropera and Viegas in order to establish the accuracy of spectroscopic data obtained from argon and helium confined arcs. Rather than solve the governing equations directly, Kruger integrated them to obtain explicit expressions for electron number density, electron and heavy particle temperatures, and the heat flux potential in terms of the measured values of electron temperature and number density. He found that measured and calculated values of electron temperature and density were in good agreement, heat flux potentials were in fair agreement, and that thermal and chemical nonequilibrium do exist in argon and helium arcs. His conclusion is that "a two-temperature ambipolar diffusion model yields satisfactory interpretation of the nonequilibrium behavior of confined arcs in atmospheric pressure argon and helium."

The most rigorous theoretical prediction of cascade arc flow known to the author was completed by Clark [9] in 1971. Using a realistic flow model which accounts for thermal and chemical nonequilibrium, he numerically obtained the flow characteristics for argon cascade arcs. The agreement of his rather extensive set of solutions with experimental data indicated that the flow model satisfactorily predicted arc flow behavior over a broad range of operating

conditions. For this reason, Clark's flow model has been selected for use in this study.

Spectroscopic studies of hydrogen cascade arcs have been done by various researchers and a brief summary of their work is appropriate. Morris and others [10] report temperature profiles and degree of nonequilibrium (percent difference in electron and gas temperature) for currents of 20, 30, 40, 50 and 70 amps at one atmosphere pressure. They also report the electric field-current (E-I) relationship for a cascade arc of radius 0.0015 meters. Wiese and others [27] also report temperatures for a 40 amp atmospheric arc with a tube radius of 0.0015 meters. Measurements taken by Maecker [11] of the E-I relationship of a hydrogen arc with a tube radius of 0.001 meters are shown in his work on transport properties in high power arcs. Temperature profiles and the degree of nonequilibrium for currents of 8, 20, 40, 60, 90, 120 and 150 amps in a 0.001 m. hydrogen arc have been obtained in the experimental studies of Steinberger [12]. Many of the above experimental results, as well as the numerical LTE studies of Greene, will be compared with the calculations of this study in a later chapter.

1.4 Objectives of this Study

It is the objective of this study to obtain solutions to a rigorous flow model of the hydrogen cascade arc that is not limited by unrealistic assumptions. As discussed in Section 2.1 on assumptions used in the flow model, only two

modes of nonequilibrium are found to be significant for a rigorous treatment of the hydrogen arc. These are the second and fourth modes of nonequilibrium which are mentioned in Section 1.2: nonequipartition of kinetic energy between the electronic and heavy particle species and chemical nonequilibrium of the various species present. The term "thermochemical nonequilibrium" will hereafter be used to describe this particular state of nonequilibrium in the arc.

The primary purpose of this study is to obtain added insight into the general physics of the cascade arc by parametric studies with the hydrogen arc flow model, comparison of the rigorous nonequilibrium solutions with equilibrium and experimental results for hydrogen arcs, and by comparison of the nonequilibrium hydrogen and argon [9] numerical data.

This work is a continuation of an extensive theoretical and experimental study of nonequilibrium cascade arc flow at the Purdue High Temperature Gas Dynamics Laboratory. Theoretical work on thermochemical nonequilibrium in argon has been completed by Clark. This study extends the knowledge of nonequilibrium arc phenomena and the theoretical methods of treating it.

CHAPTER 2   MATHEMATICAL FLOW MODEL

2.1   Assumptions

In this section the assumptions made in the derivation of the governing equations are listed and discussed and in Section 2.2 the derivation itself appears.

The assumptions which follow are numbered for future reference.

1. The flow field is steady and all properties are symmetric about the axis (axisymmetric). At the flow rates considered in this problem, the flow field is laminar.

2. Gravitational effects are negligible.

3. Externally applied magnetic fields are absent. For argon, Bower [5] found that induced magnetic fields were negligible for currents less than 1000 amps. That assumption is assumed to be equally valid for hydrogen.

4. The derivation of the macroscopic governing equations is valid from the continuum point of view since all the particle mean free paths are several orders of magnitude smaller than the tube diameter.

5. Gradients of flow properties in the axial direction
are much smaller (and, in fact, for the asymptotic
region are identically zero) than those in the radial
direction. Therefore, the usual boundary layer
assumptions are valid, i.e. axial diffusion of heat,
mass and momentum are negligible and the pressure is
uniform over the arc cross section. This assumption
is further justified by Clark [9] who utilized it in
his nonequilibrium studies and obtained good agreement
with experimental results.

6. The governing equations are applied in regions suffici-
ently far removed from the cathode and anode that the
electric field has a nonzero component only in the
axial direction. From Maxwell's equations this
further implies that the electric field is uniform
over the arc cross section.

7. Flow rates corresponding to Mach numbers significantly
less than unity are anticipated; therefore shear and
pressure work and fluid kinetic energy are negligible.

8. In the hydrogen arc, there are four chemical species
that are present in significant amounts under equi-
librium conditions. They are: electrons, positively
charged atomic ions, neutral atoms and neutral molecules.
At equilibrium, the concentration of all other species
is less, by several orders of magnitude, than those
just mentioned and it is assumed that these concentrations

remain insignificant in the nonequilibrium case as well. In this study, the presence of the molecular species has also been ignored for reasons which are discussed in Chapter 4. Therefore, governing equations are derived considering the presence of electrons, positive ions and neutral atoms.

9. Strictly speaking, Maxwellian velocity distributions do not exist in a gas wherever gradients in flow properties exist. However, for most problems the deviation from a Maxwellian distribution is slight enough to be negligible (and so the terms Maxwellian and near-Maxwellian are used interchangeably). As mentioned in Chapter 1, Maxwellian velocity distributions are assumed for each of the chemical species. Incropera and Viegas [1] have found that in an argon cascade arc, this assumption is valid except near the cool wall. However, their results have been obtained using an equilibrium flow solution which significantly under-predicts the electron temperature and number density near the wall; hence the electron self-collision frequency (which is the principal equilibrium restoration mechanism) is substantially underestimated. Therefore, it is reasonable to expect Maxwellian velocity distributions to exist in the argon cascade arc. Since the mechanisms which promote nonequilibrium velocity distributions in argon are the same as those in hydrogen,

Maxwellian distributions are assumed to exist in hydrogen as well.

10. Equipartition of translational energy in a multicomponent mixture of gases occurs by means of elastic collisions between the particles of the different species. It is well known that, if two particles of approximately equal mass collide elastically, the exchange of energy between those particles is highly efficient. However, if the two particles differ greatly in mass, then the energy exchange process is highly inefficient and each particle leaves the collision with practically the same energy it had prior to collision. Therefore, when two groups of particles of nearly equal mass but different thermal speeds are mixed, their translational energy equilibrates rapidly. This is not the case, however, with particles of greatly different mass. As far as this problem is concerned, it is therefore reasonable to assume that all the species consisting of heavy particles (ions and atoms) share a common mean energy and temperature, but since the electron is more than three orders of magnitude lighter than a heavy particle and is selectively energized by the electric field, the electron kinetic temperature cannot be assumed equal to the heavy particle temperature. Therefore, in the formulation of the flow model, it is assumed that all heavy particle

species have a common temperature and that the electron species has a different temperature.

11. The perfect gas equation of state is assumed to apply to each chemical species and Dalton's law of partial pressures is assumed valid. Griem [25] calculates a correction for the perfect gas equation in a plasma due to Coulomb interactions and concludes that it is negligible for conditions of this study.

12. In their discussion of electrical neutrality, Holt and Haskell [13] have shown that for ionized gases at the temperatures and electron number densities encountered in this work, conditions are electrically neutral on a macroscopic scale. For this work, the implication is that the hydrogen gas is electrically neutral every-where except in a microscopic region termed the plasma sheath (discussed in Section 2.2.3) which adjoins the wall.

13. Due to large gradients in the electron and ion number densities, these particles will tend to diffuse from the core of the arc toward the wall. The condition of charge neutrality implies that, in the absence of externally applied forces in the radial direction (such as in this case), the electrons and ions must diffuse together toward the wall. This condition of equal electron and ion diffusion velocities, or ambipolar diffusion, is considered in the derivation of the

governing equations. This assumption breaks down in the electrostatic sheath region which is discussed in Section 2.2.3.

14. As a result of the large value of the electronic energy for the first excited level of atomic hydrogen, the population of this level will always be quite small, even in the core of the arc. A rough calculation (based on equilibrium population densities) shows that the maximum electronic internal energy contribution from the first excited level in the core of the arc is less than 1% of the particle kinetic energy. Therefore, electronic excitation effects are completely ignored in the consideration of energy storage mechanisms. Chemical equilibrium, however, is not assumed to exist anywhere in the arc, and, in fact, the treatment of the complications arising from this form of nonequilibrium is an important feature of this work.

15. The presence of a radiation field, if treated rigorously, increases the complexity of the governing equations. For this reason, the hydrogen gas is assumed to be optically thin, and all radiation emitted by the gas is assumed to reach the cascade arc wall uninhibited by absorption. This assumption is not entirely justified, of course, due to the fact that the resonance radiation (that due to spontaneous transitions to the ground level) is quickly absorbed as it propagates through

the arc. Proper treatment of the radiation problem would involve the inclusion of the radiative transfer equation in the set of governing equations, a task which is well beyond the scope of this work.

16. In order to calculate certain terms that appear in the governing equations, it is necessary to consider the microscopic nature of the gas. Transport properties, ionization rates and other properties depend on the collision frequencies of the various particles among and between each other. Therefore, the collision frequency is an important piece of information. However, in some high temperature gases, the notion of a collision is vague since the trajectory of a particle might be simultaneously influenced by more than one neighboring particle. However, Delcroix [14] points out that for conditions of interest here, this is not the case and most collisions can be treated as binary. The exceptions are those collisions involving the recombination of ions and electrons in the presence of a third particle (which receives the recombination energy), the inverse of which is a two-body (ionization) collision.

The potentially most important collisions which need be considered in this analysis are listed below. First the elastic collisions, for which the colliding particles suffer no change in kinetic energy, are

listed and then the inelastic collisions, which involve a conversion of kinetic energy to some other form, are given.

Elastic Collisions

1. $e + e \rightleftarrows e + e$

2. $e + H^+ \rightleftarrows e + H^+$

3. $e + H \rightleftarrows e + H$

4. $H^+ + H^+ \rightleftarrows H^+ + H^+$

5. $H^+ + H \rightleftarrows H^+ + H$

6. $H + H \rightleftarrows H + H$

Inelastic Collisions

1. $e + H \rightleftarrows e + H^+ + e$ electron ionization

2. $H + H \rightleftarrows e + H^+ + H$ atom ionization

3. $e + H^+ \rightarrow H + h\nu$ radiative recombination

4. $e + H^+ \rightarrow e' + H^+ + h\nu$ Bremsstrahlung

5. $e + H \rightarrow e' + H + h\nu$ Bremsstrahlung

All of the collisions listed under Elastic Collisions are considered in deriving the transport properties of hydrogen. All of the inelastic collisions were considered in the derivation of the source terms of the governing equations except atom ionization because data on the atom ionization rate could not be found. A study of atom-atom excitation in hydrogen [29] indicates that atom ionization may be important in the wall region

of the arc. However, the uncertainty analysis in
Chapter 4 indicates that when the electron ionization
(and recombination) coefficient is perturbed by a factor
of 2, the effect on the solution is completely negligible.
Therefore, it is expected that negligence of atom ioniza-
tion has no effect on the solutions even if the atom
ionization rate is as large as that for electron
ionization.

2.2 Derivation and Discussion of Governing Equations

2.2.1 The Governing Equations

Employing the assumptions discussed in Section 2.1, the
governing equations are developed for the flow of an atomic
gas through the entrance region of a cascade arc. The equa-
tions for the asymptotic region are then a special case of the
entrance region equations. Detailed derivations are not
given, however, the physical significance of each term in
the equations is indicated.

In order to derive the necessary equations, the laws of
conservation of mass and energy and Newton's Second Law must
be applied to the gas flowing through a cylindrical differ-
ential volume fixed inside the cascade arc. A diagram of a
cylindrical control volume is shown in Figure 2-1.

The general form of the species continuity equation is
derived by applying the conservation of mass principle to
some species i as it flows through the control volume.
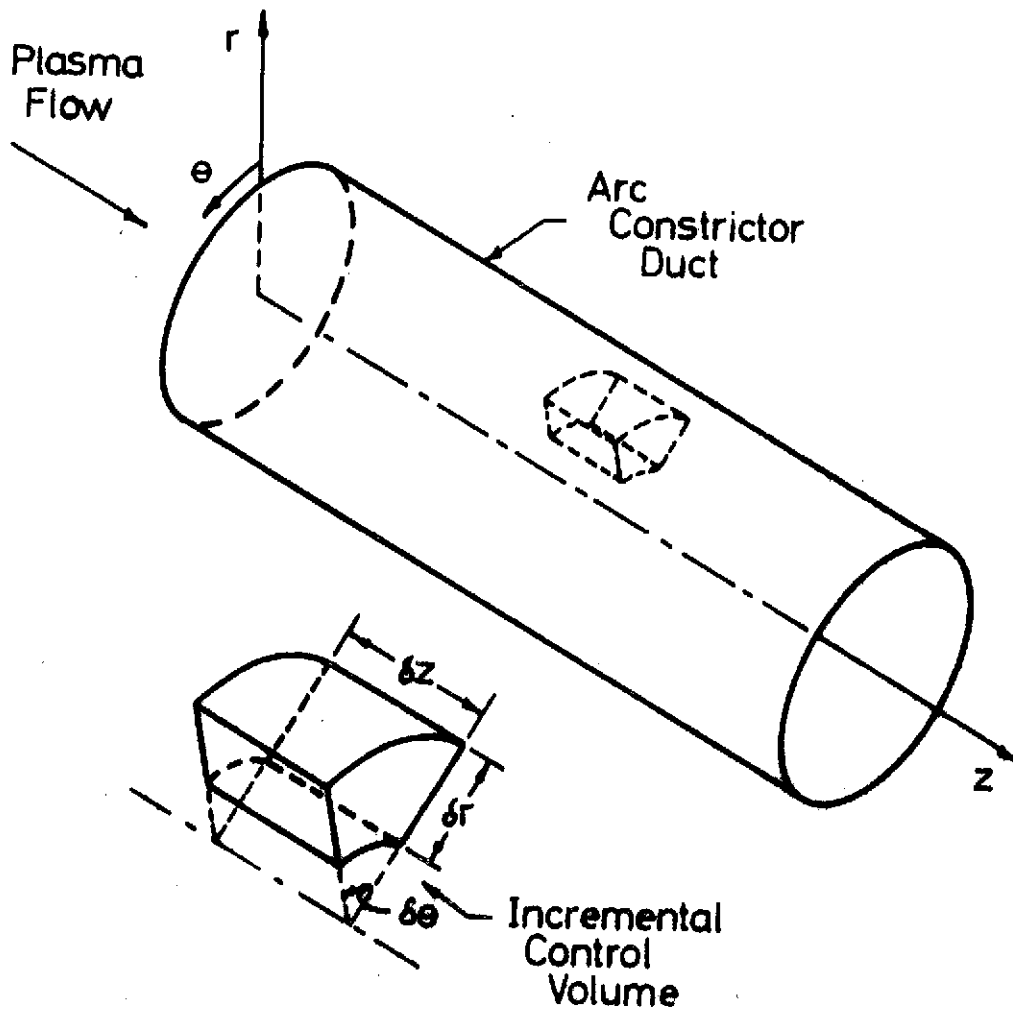
Figure 2-1. Infinitesimal Cylindrical Control Volume.

Utilizing the appropriate assumptions from Section 2.1, this
equation then becomes a balance between the net mass of i
convected out of the control volume and the rate of creation
of mass of i due to chemical reactions.

Species Continuity Equation

(1)	(2)	(3)
net rate of change of species i in control volume due to axial convection	+ net rate of change of species i in control volume due to radial convection	= net rate of change of species i in control volume due to chemical reaction

| (1) | (2) | (3) |

$$\frac{\partial [\rho_i (U+U_i)]}{\partial z} + \frac{1}{r} \frac{\partial [\rho_i (V+V_i)r]}{\partial r} = \dot{\rho}_i$$

Due to the assumed lack of large temperature and concen-
tration gradients in the axial direction, the only diffusion
force acting in that direction is due to the electric field.
Therefore U_i for neutral atoms is zero. Furthermore, due to
the large relative mass of ions, the diffusion velocity of
ions is small compared to that for electrons. Therefore,
the only significant axial diffusion velocity is that of the
electrons. This velocity will be referred to as the electron
drift velocity (U_d). Discussion of radial diffusion veloci-
ties and the source terms ($\dot{\rho}_i$) is presented in Section 2.2.2.

Applying the conservation of mass principle to the over-
all gas mixture flowing through the control volume gives the
following.

Global Continuity Equation

(1)   (2)   (3)

net rate of change   net rate of change   net rate of change
of mass in control +   of mass in control =   of mass in control
volume due to   volume due to   volume due to
axial convection   radial convection   chemical reactions

(1)   (2)   (3)

$$\frac{\partial[\rho U]}{\partial z} + \frac{1}{r}\frac{\partial[\rho Vr]}{\partial r} = 0$$

Since total mass cannot be created or destroyed, term (3) is zero.

Since the usual boundary layer assumptions have been made, the global radial momentum equation is not needed. The global axial momentum equation is derived by applying Newton's Second Law to the fluid flowing through the control volume.

Global Axial Momentum Equation

(1)   (2)   (3)

resultant of all   net rate of change   net rate of change
axially directed   of axial momentum   of axial momentum
forces acting on   =   in control volume   +   in control volume
fluid in control   due to axial   due to radial
volume   convection   convection

(1)   (2)   (3)

$$\left\{ -\frac{dP}{dz} + \frac{1}{r}\frac{\partial[r\tau_{rz}]}{\partial r} \right\} = \frac{\partial[\rho U^2]}{\partial z} + \frac{1}{r}\frac{\partial[\rho UVr]}{\partial r}$$

The method of determination of the shear stress is discussed in Appendix B.

The electron energy equation is derived by applying the
law of conservation of energy to the electron subgas flowing
through the control volume.

Electron Energy Equation

(1)	(2)	(3)	(4)
net rate of change of electron energy in control volume due to axial convection	+ net rate of change of electron energy in control volume due to radial convection	= net rate of change of electron energy in control volume due to heat conduction	+ net rate of change of electron energy in control volume due to volumetric sources and sinks

$$\frac{\partial[\rho_e(U+U_d)h_e]}{\partial z} + \frac{1}{r}\frac{\partial[\rho_e r(V+V_e)h_e]}{\partial r} = -\frac{1}{r}\frac{\partial[{}^r q_{r_e}]}{\partial r} + \left\{\sigma_e E^2 + S_{ec} + S_{ic}^e\right\}$$

    (1)   (2)   (3)   (4)

In term (4), the electrical heating term $(\sigma_e E^2)$ is a
source since it always imparts energy to the electron subgas.
The elastic collision term (S_{ec}) is always a sink when the
electron temperature is higher than the heavy particle temperature. The inelastic term (S_{ic}^e) is neither source nor
sink throughout the entire arc region but is a sink where
ionization is predominant and a source when recombination is
predominant. The term S_{ic}^e includes the radiation emitted
by the gas.

The electrical conductivity expression is derived in
Appendix C and the electron heat conduction term (q_{r_e}) is
obtained in Appendix B. The remaining source terms $(S_{ec}$ and
$S_{ic}^e)$ and the diffusion velocities $(V_e$ and $U_d)$ are discussed

in Section 2.2.2. Derivation of the diffusion coefficients is given in Appendix A.

The heavy particle energy equation is derived by applying the law of conservation of energy to the heavy particle species (ions and neutral atoms) flowing through the control volume.

Heavy Particle Energy Equation

(1)	(2)	(3)	(4)
net rate of change of heavy particle energy in control volume due to axial convection	net rate of change of heavy partical energy in control volume due to radial convection	net rate of change of heavy partical energy in control volume due to heat conduction	net rate of change of heavy particle energy in control volume due to volumetric sources and sinks

The columns above are connected by: (1) + (2) = (3) + (4)

$$\frac{\partial[\rho_i U h_i]_h}{\partial z} + \frac{1}{r}\frac{\partial[\rho_i r(V+V_i)h_i]_h}{\partial r} = -\frac{1}{r}\frac{\partial[r q_{r_i}]_h}{\partial r} + (-S_{ec})$$

with the terms labeled (1), (2), (3), (4) respectively.

The bracketed terms $[\ ]_h$ indicate a summation over the heavy particle species. For example, $[\rho_i U h_i]_h = \rho_{H^+} U h_{H^+} + \rho_H U h_H$. The source term $(-S_{ec})$ is of the opposite sign as that in the electron energy equation since the heavy particles are the recipients of the energy lost by the electrons in elastic collisions. The term q_{r_i} is the contribution of the ith species to the radial heat conduction. Derivation of the expressions for q_{r_i} is given in Appendix B.

The equation of state concludes the list of formal governing equations that mathematically describe this flow problem.

Equation of State

$$P = \rho_e R_e T_e + \left\{ \sum_{\substack{i \\ i \neq e}} \rho_i R_i T_h \right\}$$

At the conclusion of this subsection the governing equations for flow in both the entrance and asymptotic regions of the cascade arc are listed for easy reference. In order to obtain the set of equations modeling the flow in the asymptotic region from the entrance region equations, the following steps are taken. The mass average radial velocity (V) is set equal to zero and all axial derivatives, except $\frac{dP}{dz}$, are also set equal to zero. Looking at the entrance region equations it is seen that this process eliminates the global continuity equation by forcing both terms to be equal to zero and the momentum equation is no longer needed since the axial velocity (U) does not appear in any of the remaining equations. The asymptotic set of governing equations then contains two fewer equations than the set of equations governing the entrance region.

Governing Equations of the Entrance Region

Electron Continuity Equation

$$\frac{\partial[\rho_e(U+U_d)]}{\partial z} + \frac{1}{r}\frac{\partial[\rho_e(V+V_e)r]}{\partial r} = \dot{\rho}_e \qquad (2\text{-}1)$$

Global Continuity Equation

$$\frac{\partial[\rho U]}{\partial z} + \frac{1}{r}\frac{\partial[\rho V r]}{\partial r} = 0 \qquad (2\text{-}2)$$

Axial Momentum Equation

$$\frac{\partial[\rho U^2]}{\partial z} + \frac{1}{r}\frac{\partial[\rho U V r]}{\partial r} = -\frac{dP}{dz} + \frac{1}{r}\frac{\partial[r\tau_{rz}]}{\partial r} \qquad (2\text{-}3)$$

Electron Energy Equation

$$\frac{\partial[\rho_e(U+U_d)h_e]}{\partial z} + \frac{1}{r}\frac{\partial[\rho_e r(V+V_e)h_e]}{\partial r} = -\frac{1}{r}\frac{\partial[rq_{r_e}]}{\partial r} + \sigma_e E^2 + S_{ec} + S_{ic}^e \qquad (2\text{-}4)$$

Heavy Particle Energy Equation

$$\frac{\partial[\rho_i U h_i]_h}{\partial z} + \frac{1}{r}\frac{\partial[\rho_i r(V+V_i)h_i]_h}{\partial r} = -\frac{1}{r}\frac{\partial[rq_{r_i}]}{\partial r} - S_{ec} \qquad (2\text{-}5)$$

Equation of State

$$P = \rho_e R_e T_e + \left\{ \sum_{\substack{i \\ i \neq e}} \rho_i R_i T_h \right\} \qquad (2\text{-}6)$$

Governing Equations of the Asymptotic Region

Electron Continuity Equation

$$\frac{1}{r} \frac{\partial [\rho_e V_e r]}{\partial r} = \dot{\rho}_e \qquad (2\text{-}7)$$

Electron Energy Equation

$$\frac{1}{r} \frac{\partial [\rho_e V_e h_e r]}{\partial r} = -\frac{1}{r} \frac{\partial [r q_{r_e}]}{\partial r} + \sigma_e E^2 + S_{ec} + S_{ic}^{e} \qquad (2\text{-}8)$$

Heavy Particle Energy Equation

$$\frac{1}{r} \frac{\partial [\rho_i V_i h_i r]_h}{\partial r} = -\frac{1}{r} \frac{\partial [r q_{r_i}]_h}{\partial r} - S_{ec} \qquad (2\text{-}9)$$

Equation of State

$$P = \rho_e R_e T_e + \left\{ \sum_{\substack{i \\ i \neq e}} \rho_i R_i T_h \right\} \qquad (2\text{-}10)$$

2.2.2 Properties Used in Governing Equations

The dependent variables appearing in the entrance region governing equations are U, V, ρ_i, h_i, P and E (axial velocity, radial velocity, mass density of i, specific enthalpy of i, pressure and electric field). It should be remembered that the above list of variables does not form a linearly independent set since the ionic and atomic enthalpies are essentially equal and the electron and ionic mass densities differ by the electron-ion mass ratio. Hence, the dependent variables for this problem can be reduced to the following set: U, V, n_e, n_H, T_e, T_h, P and E, where n_e and n_H are the electron and atom number densities and T_e and T_h are the electron and heavy particle temperatures.

Each of the inelastic collision processes (listed in Section 2.1) can be quantified by the definition of a reaction rate, such that the product of the number densities of the reactants with the reaction rate coefficient gives the number of such reactions occurring per unit volume and time. For example, the rate of creation of electronic mass per unit volume due to the electron ionization of atoms could be given by:

$$\dot{\rho}_e = m_e n_e n_H K_{eH}$$

Therefore, in order to evaluate the term $\dot{\rho}_e$ appearing in the electron continuity equation, it is necessary to write it as the sum of those rate coefficients, multiplied by the

appropriate particle mass and number densities, which involve
a reaction resulting in the production or consumption of an
electron. This therefore requires obtaining the rate coeffi-
cients for the forward and reverse reactions of inelastic
collision number one (Section 2.1) and of the forward reac-
tion of collision three. (Recall that collision two is
insignificant.) For this study, the coefficient for colli-
sion three was obtained from Allen [15]. The coefficient
for the reverse reaction of collision one (electron-ion
recombination) was obtained by fitting the data of Hinnov
and Hirschberg [17] with a simple analytical function. The
ionization rate coefficient is then obtained by using the
law of detailed balancing together with the recombination
rate coefficient.

The term, S_{ic}^e, appearing in the electron energy equa-
tion, is closely related to the source term in the electron
continuity equation. Whenever an electron ionization (or
recombination) collision occurs, there is a loss (or gain)
of energy in the electron subgas in the amount of the ioniza-
tion potential. Therefore, the product of the appropriate
number densities with the rate for the forward (or reverse)
reaction of inelastic collision one (Section 2.1) and the
ionization potential of hydrogen gives the rate of loss (or
gain) of energy by the electrons due to the reaction. As
for radiative recombination (inelastic collision three),
there is a loss of energy in the amount of the ionization

potential plus the mean electron energy (1.5 kTe) when such a reaction occurs, and the contribution to S_{ic}^e is easily obtained. The remaining contribution to S_{ic}^e enters as a loss of electron kinetic energy due to Bremsstrahlung (inelastic collisions four and five). The derivation for the energy loss rate due to electron-ion Bremsstrahlung is given by Clark [9] and that for electron-atom Bremsstrahlung is found in Appendix E.

The electron drift velocity (U_d) appearing in the electron continuity and energy equations is defined as follows [13]

$$U_d = \frac{\sigma_e E}{e n_e}$$

where e is the absolute value of the electronic charge and σ_e is the electrical conductivity. The derivation of the electrical conductivity expression is given in Appendix C.

The transport properties (diffusion coefficients, viscosity, thermal conductivity) needed in this study, are generally provided in the literature in terms of their equilibrium values. Since the most important aspect of this work is that it treats nonequilibrium flow, equilibrium transport coefficients cannot be used. Therefore, a relatively accurate application of mean-free-path theory has been used to obtain these quantities. The derivations of the expressions for the ambipolar diffusion velocity (V_e) and coefficients, the shear stress (τ_{rz}) and the electron

and heavy particle heat fluxes (q_{r_e} and q_{r_h}) are found in Appendices A and B.

Finally, in a report by Petschek and Byron [18], an expression is derived for the rate of energy loss by electrons due to elastic collisions with a heavy particle subgas. Their expression is used in this work in order to obtain the equation for S_{ec}.

2.2.3 Boundary Conditions

Since the boundary conditions of the asymptotic equations are a subset of those of the entrance region equations, the boundary conditions of the entrance region are developed in this section. Specific discussion of the asymptotic boundary conditions is given where appropriate.

In the governing equations of the entrance region, the axial velocity (U), mass densities (ρ_i) and specific enthalpies (h_i) appear in second order radial partial derivatives when appropriate substitutions are made for the shear stress, ambipolar diffusion velocity and heat flux, respectively. Therefore, two boundary conditions must be supplied for each of these variables. For this problem, conditions are specified at the tube centerline and wall. Since the radial velocity appears only in a radial first derivative, its value needs to be specified at only one boundary (in this case, the centerline). Note that since E and P are not differentiated with respect to r, no boundary conditions are required. The centerline conditions will be discussed first.

Due to the assumed axial symmetry of the flow field,
all radial transport phenomena must vanish at the tube
centerline. Therefore, V (radial velocity) and the radial
first derivatives of U, ρ_i and h_i are all zero at the tube
centerline. The finite-difference version of the derivative
boundary conditions yields the result that the values of U,
ρ_i and h_i at the centerline equal those at the first point
away from the centerline (Figure 3-1). However, a more
rigorous set of centerline conditions may be obtained by
utilizing the governing equations in conjunction with the
first derivative boundary conditions. The governing equa-
tions must be first evaluated in the limit (using L'Hospital's
Rule) as r and V approach zero, after which the boundary con-
dition may be substituted. The "centerline" governing equa-
tions, derived according to the above procedure appear on
the following page. Note that all radial first derivatives
appearing in the ambipolar diffusion velocity, shear stress
and heat flux terms are zero in the centerline equations.

Since the value of V has been specified at the center-
line, it remains to specify boundary conditions on U, ρ_i
and h_i at the wall. The usual nonslip flow condition is
imposed at the wall, and hence, the axial velocity at the
wall is zero. Since the atom number density is between three
and four orders of magnitude larger than the electron number
density at the wall and the atom-atom mean free path is
roughly 5×10^{-5} centimeters, it is reasonable to assume that

Centerline Boundary Conditions of the Entrance Region

Electron Continuity Equation

$$\frac{\partial[\rho_e(U+U_d)]}{\partial z} + 2\rho_e\frac{\partial(V+V_e)}{\partial r} = \dot{\rho}_e \qquad (2\text{-}11)$$

Global Continuity Equation

$$\frac{\partial[\rho U]}{\partial z} + 2\rho\frac{\partial V}{\partial r} = 0 \qquad (2\text{-}12)$$

Axial Momentum Equation

$$\frac{\partial[\rho U^2]}{\partial z} + 2\rho U\frac{\partial V}{\partial r} = -\frac{dP}{dz} + 2\frac{\partial\tau_{rz}}{\partial r} \qquad (2\text{-}13)$$

Electron Energy Equation

$$\frac{\partial[\rho_e(U+U_d)h_e]}{\partial z} + 2\rho_e h_e\frac{\partial(V+V_e)}{\partial r} = -2\frac{\partial q_{r_e}}{\partial r} + \sigma_e E^2 + S_{ec} + S_{ic}^e \qquad (2\text{-}14)$$

Heavy Particle Energy Equation

$$\frac{\partial[\rho_i U h_i]_h}{\partial z} + \left[2\rho_i h_i\frac{\partial(V+V_i)}{\partial r}\right]_h = -2\frac{\partial[q_{r_i}]_h}{\partial r} - S_{ec} \qquad (2\text{-}15)$$

Equation of State

$$P = \rho_e R_e T_e + \left\{\sum_{\substack{i \\ i\neq e}} \rho_i R_i T_h\right\} \qquad (2\text{-}16)$$

the heavy particle subgas will equilibrate with the wall. Therefore, T_h at the wall is equal to the wall temperature, which is fixed at 1000°K. This is equivalent to specifying h_{H^+} and h_H at the wall. The atom mass (or number) density at the wall is determined from the equation of state and knowledge of the wall conditions for the remaining densities and enthalpies. It now remains to establish conditions for the electron temperature and number density at the wall.

Due to the nonequilibrium assumption, the electron temperature and number density at the wall are unknown. However, the necessary conditions may be obtained from consideration of what is known as the wall sheath phenomenon. Since the electron thermal speed is much higher than that of the other heavy particles, the collision frequency of electrons with the wall is higher than that of the ions. This causes the metallic wall (which does not carry a current) to maintain a negative charge relative to the gas in the constrictor. The wall sheath region extends from the wall to a point where the gas becomes electrically neutral (about ten Debye lengths away from the wall). By deriving conservation equations for the flux of electrons and electron energy across the sheath, the electron continuity and energy equations can be employed at the wall to yield two more boundary conditions.

Clark [9] gives a detailed derivation of the wall heat flux and ambipolar diffusion velocity at the edge of the sheath region, therefore, only the expressions for these

quantities will be given here. The interested reader is referred to the work of Clark [9] and Knight [16].

The outward radial flux of electrons at any point in the gas is given by the product of the electron number density and the ambipolar diffusion velocity. The ambipolar diffusion velocity at the wall does not vanish because of electron-ion recombination at the wall. If β is the fraction $(0 \leq \beta \leq 1)$ of electrons reflected from the wall without recombination, the flux of electrons to the wall is given by the product of the wall electron collision frequency, f_{e_w}, and the quantity $(1 - \beta)$. Therefore, the following equality holds

$$n_{e_w} V_{e_w} = f_{e_w} (1 - \beta) \qquad (2\text{-}17)$$

where both sides of the equation express the flux of electrons to the wall. Equation (2-17) is the expression used for the electron flux in prescribing the wall boundary condition for the electron continuity equation. Clark [9] derives the expressions needed to write f_{e_w} as a function of wall dependent variables.

An energy balance for the sheath region yields the expression

$$\overset{(1)}{(q_{r_e})_w} + \overset{(2)}{(n_e V_e \tfrac{5}{2} kT_e)_w} + \overset{(3)}{\tfrac{3}{2} kT_w \beta f_{e_w}} = \overset{(4)}{2kT_{e_w} f_{e_w}} + \overset{(5)}{(1-\beta) f_{e_w} e|\phi_w|}$$

$$(2\text{-}18)$$

where the terms in the equation are

1. Fourier heat conduction into sheath from gas,

2. Ambipolar diffusion of electron energy into sheath from gas,

3. Energy transfer to the sheath due to electron reflection from the wall, where it is assumed that the reflection of electrons is diffuse and that the reflected electrons possess a thermal energy distribution characteristic of the wall temperature [16]. Therefore the transfer of energy from the wall into the sheath is given by the product of $\frac{3}{2} kT_w$ with β and the collision frequency of electrons with the wall.

4. Clark [9] shows that the average electron arriving at the wall has an energy equivalent to $2kT_{e_w}$. Therefore, the rate of energy transfer from the sheath to the wall is given by the product of the wall electron collision frequency and $2kT_{e_w}$ as in term (4).

5. Finally, every electron which successfully traverses the sheath potential to reach the wall and recombine with an ion loses energy in the amount $e|\phi_w|$, where ϕ_w is the electrostatic wall potential. Term (5) gives the total loss due to this phenomenon.

Note that in Equations (2-17) and (2-18) several of the terms should be evaluated at the sheath edge rather than the wall. However, since the sheath is about ten Debye lengths in thickness, the difference is indistinguishable. Equation (2-18), when solved for $(q_{r_e})_w$, then provides the wall condition needed to solve the electron energy equation. The preceding wall boundary conditions appear on the following page for ease of reference.

The centerline and wall boundary conditions of the asymptotic region are obtained from those of the entrance region by simply ignoring the conditions on the axial and radial velocities. The axial momentum and global continuity equations are no longer necessary, and the remaining equations may be simplified by setting all radial velocities and axial derivatives equal to zero. It should be noted that, in the computer program used to obtain solutions in the entrance region, the sheath conditions were deleted for simplicity, and conditions were obtained by simply specifying the electron temperature and number density at the wall.

No further conditions are required for the asymptotic equations, but since there appears in the entrance region equations, first order axial derivatives of U, ρ_i and h_i, these quantities must be specified at the constrictor entrance ($z = 0$) and are referred to as "initial conditions." The initial condition on the axial velocity has been chosen to be a parabola with a centerline value that satisfies mass

Wall Boundary Conditions of the Entrance Region

Axial Velocity

$$U(R) = 0$$

Heavy Particle Temperature

$$T_h(R) = T_{wall} = 1000°K$$

Atomic Mass (or Number) Density

$$P = \rho_e R_e T_e + \left\{ \sum_{\substack{i \\ i \neq e}} \rho_i R_i T_h \right\}$$

$$P = n_e k T_e + (n_e + n_H) k T_h$$

Electron Wall Flux

$$n_{e_w} V_{e_w} = f_{e_w} (1 - \beta)$$

Electron Wall Heat Flux

$$(q_{r_e})_w = - (n_e V_e \tfrac{5}{2} k T_e)_w - \tfrac{3}{2} k T_w \beta f_{e_w} + 2 k T_{e_w} f_{e_w} + (1-\beta) f_{e_w} e |\phi_w|$$

flux requirements. Both temperature profiles are also assumed to be parabolic, with preselected centerline and wall temperatures. The electron number density profile is determined by specifying a third temperature profile and using it to compute the electron number densities from the Saha equation. The centerline and wall temperatures of this third temperature profile are adjusted to yield reasonable centerline and wall electron number densities. Finally, the entrance atom number density profile is evaluated from the equation of state and the other initial conditions. The assumed initial conditions are summarized on the following page. Note that CL stands for centerline, w for wall and R is the tube radius.

Initial Conditions of the Entrance Region

Electron Temperature

$$T_e = T_{e_w} + \left[T_{e_{CL}} - T_{e_w} \right] \left(1 - \frac{r^2}{R^2} \right)$$

Heavy Particle Temperature

$$T_h = T_{h_w} + \left[T_{h_{CL}} - T_{h_w} \right] \left(1 - \frac{r^2}{R^2} \right)$$

Electron Number Density

$$\frac{n_e^2}{n_H} = \left(\frac{2\pi m_e kT'}{h^2} \right)^{\frac{3}{2}} e^{-I_p/kT'}$$

$$n_H = \frac{P}{kT_h} - n_e \frac{T_e}{T_h} - n_e$$

$$T' = T_w' + \left[T_{CL}' - T_w' \right] \left(1 - \frac{r^2}{R^2} \right)$$

Atom Number Density

$$n_H = \frac{P}{kT_h} - n_e \frac{T_e}{T_h} - n_e$$

Axial Velocity

$$U = U_{CL} \left(1 - \frac{r^2}{R^2} \right)$$

$$U_{CL} = \dot{m} \left[\int_0^R 2\pi \rho \left(1 - \frac{r^2}{R^2} \right) r \, dr \right]^{-1}$$

$$\dot{m} = \text{mass flux.}$$

CHAPTER 3   NUMERICAL SOLUTION TECHNIQUES

3.1   General Discussion

The primary purpose of this study is to obtain accurate information concerning the flow of hydrogen through a cascade arc by using theoretical procedures. To obtain accurate results, it is necessary to incorporate numerous microscopic and macroscopic phenomena in the governing equations, thus causing the equations to assume a complex form. Expressions for the source terms and the diffusion velocities are complicated and involve three or four dependent variables. Due to the high degree of coupling and the presence of highly non-linear terms in the governing equations, exact solutions to the equations cannot be obtained. The only recourse is then to use finite-difference solution techniques.

Finite-difference methods in general have several properties in common. The most basic of these common elements is the idea of breaking up the real, continuous solution domain into a finite set of discrete points. The solution of a problem by finite differences therefore consists of calculating values of the dependent variables at these points. This is accomplished by replacing the derivatives in the governing equations by approximations involving the values of the dependent variables at neighboring points of

the finite-difference grid. Two important aspects of the procedure include determination of the spacing of the discrete solution points (grid, stencil or star) in the domain of the independent variables and the selection of the finite difference operators which will replace the derivatives.

It is not the purpose of this chapter to present in great detail the particular finite-difference techniques utilized in this study but rather to present an overview, such that the reader can supply the details and derivations necessary for full understanding. Also, the numerical methods discussed in this chapter apply only to the solution of the asymptotic equations. The solutions to the equations of the entrance region require different techniques and are of relatively minor importance in this study. The reader who is interested in entrance equation solution techniques is referred to the work of Clark [9].

There are two basic choices available regarding the spacing of finite difference grid points: uniform or non-uniform spacing. Uniform spacing is to be preferred because it permits the simplification of the finite-difference operators and if, as in many cases, computer run time is small, the grid spacing can be easily reduced for greater accuracy. However, if computer time is expected to be large, as in this case, an optimally spaced variable grid is the wisest choice. The spacing can be made coarse in regions of small gradients and fine in regions of large gradients.

Therefore, the nonuniform grid, with accompanying compli-
cated expressions for difference operators, has been selected
for this work. The grid consists of 20 points with center-
line spacing six times greater than at the wall. A schematic
drawing of this grid appears in Figure 3-1.

At first glance, it appears that all derivatives in the
asymptotic equations (Section 2.2.1) are of the first order.
However, the ambipolar diffusion velocity (V_e and V_i) and
the heat fluxes (q_{r_e} and q_{r_i}) involve first order derivatives
of the dependent variables. Therefore, each derivative term
of the asymptotic equations, after substitution and expan-
sion, takes the form, $\frac{1}{r} \frac{\partial}{\partial r} \left[r\alpha(\phi, \ldots) \frac{\partial \phi}{\partial r} \right]$, where ϕ is a
dependent variable and α is a single term or product of terms
which are a function of ϕ and possibly other dependent
variables.

The derivation of a finite-difference operator for the
above derivative takes place in two steps. First, an expres-
sion is found to approximate $\frac{\partial f}{\partial r}$ evaluated at the grid point n
in terms of the values of f at the half grid points $(n - \frac{1}{2})$
and $(n + \frac{1}{2})$. Note that $f(n \pm \frac{1}{2}) = [f(n) + f(n \pm 1)]/2$.
Half grid points are used for accuracy and for reasons that
will be obvious in succeeding paragraphs. Deriving expres-
sions for $f(n + \frac{1}{2})$ and $f(n - \frac{1}{2})$ by expanding a Taylor series
about the point n and manipulating the resulting two equa-
tions in order to cancel the lowest order error term gives
the equation
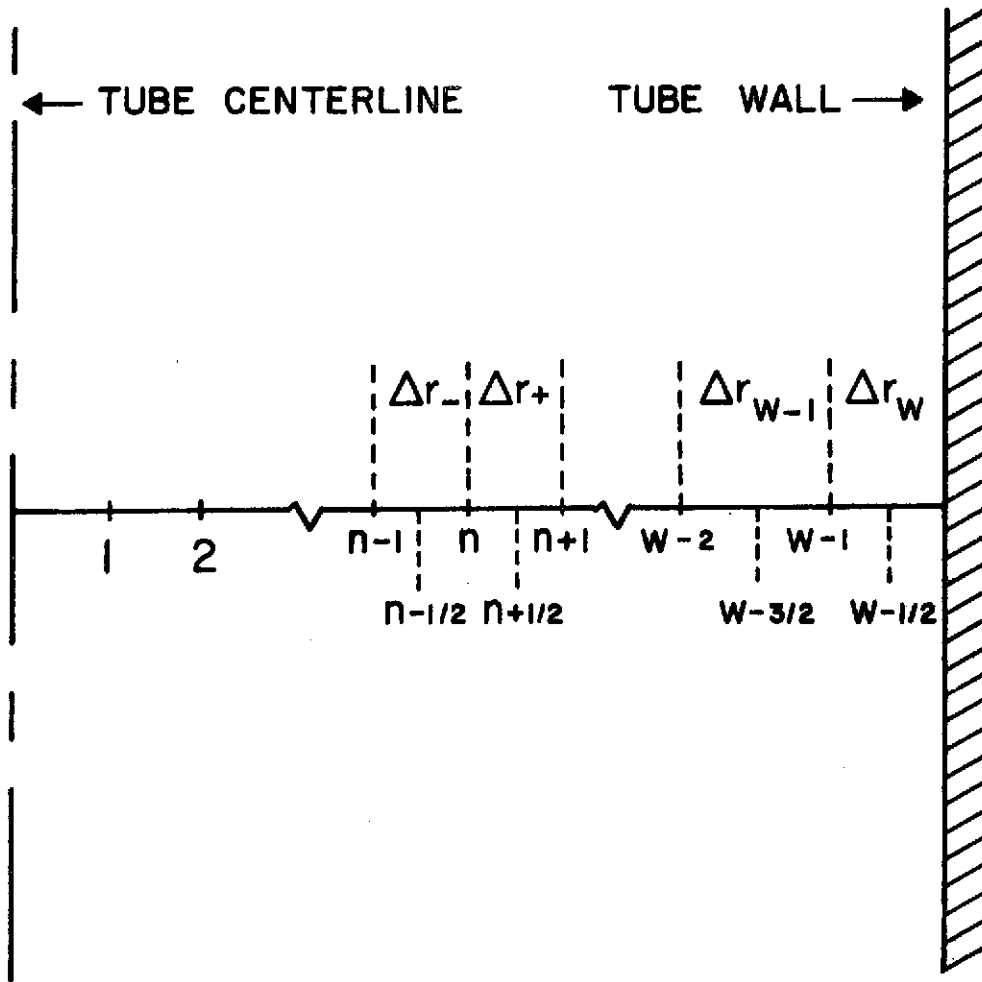
Figure 3-1. Schematic of Finite Difference Grid.

$$\left(\frac{\partial f}{\partial r}\right)_n \approx \frac{2\Delta r_-}{\Delta r_+ (\Delta r_- + \Delta r_+)} f_{n+\frac{1}{2}} + \left(\frac{2}{\Delta r_- + \Delta r_+}\right)\left(\frac{\Delta r_+}{\Delta r_-} - \frac{\Delta r_-}{\Delta r_+}\right) f_n$$

$$- \frac{2\Delta r_+}{\Delta r_- (\Delta r_- + \Delta r_+)} f_{n-\frac{1}{2}} \qquad (3\text{-}1)$$

where Δr_- and Δr_+ are the differences in the independent radial variable, as shown in Figure 3-1.

Substituting $r\alpha(\phi,\ldots)\frac{\partial\phi}{\partial r}$ for f in Equation (3-1); setting

$$\left(\frac{\partial\phi}{\partial r}\right)_{n+\frac{1}{2}} = \frac{\phi_{n+1} - \phi_n}{\Delta r_+}$$

and

$$\left(\frac{\partial\phi}{\partial r}\right)_{n-\frac{1}{2}} = \frac{\phi_n - \phi_{n-1}}{\Delta r_-} \quad ;$$

evaluating $\left(\frac{\partial\phi}{\partial r}\right)_n$ by means of Equation (3-1) by replacing $n+\frac{1}{2}$ with $n+1$, $n-\frac{1}{2}$ with $n-1$, $\Delta r_-/2$ with Δr_- and $\Delta r_+/2$ with Δr_+ as shown below

$$\left(\frac{\partial\phi}{\partial r}\right)_n = \frac{\Delta r_-}{\Delta r_+ (\Delta r_- + \Delta r_+)} \phi_{n+1} + \left(\frac{1}{\Delta r_- + \Delta r_+}\right)\left(\frac{\Delta r_+}{\Delta r_-} - \frac{\Delta r_-}{\Delta r_+}\right) \phi_n$$

$$- \frac{\Delta r_+}{\Delta r_- (\Delta r_- + \Delta r_+)} \phi_{n-1} \quad ;$$

the following expression for the desired derivative is obtained

$$\frac{1}{r} \frac{\partial}{\partial r} \left[r\alpha(\phi, \ldots)\frac{\partial \phi}{\partial r} \right]_n = \left(R_{4n}\alpha_{n+\frac{1}{2}} + R_{5n}\alpha_n \right) \phi_{n+1}$$

$$- \left(R_{4n}\alpha_{n+\frac{1}{2}} - R_{7n}\alpha_n + R_{6n}\alpha_{n-\frac{1}{2}} \right) \phi_n$$

$$+ \left(R_{6n}\alpha_{n-\frac{1}{2}} - R_{8n}\alpha_n \right) \phi_{n-1} \qquad (3\text{-}2)$$

where

$$R_{4n} = \frac{2\Delta r_-}{\Delta r_+^2 (\Delta r_- + \Delta r_+)} \frac{r_{n+\frac{1}{2}}}{r_n}$$

$$R_{5n} = \frac{2(\Delta r_+ - \Delta r_-)}{\Delta r_+^2 (\Delta r_- + \Delta r_+)}$$

$$R_{6n} = \frac{2\Delta r_+}{\Delta r_-^2 (\Delta r_- + \Delta r_+)} \frac{r_{n-\frac{1}{2}}}{r_n}$$

$$R_{7n} = \frac{2(\Delta r_+ - \Delta r_-)^2}{(\Delta r_+ \Delta r_-)^2}$$

$$R_{8n} = \frac{2(\Delta r_+ - \Delta r_-)}{\Delta r_-^2 (\Delta r_- + \Delta r_+)}$$

Substitution of the above approximation in the governing equations yields the desired finite-difference approximation, the treatment of which is discussed in the following section. The truncation error of Equation (3-2) is complicated, but the lowest order terms are written below.

$$(\Delta r_+ - \Delta r_-) \frac{(r\alpha)_n}{3} \frac{\partial^3 \phi}{\partial r^3}\bigg|_n + \frac{\Delta r_- \Delta r_+}{24} \frac{\partial^3}{\partial r^3} \left[r\alpha(\phi, \ldots)\frac{\partial \phi}{\partial r} \right]_n$$

The largest error (which is of the first order) is reduced by selecting a variable grid in which grid spacing increases

or decreases gradually. If this is done, the truncation
error is of the second order.

The centerline boundary equations, Equations (2-11)
through (2-16), must also be approximated by use of second
order finite-difference operators. However, the grid can
be assumed uniform at the centerline and the second deriva-
tives approximated by difference operators using values of
variables at the centerline and the first point on either
side of it (the variables at the latter two points being
equal). Since the standard expression for the second order
difference operator (which has a second order error) for a
uniform grid is well known, it will not be written here.

A special difference operator must be developed for
Equations (2-7) and (2-8) which are used in conjunction with
Equations (2-17) and (2-18) for wall boundary conditions on
electron wall particle and heat fluxes. Since the expres-
sions for the heat flux and ambipolar diffusion velocity at
the sheath edge do not contain derivatives, these equations
are only of the first order in the radial derivative.
Therefore, a finite difference expression must be obtained
which approximates the first derivative of a quantity ϕ at
the wall. This is accomplished by using a Taylor series
expansion at the wall to approximate the value of the vari-
able ϕ at the points $w-\frac{1}{2}$ and $w-\frac{3}{2}$ (see Figure 3-1) in terms
of the value of ϕ and its derivatives at the wall. Two
equations are obtained from this procedure and are solved

simultaneously in order to eliminate the second derivative terms in each. When this is done, the following expression is obtained for the first radial difference at the wall

$$\left.\frac{\partial \phi}{\partial r}\right|_w = R_{w_1} \phi_{w-\frac{3}{2}} - R_{w_2} \phi_{w-\frac{1}{2}} + R_{w_3} \phi_w$$

where

$$R_{w_1} = \frac{2\Delta r_w}{(2\Delta r_w + \Delta r_{w-1})(\Delta r_w + \Delta r_{w-1})}$$

$$R_{w_2} = \frac{2(2\Delta r_w + \Delta r_{w-1})}{\Delta r_w(\Delta r_w + \Delta r_{w-1})}$$

$$R_{w_3} = \frac{2(3\Delta r_w + \Delta r_{w-1})}{\Delta r_w(2\Delta r_w + \Delta r_{w-1})}$$

and Δr_w and Δr_{w-1} are defined in Figure 3-1. The truncation error of the above formula is of the second order as shown below

$$\frac{\Delta r_w(2\Delta r_w + \Delta r_{w-1})}{24}$$

When this difference formula is directly applied to the wall electron continuity and energy equations, the resulting difference expression will contain the ambipolar diffusion velocity and heat flux evaluated at $w-\frac{3}{2}$, $w-\frac{1}{2}$ and w. At the first two of these three points, the standard differential forms of the ambipolar velocity and the heat flux are substituted (see Appendices A and B) but at the last point, w, the sheath expressions, Equations (2-17) and (2-18), are substituted.

3.2 Solution of Finite Difference Governing Equations

In order to introduce the method used to solve the difference equations, an illustrative example is first described. Suppose that it is necessary to solve a system of two transcendental equations in two unknowns. Due to the nonlinearity and coupling of the various terms of the equations it is impossible to obtain a direct solution and, therefore, an iterative technique must be utilized. Assume that the unknowns in the equations are labeled x and y and that the equations have been written such that all terms are on the left hand side. Therefore, the system of equations appears as

$$f_1(x,y) = 0; \quad f_2(x,y) = 0$$

The Newton-Raphson method is to be utilized to obtain the values of x and y which satisfy the above expressions. First, expand each of the above functions to the first order in a Taylor series about x and y.

$$f_1\left(x^{i+1},y^{i+1}\right) = f_1\left(x^i,y^i\right) + \left.\frac{\partial f_1}{\partial x}\right|^i\left(x^{i+1} - x^i\right) + \left.\frac{\partial f_1}{\partial y}\right|^i\left(y^{i+1} - y^i\right)$$

$$f_2\left(x^{i+1},y^{i+1}\right) = f_2\left(x^i,y^i\right) + \left.\frac{\partial f_2}{\partial x}\right|^i\left(x^{i+1} - x^i\right) + \left.\frac{\partial f_2}{\partial y}\right|^i\left(y^{i+1} - y^i\right)$$

The above equations indicate that, if values of f_1^{i+1} and f_2^{i+1} are arbitrarily selected, it is possible to find the set of variables (x,y) which will satisfy the above equations. It is desired now to find the values of x and y which result

54

in f_1^{i+1} and f_2^{i+1} being identically zero. Suppose a set of variables (x^i, y^i) have been arbitrarily substituted into the functions and have failed to yield zero. A second estimate of variables (x^{i+1}, y^{i+1}) which will accomplish this is acquired by setting the left hand sides of the above equations equal to zero and solving for (x^{i+1}, y^{i+1}). Using matrix notation, this results in the following expression.

$$\begin{bmatrix} x^{i+1} \\ y^{i+1} \end{bmatrix} = \begin{bmatrix} x^i \\ y^i \end{bmatrix} - \begin{bmatrix} \frac{\partial f_1}{\partial x}\Big|^i & \frac{\partial f_1}{\partial y}\Big|^i \\ \frac{\partial f_2}{\partial x}\Big|^i & \frac{\partial f_2}{\partial y}\Big|^i \end{bmatrix}^{-1} \begin{bmatrix} f_1^i \\ f_2^i \end{bmatrix} \qquad (3-3)$$

Since the Taylor series expansion was terminated after the first order, the above matrix equation is only approximately correct. Therefore, the variables (x^{i+1}, y^{i+1}) are only approximations of the true solution of the two transcendental equations. In order to obtain the true solution, the variables (x^{i+1}, y^{i+1}) must be used in place of the values (x^i, y^i) to completely reevaluate the right hand side of the above matrix equation. Then, another matrix inversion, multiplication and subtraction must be carried out to obtain a yet more refined set of variables (say x^{i+2}, y^{i+2}). This process is continued until sufficient accuracy is obtained in the solution. This method can, in general, be used for large systems of equations where it is possible to invert matrices quickly by the computer.

By utilizing the difference operators of the previous
section to obtain the finite difference forms of the govern-
ing equations and the boundary conditions, a large system of
equations is generated in which the unknown variables are
the densities and enthalpies at each of the individual grid
points. Actually, the final form of the governing differ-
ential equations used in this study has been simplified so
that the variables are electron and atom number densities
and electron and heavy particle temperatures. Therefore,
there are four unknowns in the four governing equations of
the asymptotic region (Section 2.2.1).

For each grid point at which it is desired to obtain a
solution, there are four unknowns (two temperatures and two
number densities) and four finite-difference governing equa-
tions. Suppose there are n such grid points. Therefore,
there are 4n unknowns (n_{e_i}, n_{H_i}, T_{e_i}, T_{h_i}, $i = 1,n$) and 4n
finite difference equations. The Newton-Raphson method has
been employed in this study to solve this system of equations
and its development proceeds as follows.

The most direct approach is to choose an initial estimate
of the variables at each grid point; calculate the values of
the functions and their derivatives which appear in the
matrix to be inverted, as in Equation (3-3), (it is assumed
that all terms in the difference equations are on the left
hand side); invert the matrix; calculate the new set of
variables; and then repeat the cycle until convergence is

obtained. In practice, this procedure did not yield convergence due to the strong coupling between equations and the following modification was employed. The electron continuity equation and equation of state were "decoupled" from the two energy equations in the finite-difference scheme as follows. Initial estimates of variables at all grid points were first obtained, and all temperatures were assumed to be fixed. The matrix inversion routine then only involved the electron continuity equation and the equation of state. Therefore, only the number densities were recomputed until convergence was obtained. Then, the number densities were fixed and the matrix inversion routine involved only the energy equations. The temperatures were then recomputed until convergence was obtained. This procedure was repeated until successive cycles produced unchanging number density and temperature profiles, indicating total convergence. It was also necessary to introduce the following additional step in the actual computer program. Rather than specify the electric field (which appears explicitly in the electron energy equation), the current was actually read into the computer program and the electric field was estimated. Therefore, after convergence was obtained on the temperature profiles (with fixed number densities), the integration of the electrical conductivity was carried out to calculate the current corresponding to the estimated electric field. This was done according to the expression

$$I = E \int_0^R 2\pi\sigma_e r \, dr \qquad (3\text{-}4)$$

If the calculated current did not agree with that which was read into the program, an iteration procedure (Newton-Raphson) was initiated to obtain the correct electric field by estimating a new value of E, substituting it back into the energy equations (with fixed number densities) and obtaining the new converged set of temperatures and electrical conductivity. Integration was again repeated according to Equation (3-4) and the process continued until the correct electric field was obtained.

One final comment needs to be made regarding the selection of the first estimate of the unknown variables. It has been found that this program is sensitive to the accuracy of the input variables. For this reason another computer program (program MARCH) was developed to use an explicit, finite-difference scheme to solve the governing equations of the entrance region. As the solution of program MARCH progresses in the axial direction of the cascade arc, it approaches the asymptotic region and yields number density and temperature profiles suitable for the initial values of the asymptotic solution method. However, most of the initial profiles used in this work were provided by solutions of the asymptotic region program for other operating parameters (current, pressure, tube radius). Therefore, due to the insignificance of program MARCH, the explicit finite-difference

scheme for the entrance region equations has not been dis-
cussed here. The interested reader is referred to the work
of Clark [9].

CHAPTER 4   RESULTS AND DISCUSSION

4.1   Preliminary Discussion

Development of the finite-difference and computer pro-
gramming techniques in order to obtain stable, convergent
solutions to the governing equations has proved to be a
formidable task.   It is not possible to mention all of the
intricate details which have become necessary to obtain solu-
tions, however, some of the more important aspects of the
methods should be discussed.

As mentioned previously, a computer program (MARCH) was
developed to solve the governing equations of the entrance
region.   Since this program proved to be stable only at low
currents, it was of limited value and has not been discussed
to any great extent.   However, this program has been used to
obtain a solution for I = 50 amps, P = 1 atm. and R = 0.005
meters, and the results were sufficiently accurate to serve
as the starting data for the iterative solution (the Newton-
Raphson method) of solving the asymptotic equations.   In
this study, three separate computer programs were used to
obtain the solution to the asymptotic equations in final
form.   The first program (NRHEQD) provided solutions to the
equations for the case of thermal equilibrium ($T_e = T_h$) with
fixed (rather than electrostatic sheath) boundary conditions.

This program was used to obtain approximate densities and temperature for new operating conditions because it was faster than the other two. When a set of profiles was obtained from program NRHEQD, they were read into a second program (NRHD) which obtained the solution to the governing equations without the thermal equilibrium restriction but, again, with fixed boundary conditions. This then provided a sufficiently accurate set of data for the more sensitive program (NRHDS) which accounted for the sheath electrostatic wall phenomena. The output from NRHDS was then the final solution. The computer time required to obtain each solution by this procedure on a CDC 6500 computer ranged from about 10 minutes to an hour.

In order to maintain numerical stability of the asymptotic computer programs at higher currents, it became necessary to fix the electron and heavy particle temperatures at the grid point adjacent to the wall (w-1 in Figure 3-1). Reasonable values were selected on the basis of experience with the solutions, and solutions for the lower currents which did not require this restriction indicated that temperatures adjacent to the wall are relatively insensitive to values of the reflection coefficients.

The criterion used to determine whether a solution had converged sufficiently was that successive iterates of the densities and temperatures at all grid points must not vary by more than 0.0005%. Therefore, if the temperature at a

certain grid point is about 10,000°K, at the time of con-
vergence it changes less than 0.05°K from one iteration to
the next. In addition, a global energy balance was also
used to check the convergence of each of the final solutions.
The amount by which this balance was not satisfied averaged
about 2.5% for all parametric solutions. Undoubtedly, this
figure could have been reduced by substantially decreasing
the grid spacing, but this would have resulted in prohibitive
computer run times. Also, the accuracy demonstrated by the
convergence criterion and the energy balance is considered
to be much greater than that of the basic data (such as
recombination coefficients, transport properties, etc.) used
in the program (see Section 4.4). Therefore, it was deemed
of little benefit to obtain greater numerical accuracy.

Solutions were obtained for two purposes. First,
parametric predictions were obtained to gain more insight
to the physical nature of high temperature, nonequilibrium
arcs. In addition, solutions were obtained specifically
for the purpose of comparison with experimental data and
equilibrium solutions. The parametric predictions obtained
covered the following range of operating conditions:

1. P = 1 atm, R = 0.005 meters, $50 \leq I \leq 200$ amps.

2. I = 200 amps, R = 0.005 meters, $1 \leq P \leq 10$ atm.

3. I = 200 amps, P = 1 atm, $0.005 \leq R \leq 0.05$ meters.

Predictions were obtained for comparison with the experimental results of Steinberger [12], Morris and Rudis [10], Wiese [27] and Maecker [11] and with the equilibrium predictions of Greene [6]. The range of operating conditions used in these comparisons is as follows:

1. P = 1 atm, R = 0.0015 meters, 20 $\leq$ I $\leq$ 50 amps.

2. P = 1 atm, R = 0.0010 meters, 20 $\leq$ I $\leq$ 40 amps.

3. P = 1 atm, R = 0.005 meters, 50 $\leq$ I $\leq$ 200 amps.

Before discussing the solutions to the atomic hydrogen nonequilibrium model it would be beneficial to briefly consider the individual terms in the electron continuity and energy equations.

Figure 4-1 illustrates the two terms of the electron continuity equation which exactly balance each other. It is evident that electron production in the core due to ionization is balanced by ambipolar diffusion of electrons away from that region. As the wall is approached, $\dot{n}_e$ reverses sign indicating that electrons diffusing into the wall region are being consumed by radiative and three-body recombination processes.

Figure 4-2 is plotted in such a way that positive values indicate energy transfer to the electron gas and negative values indicate energy transfer from the gas. As expected, the Ohmic heating term $(\sigma_e E^2)$ supplies energy to the electron gas over the entire arc cross section. Also
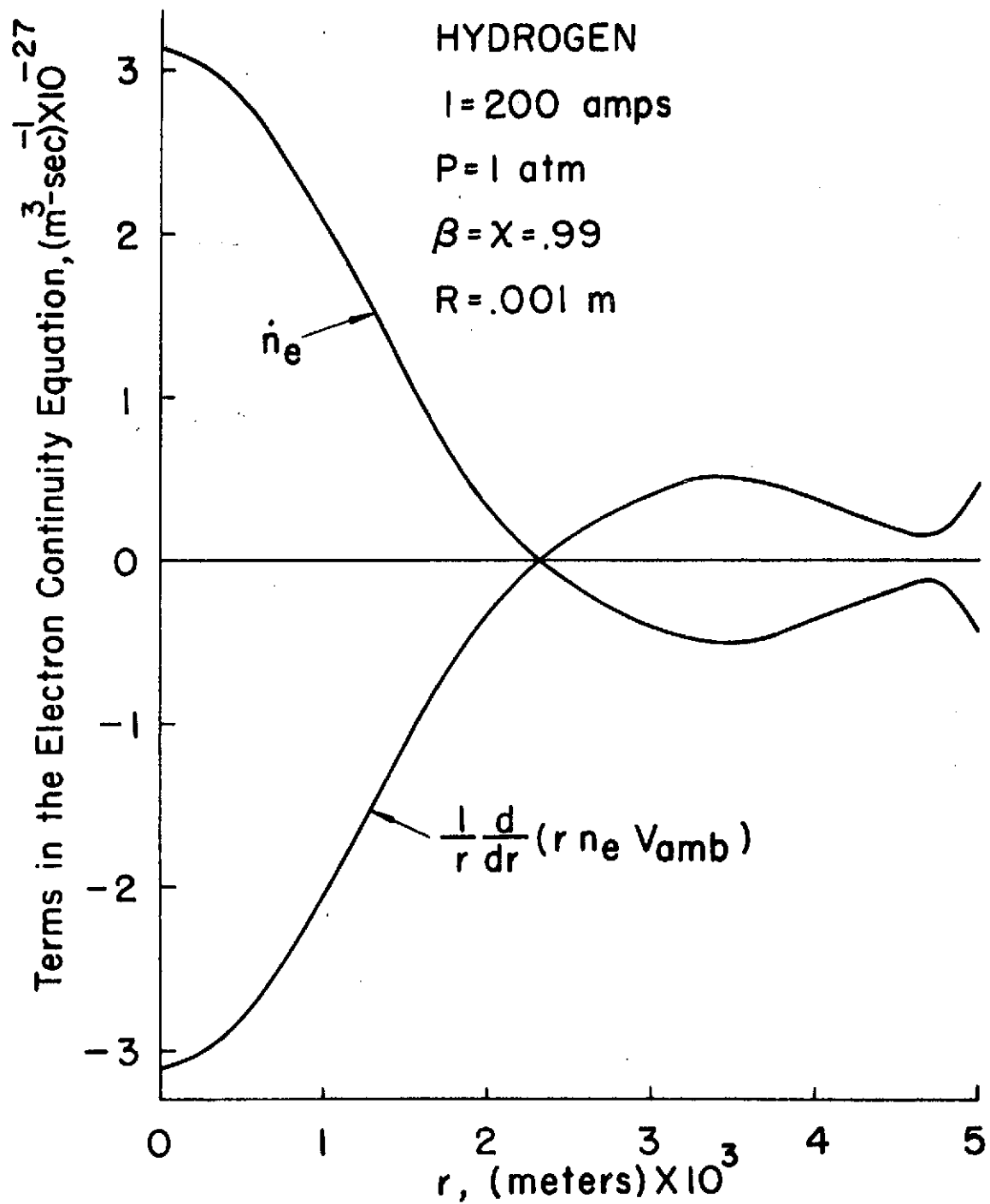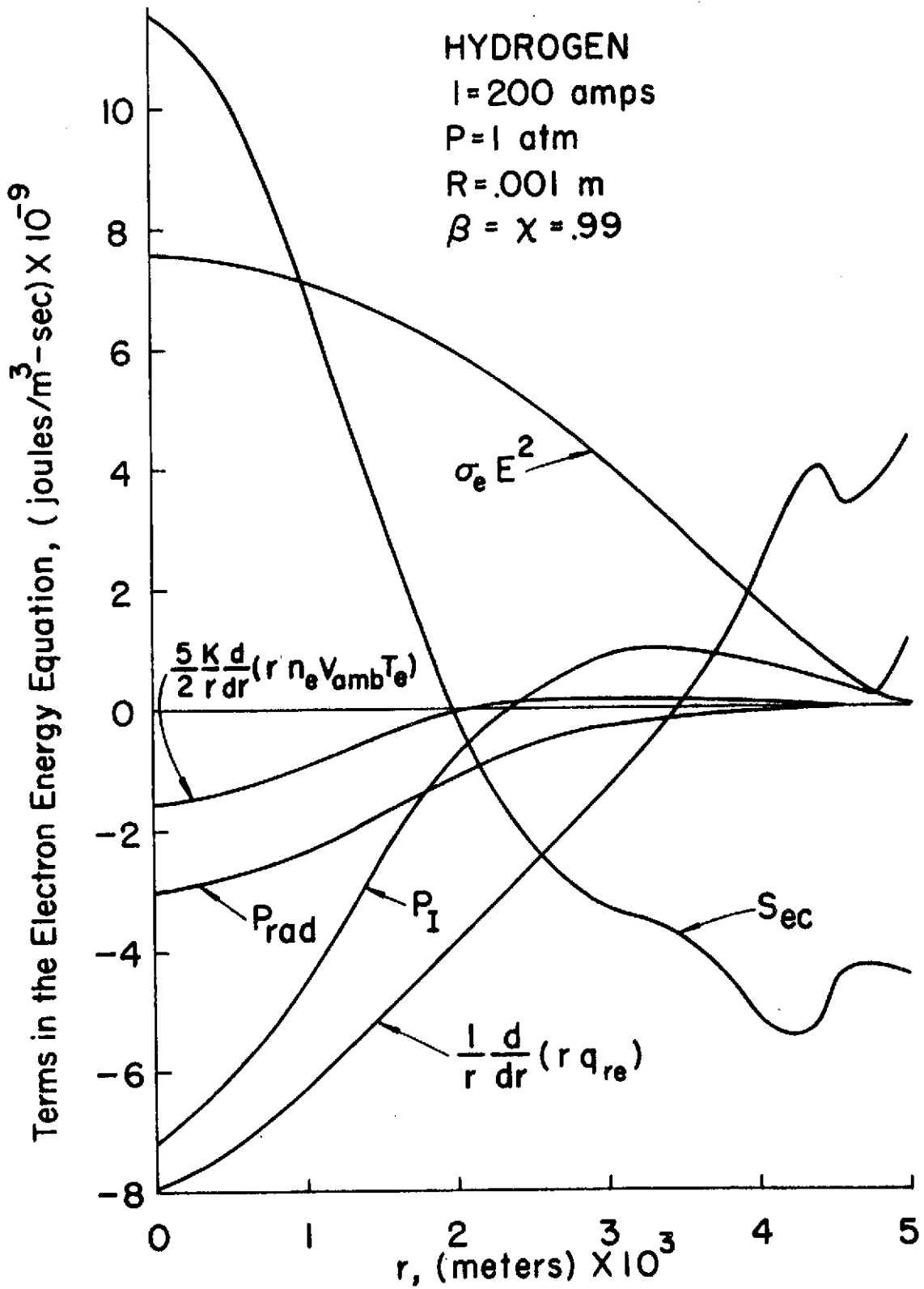
Figure 4-1. Terms in the Electron Continuity Equation.

Figure 4-2. Terms in the Electron Energy Equation.

radiative emission (P_{rad}) depletes the electron gas energy, especially in the core. The term (P_I) refers to the diffusion of ionization energy. Since electron-ion pairs are being produced in and diffused away from the core, P_I is negative there. However, as the wall is approached, the electron-ion pairs recombine transferring ionization energy to electron third particles and P_I is positive. The term S_{ic}^e appearing in the electron energy equation (2-8) is equivalent to $-(P_{rad} + P_I)$. The core also loses thermal energy through ambipolar diffusion and electron heat conduction as shown in Figure 4-2, but as the cooler wall region is approached the electron subgas begins to gain energy due to these processes. Finally, note that the exchange of elastic collisional energy between electrons and heavy particles (S_{ec}) behaves unexpectedly. In fact, the heavy particles transfer energy to the electrons in the core region (for these operating conditions) indicating that the heavy particle temperature is slightly higher (by about .05%) than the electron temperature. The reason for the magnitude of S_{ec} being so large for such a small difference in temperature is because S_{ec} is proportional to the product of the electron density and the electron-heavy particle collision frequency, both of which are much larger in the core than elsewhere. From Figure 4-2 it is evident that the high rate of depletion of electron energy in the core by electron heat conduction and electron ionization (as evidenced by the P_I term) tends to depress the

electron temperature. Note that from Equation (2-9), the integral $\left[-\frac{1}{r} \int_0^r rS_{ec}dr \right]$ gives the heavy particle heat conduction and that from Figure 4-2 this indicates that there is a net heavy particle conduction of energy to the core from the periphery. This is impossible for simple Fourier conduction, but the mean free path theory of this model predicts a large diffusion-thermo effect (heat transfer induced by a concentration gradient) which is responsible for this effect (the heavy particle concentration increases rather than decreases with increasing r). Nevertheless, at the wall, Fourier conduction takes over and results in a positive transfer of heavy particle energy to the wall. The consequence of this diffusion-thermo effect, coupled with the depletion of electron energy by conduction and ionization, is that the heavy particle temperature can be elevated slightly above the electron temperature because there is a source of energy for the heavy particle subgas in the core. Nevertheless, the effect is small resulting in only a few degrees temperature difference.

The comparative studies are discussed in detail in Section 4.2 and the parametric studies are discussed in Section 4.3. The chapter is concluded with an uncertainty analysis and a discussion of the molecular hydrogen arc in Sections 4.4 and 4.5, respectively.

4.2 Comparisons with Other Data

In this section, comparison of the numerical solutions is made with both experimental results and equilibrium predictions obtained by other researchers. Morris and others [10] have published the results of their study for an atmospheric hydrogen arc with a radius of 0.0015 m and sample temperature measurements are shown in Figure 4-3. The curve shown is for a current of 40 amps and its relationship to the numerical results of this study is representative of the other currents for which data were obtained. Therefore, only the 40 amp curves are shown. The Morris profile is much more "peaked" than the results of this study, producing a higher centerline temperature. Wiese [27] has also obtained spectroscopic measurements of a hydrogen arc at the specified operating conditions and his results are also shown on Figure 4-3. In contrast to the Morris results, the Wiese data agree closely with the results of this study. Actually, Wiese reports temperature profiles determined by two different methods. One set of data is obtained from spectroscopic measurements of the continuum radiation intensity and the other by measuring the intensity of the Balmer line of hydrogen. According to Wiese [27] however, the continuum measurements are the less reliable of the two (due to the contribution of several molecular processes to the continuum emission and the presence of weak, highly broadened impurity lines). For this reason only the temperature profile resulting from
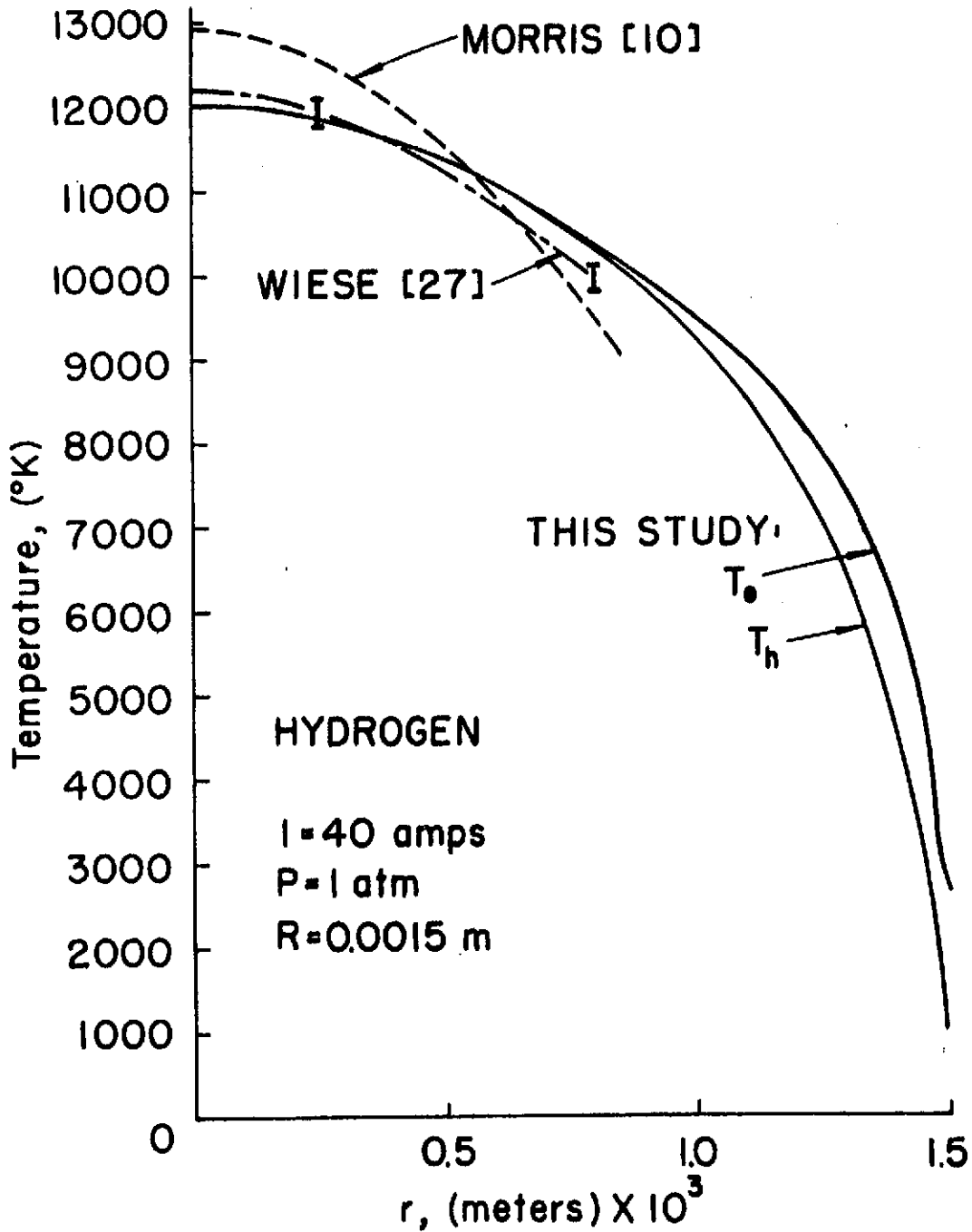
Figure 4-3.   Comparison of Theoretical and Experimental
Temperature Distributions for a 40 amp, .0015 m
Radius Hydrogen Arc.

Wiese's measurement of the Balmer line intensity is shown in Figure 4-3. His other temperature profile (not shown) is more in agreement with that of Morris, who obtained the temperature from a measurement of the continuum intensity.

Figure 4-4 provides the comparison of experimental temperature profiles for a 0.001 m radius atmospheric arc with the solutions of this study. In his experiments, Steinberger [12] also used the Balmer line intensity to obtain his temperatures. Note that at 20 amps, the agreement between theory and experiment is rather poor. Moreover, for this current, the predictions reveal the existence of thermal nonequilibrium over most of the arc cross section. Much time has been spent in thoroughly checking the solution procedures, computer logic, and programs of this study and there is no apparent reason why the low current solution should be any less valid than the high current results. It is to be expected that, at lower currents, nonequilibrium effects extend over a greater portion of the arc and that accurate intensity measurements are more difficult to obtain because of arc instabilities and asymmetry. The agreement between Steinberger's data for 40 amps and the solution from this study is good.

Greene [6] has compiled a set of numerical solutions for the mathematical model of a hydrogen arc in thermochemical equilibrium and representative results appear in Figure 4-5 along with the solutions of this study. These solutions are
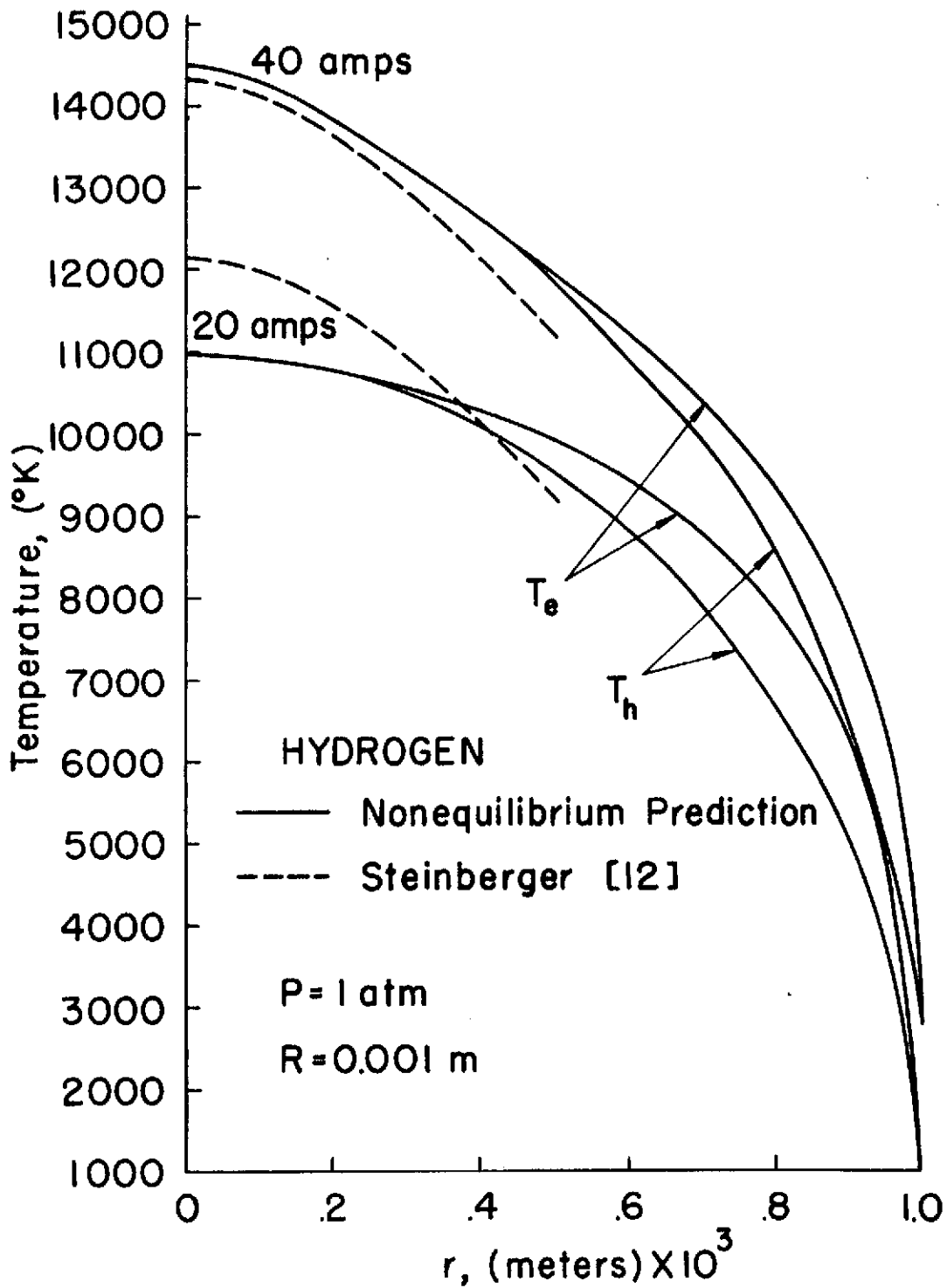
Figure 4-4. Comparison of Theoretical and Experimental Temperature Distributions for a .001 m Radius Hydrogen Arc.
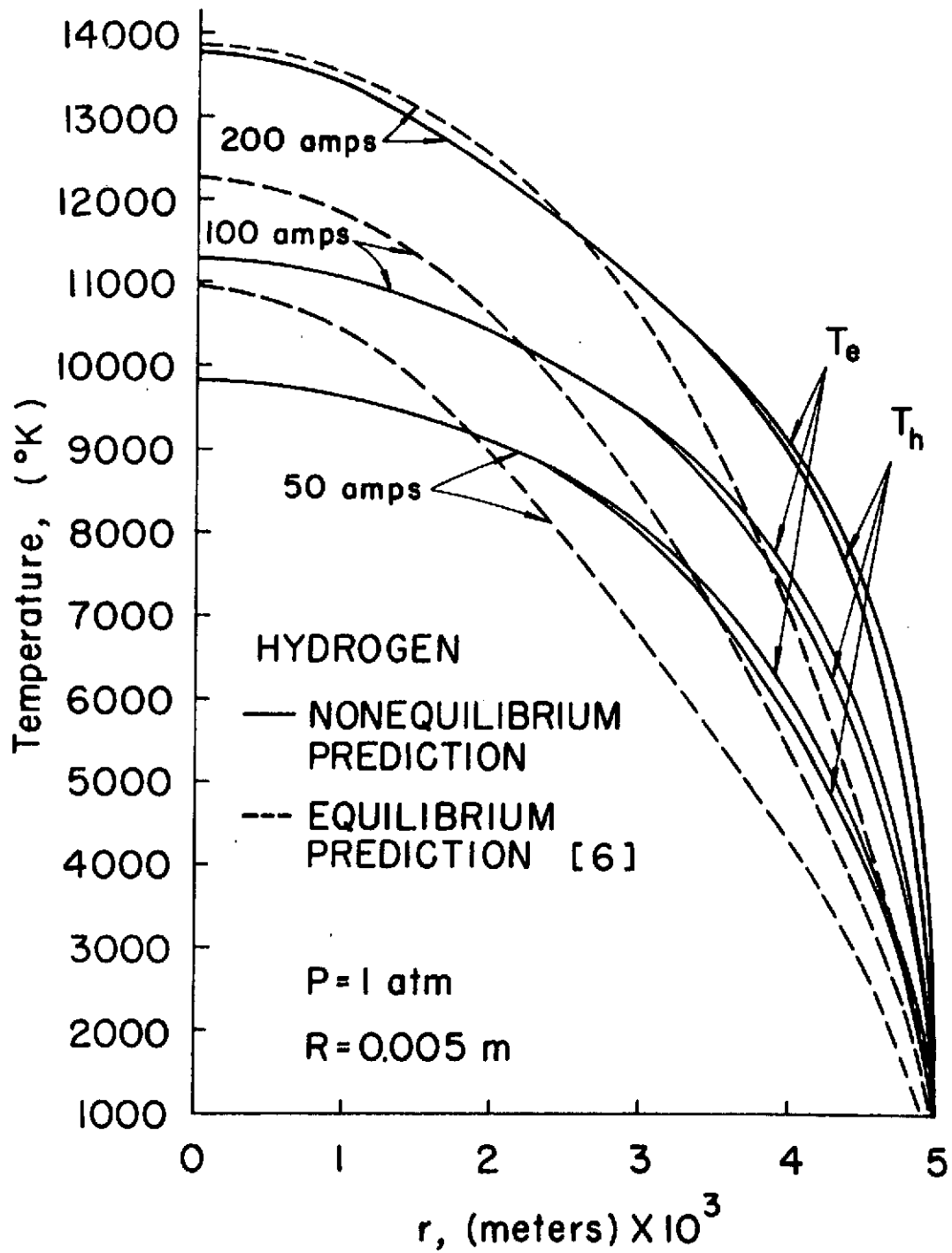
Figure 4-5. Comparison of Temperature Profiles for Equi-
librium and Nonequilibrium Hydrogen Cascade
Arcs.

for an arc of radius .005 m and pressure of 1 atmosphere. The comparisons of this figure reflect the effect of thermo-chemical nonequilibrium in the arc.

At first glance, agreement seems to be poor, but it must be remembered that Greene's [6] solutions are for an arc in local thermodynamic equilibrium. This means that the number densities calculated near the wall are several orders of magnitude lower than for the nonequilibrium case. Therefore, his electrical conductivity is much smaller and the Ohmic heating term $(\sigma_e E^2)$ in his energy equation is very small in the wall region. (See Figure 4-2). Note that, from Table 4-1, although the square of his electric field intensity is as much as twice the nonequilibrium value, his electrical conductivity is orders of magnitude smaller. Therefore, the equilibrium model, as expected, greatly underpredicts the temperature in the wall region due to its failure to include Ohmic dissipation effects in this region. Furthermore, since the electric field is inversely proportional to the integral of the product of the radial coordinate and the electrical conductivity across the tube radius, the electric field of the equilibrium arc is higher due to the smaller electrical conductivities in the wall region. The elevated centerline temperatures for the equilibrium arc tend to com-pensate for this effect on the electric field but fail to do so completely because of the small value of the radial coordinate and the fact that electrical conductivity is

comparatively insensitive to temperature at the higher arc temperatures (Figure C-1). Therefore, the higher electric field provides more Ohmic heating at the centerline in the equilibrium case and hence produces the higher centerline temperatures shown in Figure 4-5.

As the current increases, the equilibrium and nonequilibrium electric fields converge (see Table 4-1). This effect is reflected by the results of Figure 4-5. As the current increases, the centerline temperatures converge, and good agreement between the theories exists over a larger portion of the arc cross section. The difference between the temperatures in the arc periphery is due to thermochemical nonequilibrium effects which persist at the higher currents.

In addition to determining the experimental temperature profiles, Morris [10] and Wiese [27] also measured the electric field intensity, and the results are presented in Table 4-1. Agreement between the experimental and nonequilibrium theoretical electric field intensities is poor at low currents but improves with increasing current. The best comparison is with the data of Wiese [27] which also provided the best agreement for the temperature profiles.

The reason for the poor agreement between theory and experiment is thought to rest largely with the theoretical method because of convergence errors in the numerical procedure at small tube radii. Consider the error in the

Table 4.1   Comparison of Experimental, Equilibrium and
            Nonequilibrium Electric Field Intensity Data
            and Predictions for Various Arc Operating
            Parameters.

P = 1 atm, R = .001 m

I (amps)	E (volts/meter)	
	Maecker [11]	Nonequilibrium
20	12000	5572
40	9800	5261
50	9000	—

P = 1 atm, R = .0015 m

I (amps)	E (volts/meter)		
	Morris [10]	Wiese [27]	Nonequilibrium
20	9300	—	4040
30	7400	—	3779
40	6800	5600	3672
50	6200	—	3617

P = 1 atm, R = .005 m

I (amps)	E (volts/meter)	
	Equilibrium [6]	Nonequilibrium
50	1824	1343
100	1468	1200
150	1375	1191
200	1348	1223
300	1361	—
400	1398	—

second order finite-difference formula given in Chapter 3 and repeated here for reference.

$$\text{error} = (\Delta r_+ - \Delta r_-) \; \frac{(r\alpha)_n}{3} \; \left. \frac{\partial^3 \phi}{\partial r^3} \right|_n$$

It is of interest to see how the error is affected by reducing the tube radius and grid spacing by some factor "a" (less than unity) and assuming that the arc operating parameters are adjusted such that the profiles of α and ϕ maintain the same relative shape. Let the new values of tube radius and grid spacing be denoted by a primed (') superscript such that $r' = ar$ and $\Delta r' = a\Delta r'$. The new error is then

$$(\Delta r'_+ - \Delta r'_-) \; \frac{(r'\alpha)_n}{3} \; \left. \frac{\partial^3 \phi}{\partial (r')^3} \right|_n = a(\Delta r_+ - \Delta r_-) \; \frac{(ar\alpha)_n}{3} \; \left. \frac{\partial^3 \phi}{\partial (ar)^3} \right|_n$$

$$= \frac{1}{a} (\Delta r_+ - \Delta r_-) \; \frac{(r\alpha)_n}{3} \; \left. \frac{\partial^3 \phi}{\partial r^3} \right|_n$$

Therefore if the number and relative spacing of grid points with respect to each other is maintained the same and the values of α and ϕ remain the same at each of the grid points, the error is proportional to $\frac{1}{a}$. To be specific, the profiles of temperature and number density for the solution at I = 40 amps and R = .001 m are roughly the same shape as profiles obtained for a radius of .005 m (which is used for parametric studies) and a current of 200 amps. Therefore, the finite difference convergence error is $\frac{1}{a} = \frac{1}{.2} = 5$ times greater at

I = 40 amps and R = .001 m than at I = 200 amps and R = .005 m. In order to obtain the same accuracy at R = .001 m as at R = .005 m then it is necessary to increase the number of grid points from 20 to 100. Since computer time is roughly proportional to the square of the number of grid points for this type of problem, 25 times as much computer time would be required to obtain this accuracy. This would then involve computer run times of several hours per solution, which is indeed prohibitive. The above calculation of the tube radius dependence of the convergence error is born out by the fact that at the tube radius of .001 m, energy balances of the final solutions showed discrepancies as high as 15%, while at R = .005 m the discrepancies are less than 1%.

It is unfortunate that experimental studies have not been performed for larger tube radii where the convergence error of this numerical method is tolerable. Although the solutions of this model are not accurate at low tube radii (R = .001 m), good accuracy is expected at all the tube radii used in the parametric studies of Section 4.3.

Comparison of the equilibrium and nonequilibrium predictions of the electric field intensity is also shown in Table 4-1 as well as Figure 4-11. As mentioned previously, the difference in these predictions is due to the failure of the equilibrium model to account for thermochemical nonequilibrium effects.

Comparisons between the experimental and nonequilibrium total wall heat flux exhibit the same trends as the electric field comparisons, since the wall heat transfer is equal to the product of the electric field intensity and current in the asymptotic region. The equilibrium and nonequilibrium predictions of total wall heat flux are compared in Figure 4-12 for both hydrogen and argon. Because of the larger value of the field intensity, the equilibrium solution predicts a larger value of the heat flux than the nonequilibrium solution for the hydrogen arc.

Finally, a comparison between equilibrium and nonequilibrium predictions of the radiation heat flux fraction is shown in Figure 4-13, along with the corresponding predictions for argon. Before discussing Figure 4-13, it is useful to discuss the radiation model used in this study.

In the nonequilibrium model of this study, it is difficult to rigorously treat the radiation power loss. Such a treatment would require solution of the conservation equations for the atomic energy level populations and the equation of radiative transfer simultaneously with the governing equations of this study. Since the inherent computational difficulties are prohibitive, an approximation to the radiative loss term is made. It is assumed that all electrons recombining radiatively with an ion would, after recombination to an upper level, radiatively decay to the ground state. Likewise it is assumed that any electron recombining with an

ion collisionally would continue to de-excite collisionally to the ground state. If such is the case, the energy radiated for each radiative recombination would equal the ionization potential plus the mean electron thermal energy $(I_p + \frac{3}{2} kT_e)$. Therefore, the radiative emission rate would be equal to the product of the radiative recombination rate and $(I_p + \frac{3}{2} kT_e)$ plus whatever energy is released due to Bremmstrahlung.

The radiative recombination coefficient, though it can be accurately calculated for atomic hydrogen, is not strictly appropriate for use in the calculations of this study. In the calculation of this property from atomic theory, it is assumed that the presence of other modes (collisional) of recombination and excitation have no effect on the radiative recombination coefficient. This assumption is good for plasma afterglows and atmospheric radiation studies because of the very low pressures involved, but in an atmospheric pressure arc the collisional modes of recombination and excitation are dominant. This means that, when a radiative recombination takes place to an energy level other than the ground level, the probability of an electron colliding with that excited atom and re-ionizing or de-exciting it is significant. This is especially true in hydrogen since the ionization energy for atoms in the upper energy levels is roughly equal to the mean electron kinetic energy. Therefore, the effect on the radiative recombination coefficient

of having a collisionally dominant gas is to reduce it by some factor less than unity. Comparing the radiative emission rate predicted by the above model, in the equilibrium limit, with the results of Yos [21], indicates that this multiplicative factor is roughly 0.4 for hydrogen. Therefore, in this study, the low pressure radiative recombination coefficient given by Allen [15] is corrected for high pressure collisional interactions by the factor 0.4.

Looking again to Figure 4-13 in conjunction with Figure 4-12, the equilibrium radiative flux at 50 amps exceeds the nonequilibrium flux by 35% but at 200 amps the discrepancy is reduced to about 4%. The reason for the rather large discrepancy at 50 amps is evident in Figure 4-5 where the equilibrium and nonequilibrium temperature profiles are plotted. The equilibrium core temperatures far exceed those at nonequilibrium. Since the radiative flux is a sensitive function of temperature, it is expected that at low currents the equilibrium model will overpredict radiative flux. Discussion of the equilibrium and nonequilibrium temperature comparisons has been given previously in this section. Although for argon the equilibrium and nonequilibrium radiative flux fractions do not agree well, the nonequilibrium predictions agree very well with available experimental argon data. The difference in the argon and hydrogen radiative flux fractions is discussed in the following section.

4.3 Parametric Study

There are three critical parameters which have been varied in order to examine the phenomenological behavior of a hydrogen cascade arc. They are: current, pressure and tube radius. The heavy particle temperature at the wall has been fixed at 1000°K for all results presented. Other variables which have been considered are the reflection coefficients for electrons (β) and ions (χ), which are allowed to vary from a maximum of 0.99 to a minimum of 0.0 (or somewhat higher depending on the stability of the numerical scheme). Because the influence of the reflection coefficients on the flow profiles and the integrated quantities (E, heat flux, etc.) are relatively minor, they are not considered to be important parameters.

Results typical of those obtained for the influence of the reflection coefficients are shown in Figures 4-6 and 4-7 for the case of I = 200 amps, P = 1 atm and R = 0.005 meters. These results illustrate the electron temperature and number density profiles for values of β and χ equal to 0.99 and 0.20. Notice that β and χ influence the profiles only in the region very close to the wall. As the reflection coefficients decrease, more electron-ion pairs are combined into atoms at the wall (Figure 4-7), and it is therefore not surprising to note a decrease in electron number density at the wall. Due to the fact that the heavy particle temperature profile is virtually unaffected by β and χ, the heavy particle heat
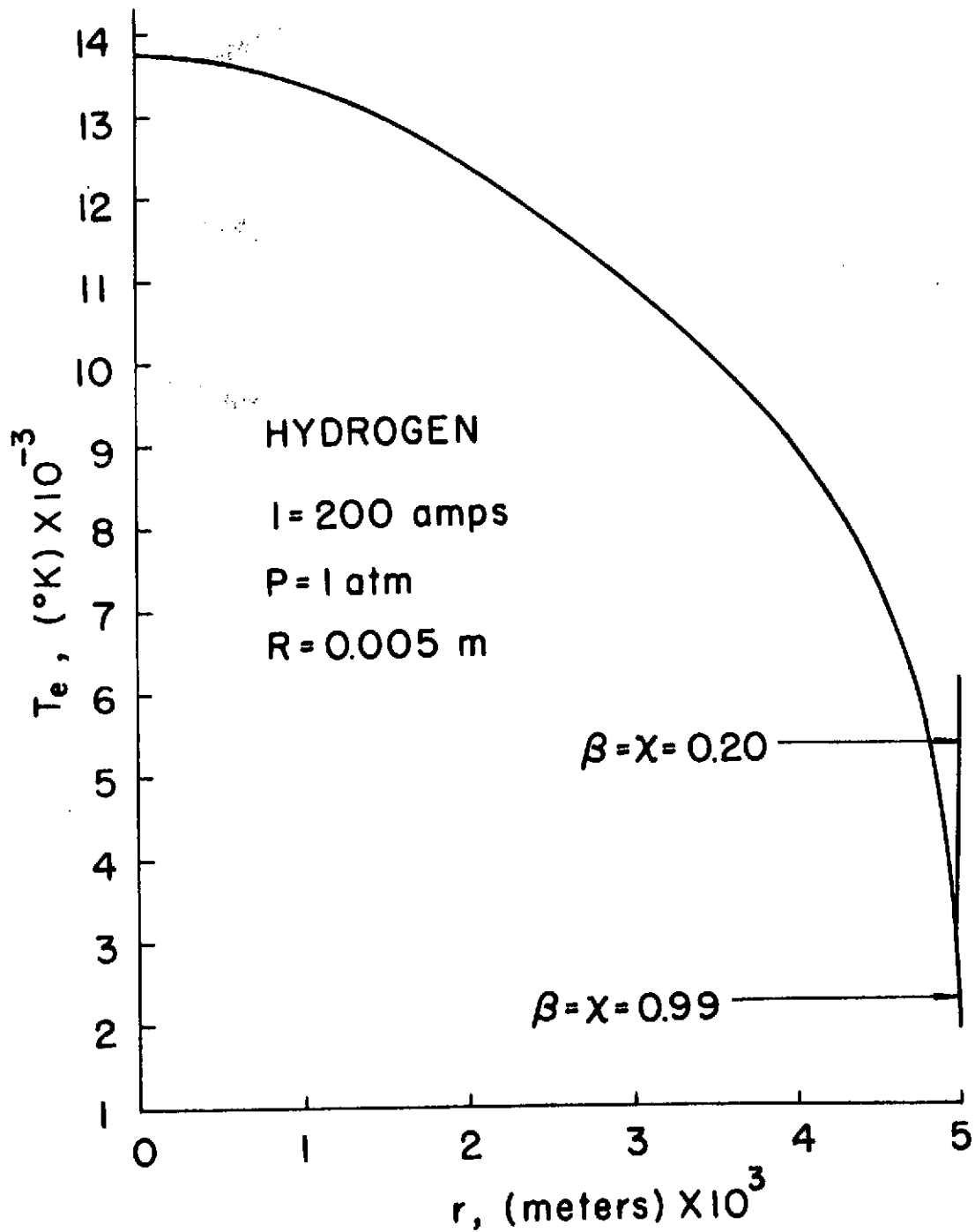
Figure 4-6. Illustration of Electron Temperature Profile
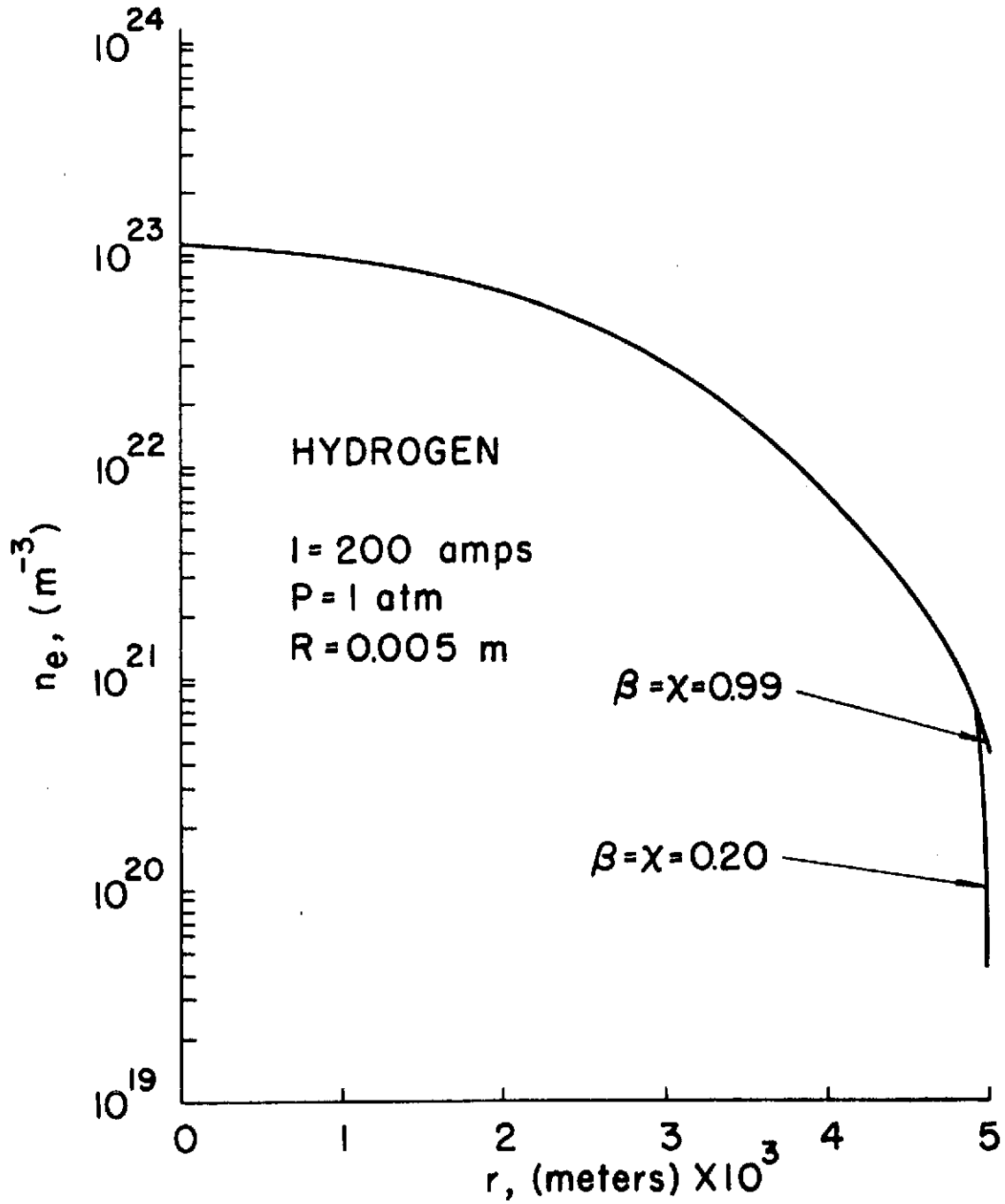Variation as a Function of the Reflection
Coefficients.

Figure 4-7. Illustration of Electron Number Density Profile Variation as a Function of the Reflection Coefficients.

conduction varies by only 1% between the two conditions shown. Since the radiation level is essentially determined by the high temperatures in the arc core, it too is independent of β and χ. In contrast, electron heat conduction and diffusion effects are directly related to sheath parameters and are therefore relatively sensitive to the reflection coefficients. However, these terms have been shown to be insignificant in the present study since, for all operating conditions, their sum accounts for less than 2% of the total energy balance and, on the average, for less than 0.5%. Finally, it has also been shown that the electric field intensity, and therefore the total power input, is also virtually independent of the values of β and χ. Due to their comparative unimportance, the reflection coefficients have therefore been fixed at 0.99 for all further calculations.

The parametric studies are now discussed in three parts. These pertain to consideration of the current, the pressure, and the tube radius as independent variables. The temperature and electron number density profiles calculated for a pressure of 1 atm and a radius of 0.005 meters are shown in Figures 4-8 and 4-9 for arc currents of 50, 100, 150 and 200 amps. In Figure 4-8, the upper curve of each pair originating from the same centerline temperature is the electron temperature and the lower curve is the heavy particle temperature. The electron wall temperature varies from 1260°K for
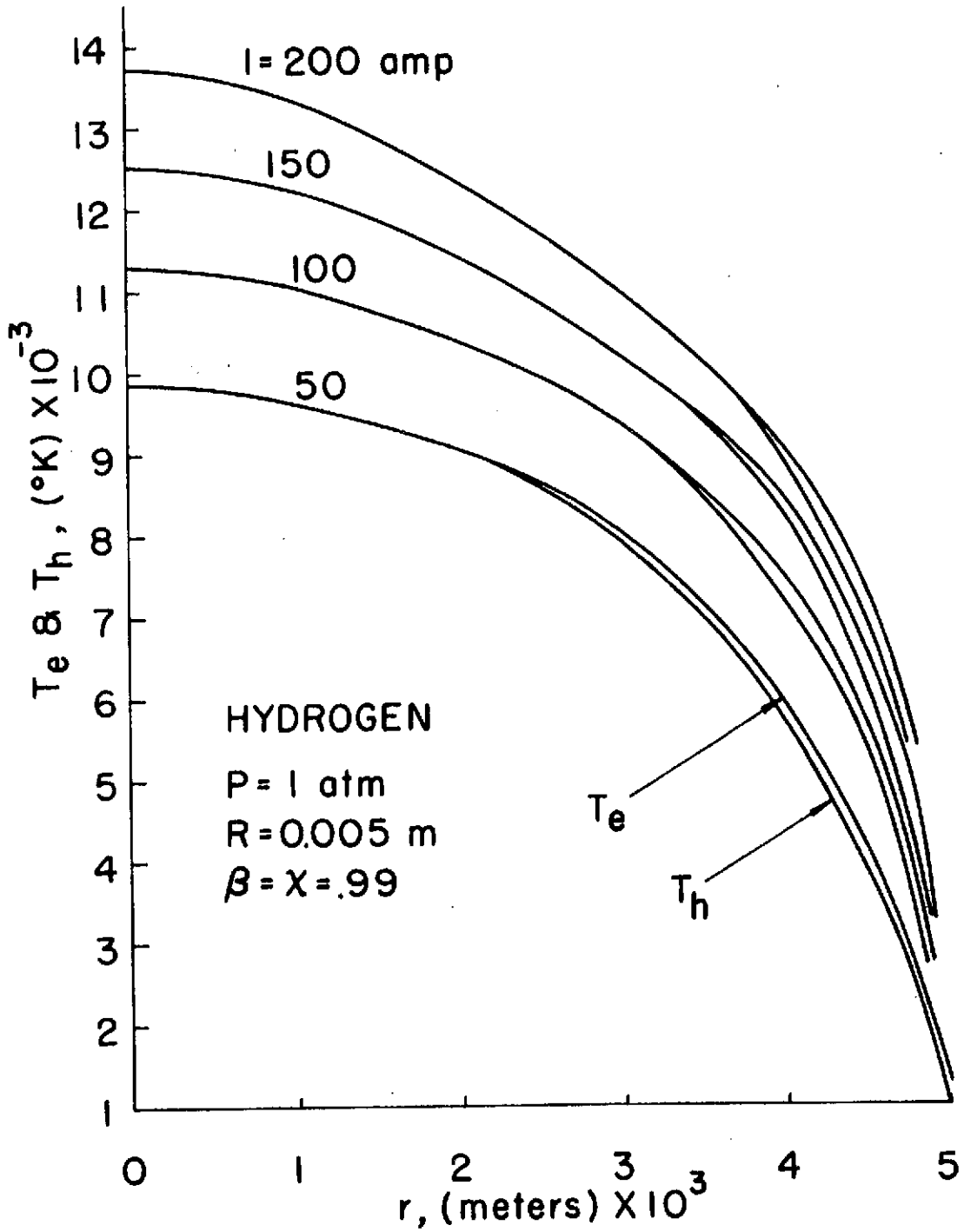
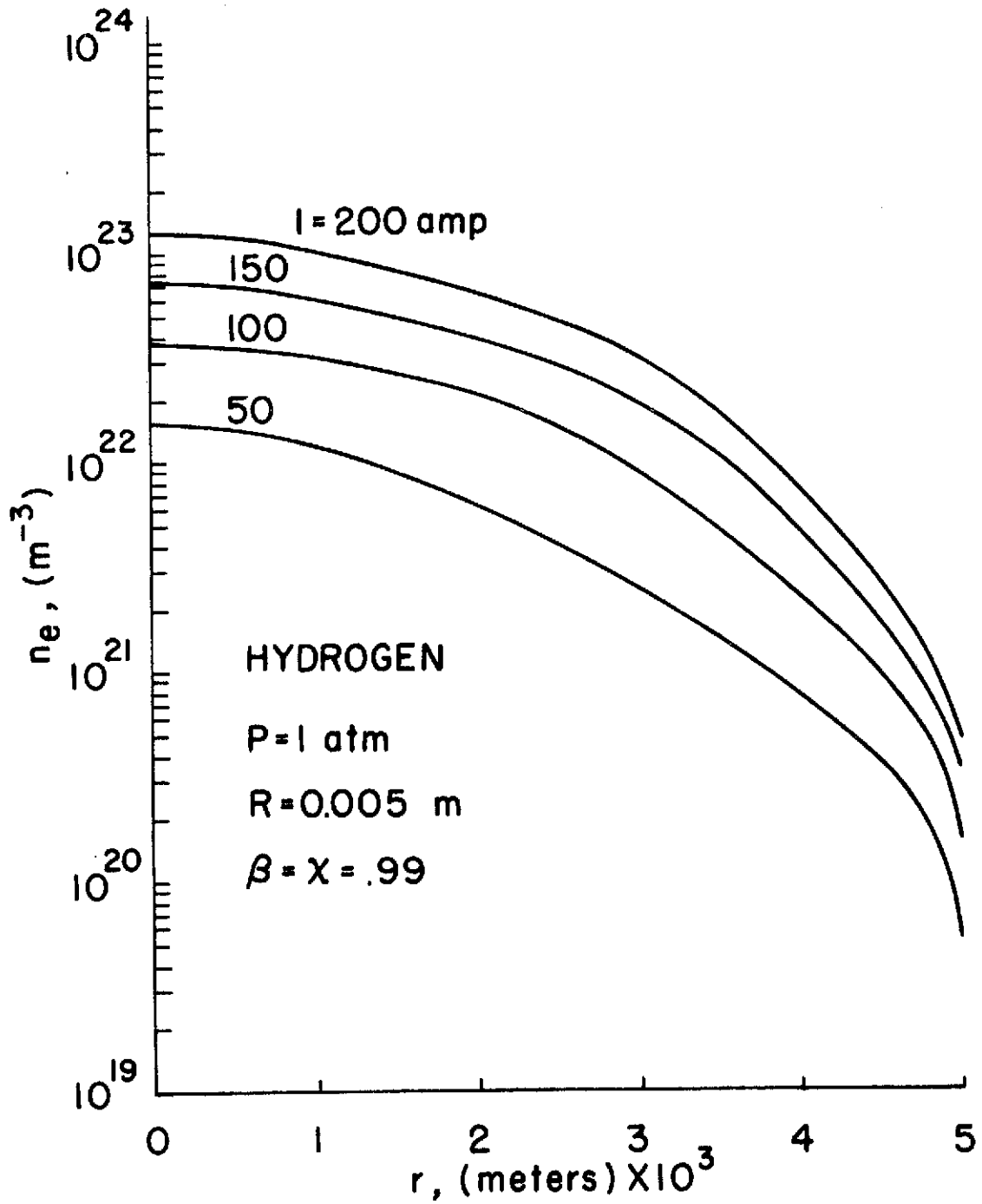Figure 4-8. Electron and Heavy Particle Temperature Versus Current at P = 1 atm and R = .005 m.

Figure 4-9. Electron Number Density Versus Current at
P = 1 atm and R = 0.005 m.

I = 50 amps to 1930°K for I = 200 amps. The figures reflect
typical arc behavior. As the operating current increases,
there is an increase in temperature due to the increased
energy input. Also, due to increased temperature, there is
a corresponding increase in electron number density. One
interesting aspect of Figure 4-8 is that there is little
difference between the electron and heavy particle tempera-
ture profiles for all currents, indicating that for these
conditions thermal equilibrium is closely approached. In
fact, for all solutions which were obtained, the thermal
nonequilibrium effect is minor compared with chemical non-
equilibrium. As mentioned in Chapter 2, the degree of
thermal nonequilibrium in a gas is dependent upon, among
other things, the atomic weight of the gas. That is, lighter
gases exchange kinetic energy with electrons more efficiently
than heavier gases. It is therefore not surprising to note
that, for a heavier gas such as argon, Clark [9] reports a
high degree of thermal nonequilibrium with electron wall
temperatures "freezing" at values between 6000 and 8000°K.

Figure 4-10 illustrates the nature of the chemical
nonequilibrium condition for currents of 50 and 200 amps.
The solid lines represent the computed nonequilibrium elec-
tron number density, and the solid lines with circles are
the electron density calculated from the Saha equation at
the electron temperature. Severe chemical nonequilibrium
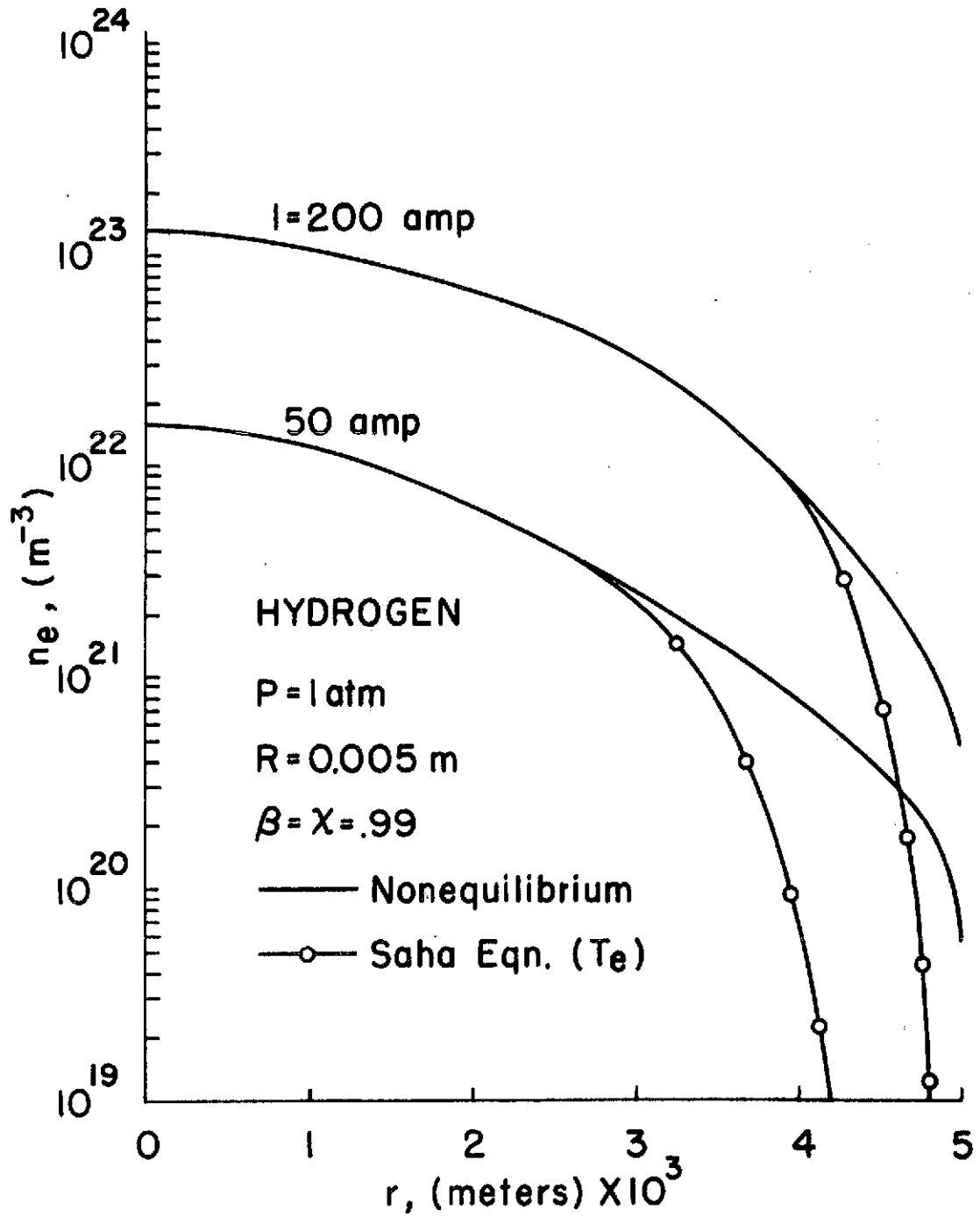in the wall region is evident in all results of this study.

Figure 4-10. Illustration of Current Dependence of Chemical Nonequilibrium.

The nonequilibrium is induced by the ambipolar diffusion of electron-ion pairs. In the wall region the net flux of electrons to a differential element increases above the rate at which electron recombination occurs. The net effect is the elevation of the electron concentrations in the arc periphery above the values which would exist under equilibrium conditions. Note in Figure 4-10 that the radial location which marks the onset of chemical nonequilibrium increases with increasing current. This is because, at a given radial location, increasing the current increases both the electron temperature and concentration, which in turn increases the rate of the equilibrium restoration processes (in this case collisional and radiative recombination).

In the computer program, the electric field is calculated through numerical integration of Equation (3-4). Figure 4-11 displays the influence of arc current on the electric field intensity of the hydrogen cascade arc. It is interesting to note that both equilibrium and nonequilibrium models predict a local minimum of the electric field. For the non-equilibrium curve, the minimum occurs near 130 amps. The existence of this minimum may be explained by considering the electric field to be equal to the current divided by the over-all conductivity of the arc column, as in a solid conducting rod. An increase in current results in an increased degree of ionization and, therefore, an increase in the conductivity of the arc column. At lower currents, a small
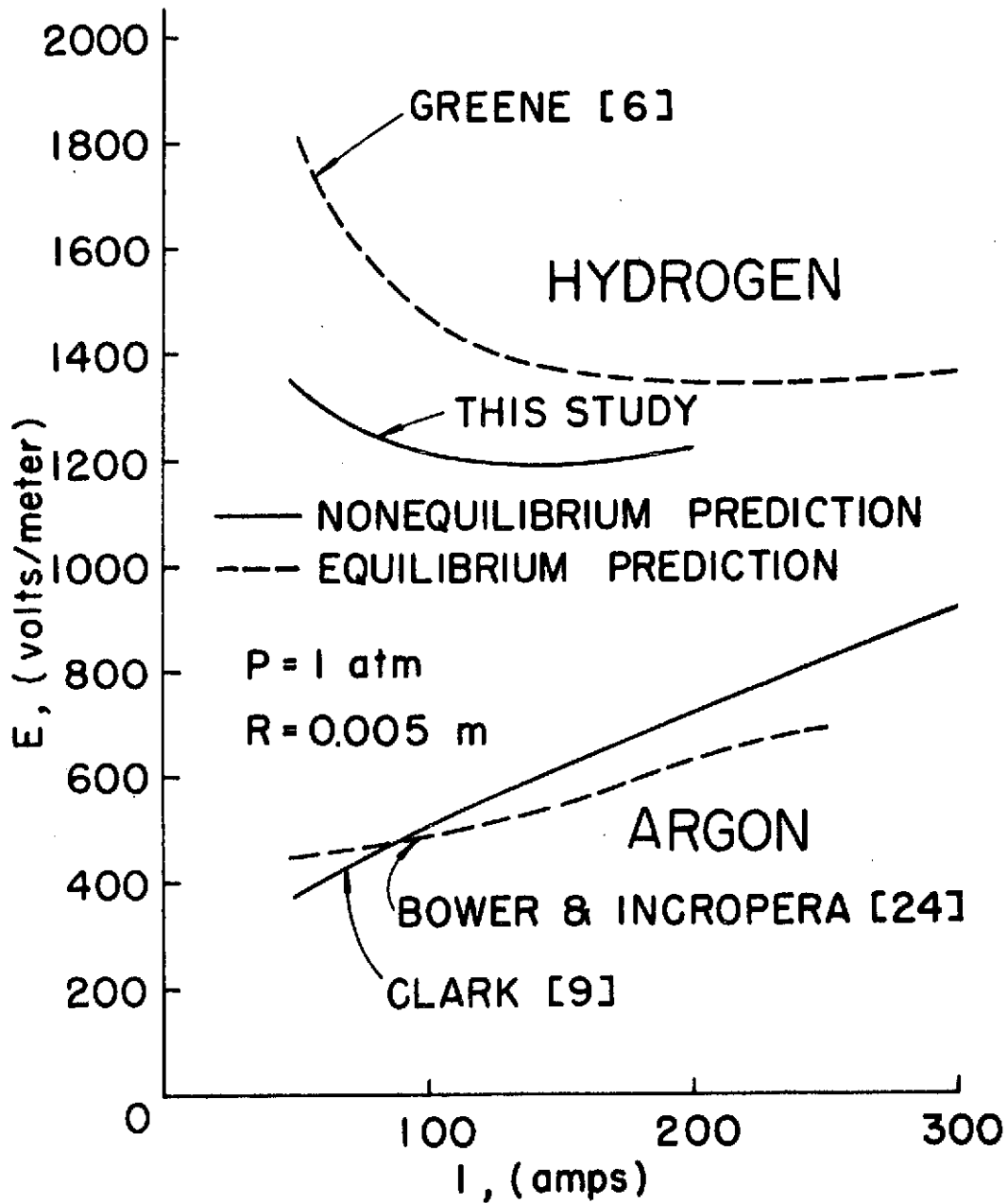
Figure 4-11. Equilibrium and Nonequilibrium Calculations of Electric Field-Current Characteristic in Hydrogen and Argon.

increase in current results in a large enough increase in
the degree of ionization, and hence the conductivity, to
provide for a decrease in the electric field intensity. At
higher currents, the degree of ionization is less responsive
to a current increase and any increase in current increases
the electric field intensity. As mentioned in Section 4.2,
the reason for the discrepancy in the equilibrium and non-
equilibrium predictions of electric field intensity is due
to the inability of the equilibrium model to accurately
calculate the electrical conductivity outside the core
region.

The reason for the hydrogen electric field intensity
exceeding that for argon is due to the fact that because of
its greater atomic mass (hence, less efficient transfer of
elastic energy from electrons to heavy particles), the elec-
tron concentration and temperature of argon far exceed that
for hydrogen outside the core. Therefore, the integral of
the electrical conductivity is greater and the electric
field lower in argon.

Before discussing the heat transfer properties of the
hydrogen arc, it is important to understand how the heat
fluxes are computed. In Section 2.2.3 reference was made
to the method of calculating the electron wall heat conduc-
tion by consideration of the electrostatic sheath. Without
derivation, the equations used in calculating the electron
wall heat conduction are

$$(\Gamma_{H+})_w = .25 \; n_{e_w} \; \overline{c_{H_w}} \qquad\qquad (4\text{-}1)$$

$$f_{e_w} = \frac{J_w}{e(1-\beta)} + \frac{(1-\chi)}{(1-\beta)} \; (f_{H+})_w \qquad\qquad (4\text{-}2)$$

$$|\phi_w| = - \frac{kT_{e_w}}{e} \; \ln\left[\frac{4f_{e_w}}{n_{e_w} \; \overline{c_{e_w}}}\right] \qquad\qquad (4\text{-}3)$$

$$(q_{r_e})_w = f_{e_w}\left[kT_{e_w} \; \frac{5\beta-1}{2} + (1-\beta)e|\phi_w| - \frac{3}{2} \; kT_{h_w}\beta\right] \qquad (4\text{-}4)$$

where f_{H+_w} and f_{e_w} are the ion and electron wall fluxes, $\overline{c_{H_w}}$ and $\overline{c_{e_w}}$ are the ion and electron thermal speeds, J_w is the wall current (zero in this study), ϕ_w is the electrostatic wall potential and e is electronic charge. In addition, the wall ambipolar diffusion velocity is:

$$V_{amb_w} = \frac{f_{e_w}}{n_{e_w}} \; (1 - \beta) \qquad\qquad (4\text{-}5)$$

Equation (4-4) is used to obtain electron wall heat conduction. For atomic hydrogen, the summation over diffusion velocities in the heavy particle energy equation (2-9) reduces to zero. The heavy particle energy equation, when multiplied by the radial coordinate and integrated from centerline to wall, then yields, for the heavy particle heat conduction,

$$(q_{r_h})_w = - \frac{1}{R} \int_0^R r \; S_{ec} \; dr \qquad\qquad (4\text{-}6)$$

The remaining heat flux quantities are obtained from the electron energy equation (2-8). Expressing this equation in terms of electron temperature and number density, multiplying by the radial coordinate, and integrating, the equation becomes

$$\frac{5}{2} kR(n_e T_e V_{amb})_w = - R(q_{r_e})_w + \frac{EI}{2\pi} + \int_0^R rS_{ec}dr + \int_0^R rS_{ic}^e dr$$

$$(4-7)$$

The term S_{ic}^e can be rewritten as the sum of a radiation and a three body collision term. When this is done, the three body collision term simply becomes the product of the ionization potential and the electron creation rate, $I_p \dot{n}_e$. Making these substitutions and dividing Equation (4-7) by R gives

$$\frac{5}{2} k(n_e T_e V_{amb})_w = - (q_{r_e})_w + \frac{EI}{2\pi R} - (q_{r_h})_w - \frac{1}{R} \int_0^R r \, Rad \, dr$$

$$- \frac{1}{R} \int_0^R rI_p \dot{n}_e dr \qquad (4-8)$$

Finally, recognizing that the last term of Equation (4-8) is simply the product of I_p and the integral of the electron continuity equation (2-7), the energy equation may be rewritten as

$$\frac{EI}{2\pi R} = (q_{r_e})_w + (q_{r_h})_w + \frac{5}{2} k(n_e T_e V_{amb})_w + \frac{1}{R} \int_0^R r \, Rad \, dr$$

$$+ I_p(n_e V_{amb})_w \qquad (4-9)$$

The left-hand side of Equation (4-9) is then the total power input to the gas and the right-hand side contains the various energy loss terms. The first and second terms of the right-hand side are the electron and heavy particle heat conductions calculated by Equations (4-4) and (4-6). The third term is the flux of electron kinetic energy to the wall due to ambipolar diffusion, and the fourth term is the radiation heat flux to the wall. Note that, since the cascade arc is assumed to be an infinitely long cylinder and the gas is assumed to be optically thin, the energy radiated per unit length of tube by the gas is equal to the radiation energy absorbed per unit length by the tube wall. The fifth term is the product of the ionization potential and the ambipolar electron flux at the wall and is therefore equivalent to the diffusion of ionization energy to the wall. The third and fifth terms are calculated with the aid of Equation (4-5) and the fourth term by numerical integration. In all of the calculations of this study, the combined electron heat conduction and diffusion terms accounted for less than 2% of the total energy loss. Due to their minor influence on total wall heat transfer, the values of these terms are not plotted in succeeding graphs. It cannot be said, however, that ambipolar diffusion, electron heat conduction and the diffusion of ionization energy within the arc do not have a very important influence on the temperatures and densities and hence, indirectly upon the radiation, heavy particle conduction and total power input, of the hydrogen arc.

The very nature of the asymptotic region is such that
the total power input is equal to the heat transfer to the
wall. Therefore the total wall heat flux is given by the
term on the left-hand side of Equation (4-9) and is shown
plotted in Figure 4-12. The reason, then, for the hydrogen
heat flux exceeding that for argon is the higher electric
field of argon. The higher electric field for argon was
explained earlier in this section as being due to the higher
electron concentrations and temperatures outside the core
region. The wall heat flux is primarily composed of radia-
tion and heavy particle conduction.

The percentage radiative heat flux is shown in Figure
4-13. The percentage of heavy particle conduction is approx-
imately 100% minus the percentage radiation. Figure 4-13
demonstrates that at lower currents, heat transfer from the
arc is almost completely due to heavy particle conduction.
However, at higher currents radiation assumes part of the
burden of transferring heat from the gas. Due to the much
higher electron concentration and temperature outside the
core in argon, the radiative recombination rate (which is
proportional to n_e^2) is higher and a larger portion of the
argon arc will be radiating significantly. Hence, the radia-
tion percentage is higher for argon than for hydrogen.

Figures 4-14 and 4-15 reveal the effect of arc pressure
on the electron temperature and concentration profiles. In
Figure 4-14, the electron and heavy particle temperatures

Figure 4-12. Equilibrium and Nonequilibrium Calculations of Total Wall Heat Flux as a Function of Current in Hydrogen and Argon.
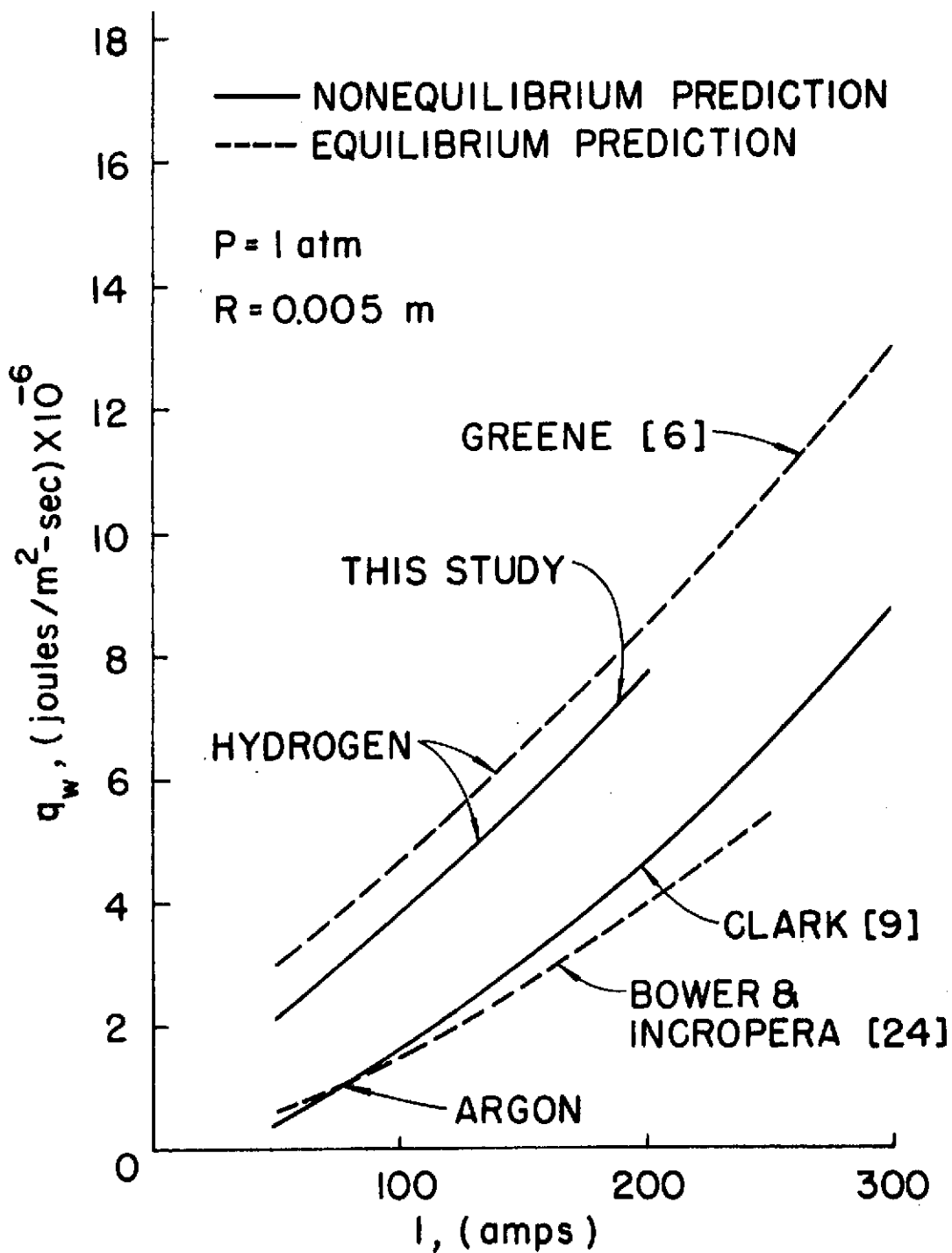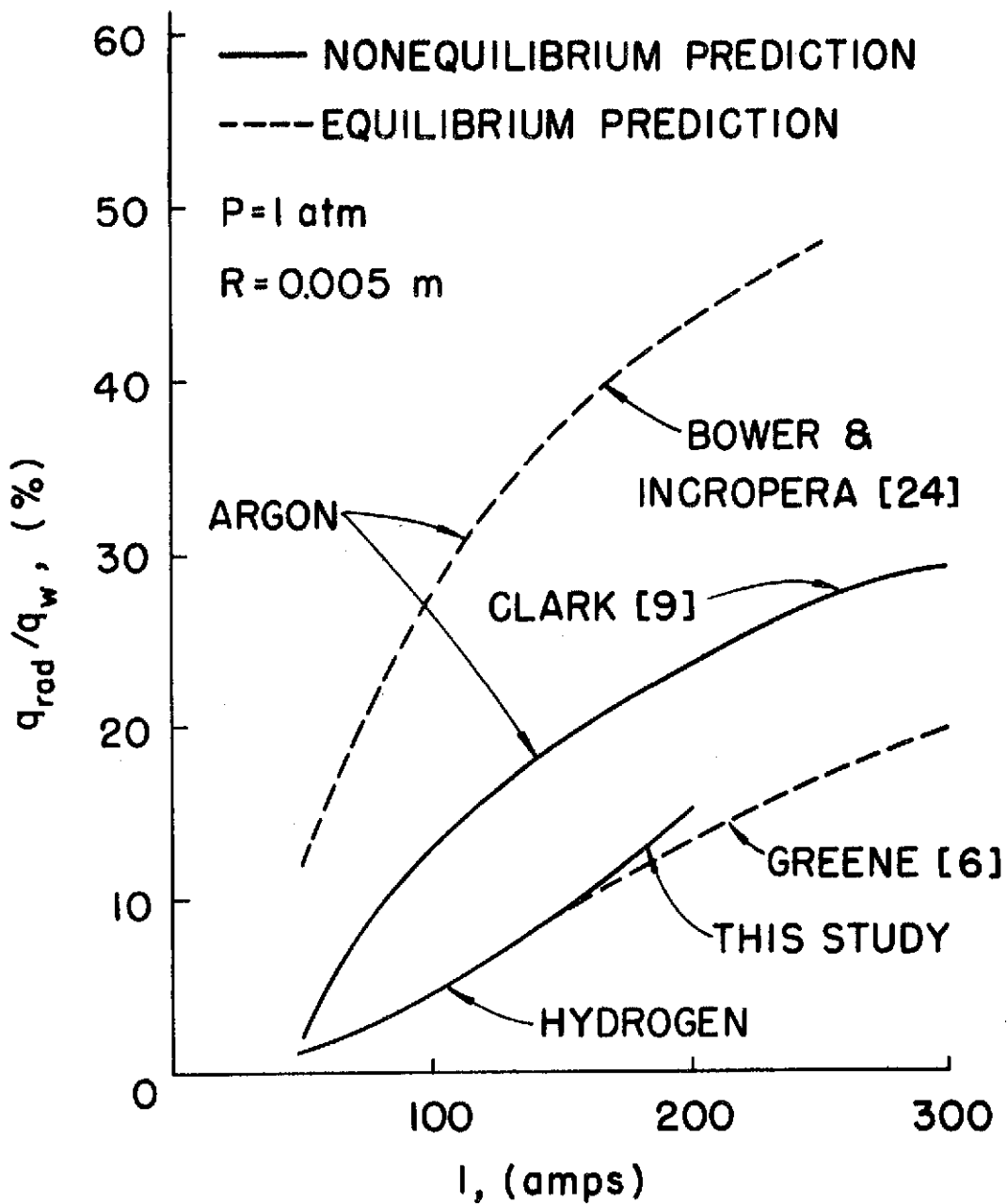
Figure 4-13. Equilibrium and Nonequilibrium Calculations of Radiative Wall Heat Flux Fraction as a Function of Current in Hydrogen and Argon.
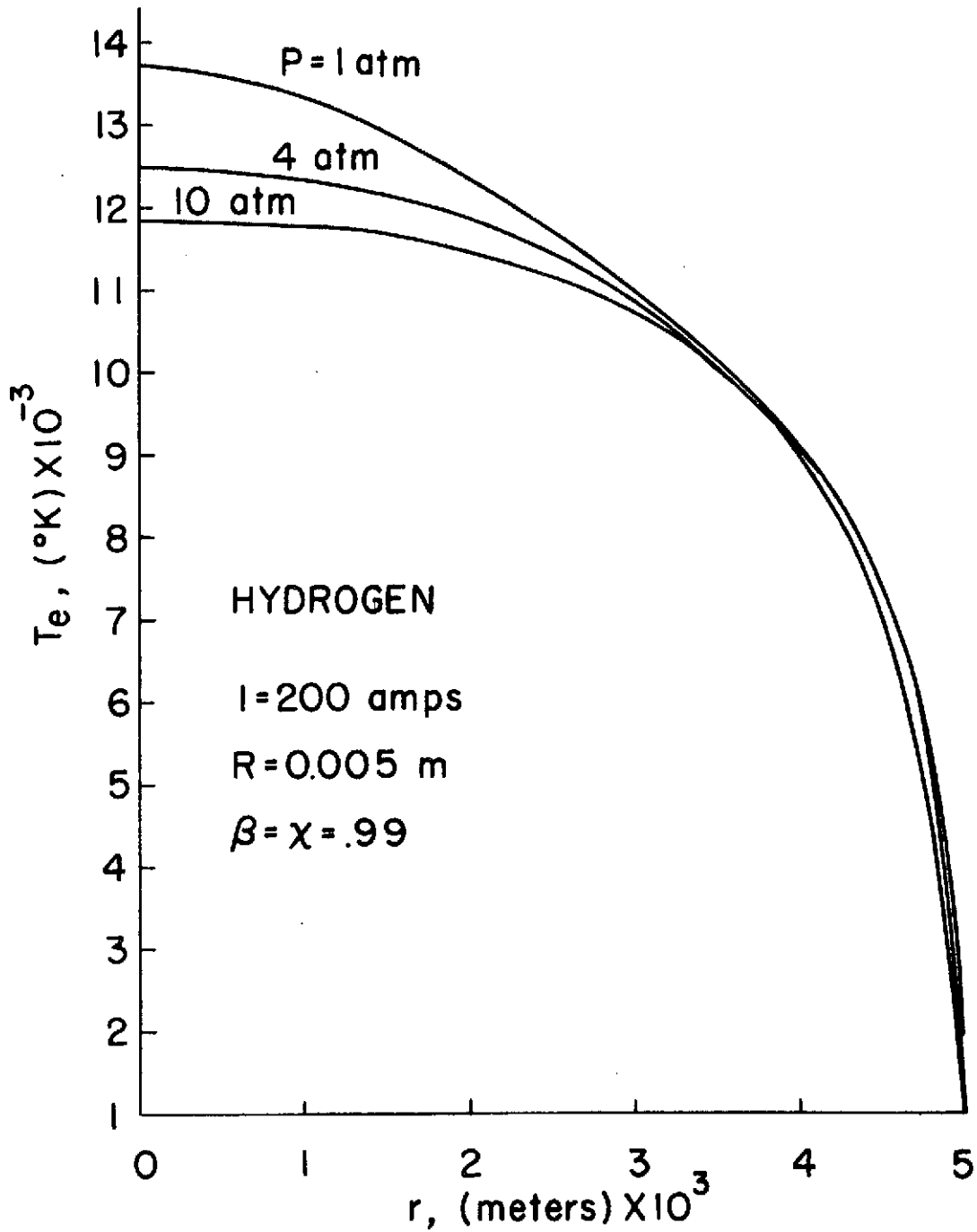
Figure 4-14.   Electron Temperature Profiles Versus Pressure
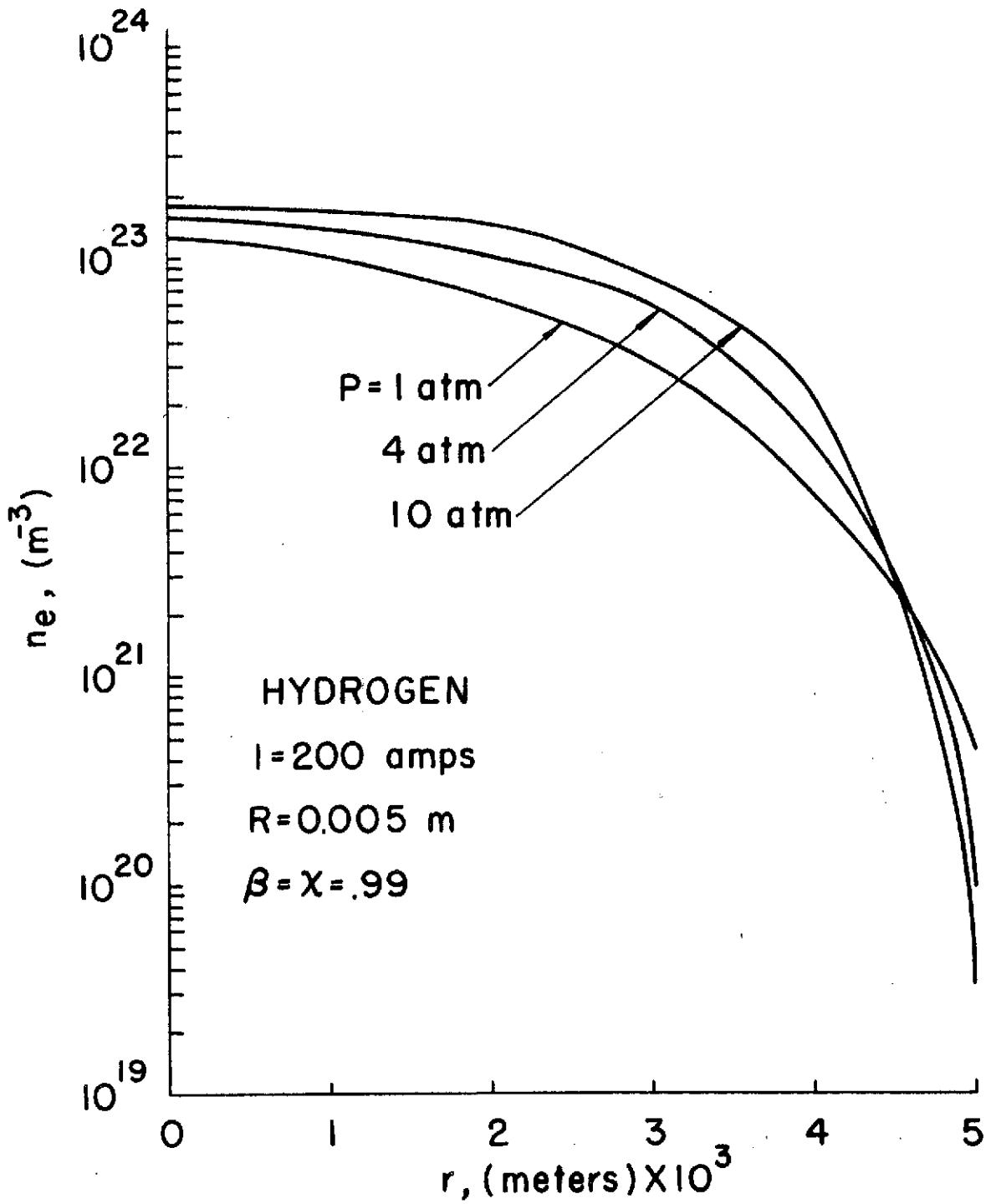at I = 200 amps and R = 0.005 m.

Figure 4-15. Electron Number Density Versus Pressure at
I = 200 amps and R = 0.005 m.

are close enough to be indistinguishable, hence only T_e is plotted. The electron wall temperature varies from 1930°K for P = 1 atm to 1032°K for P = 10 atm. The decrease in centerline temperature with increasing pressure is best explained by referring to Figure 4-19. Through this range of pressure, the radiation flux increases from 15% at 1 atm to about 55% at 10 atm. This increase of radiation transfer from the arc core causes the reduction in temperature shown in Figure 4-14. Also, as pressure rises, electron-heavy particle collision rates increase resulting in a stronger tendency toward equilibrium and thus the decrease of wall electron temperature and wall number density. The increase in electron number density in the core with pressure is a result of the increasing atom number density and subsequent ionization rate. Figure 4-16 illustrates the nature of the chemical nonequilibrium dependence on pressure. The increase of electron-heavy particle collision rates with pressure suppresses chemical nonequilibrium for a greater distance from the centerline.

Both Clark's results and those of the present study show an increase in electric field intensity with pressure as shown in Figure 4-17. Since the current is fixed, this implies a decrease in the integrated electrical conductivity with pressure. Hence, the positive influence of increasing electron number density on the electrical conductivity is not as strong as the negative influence of increased elastic collision rates (see Equation (C-2)).
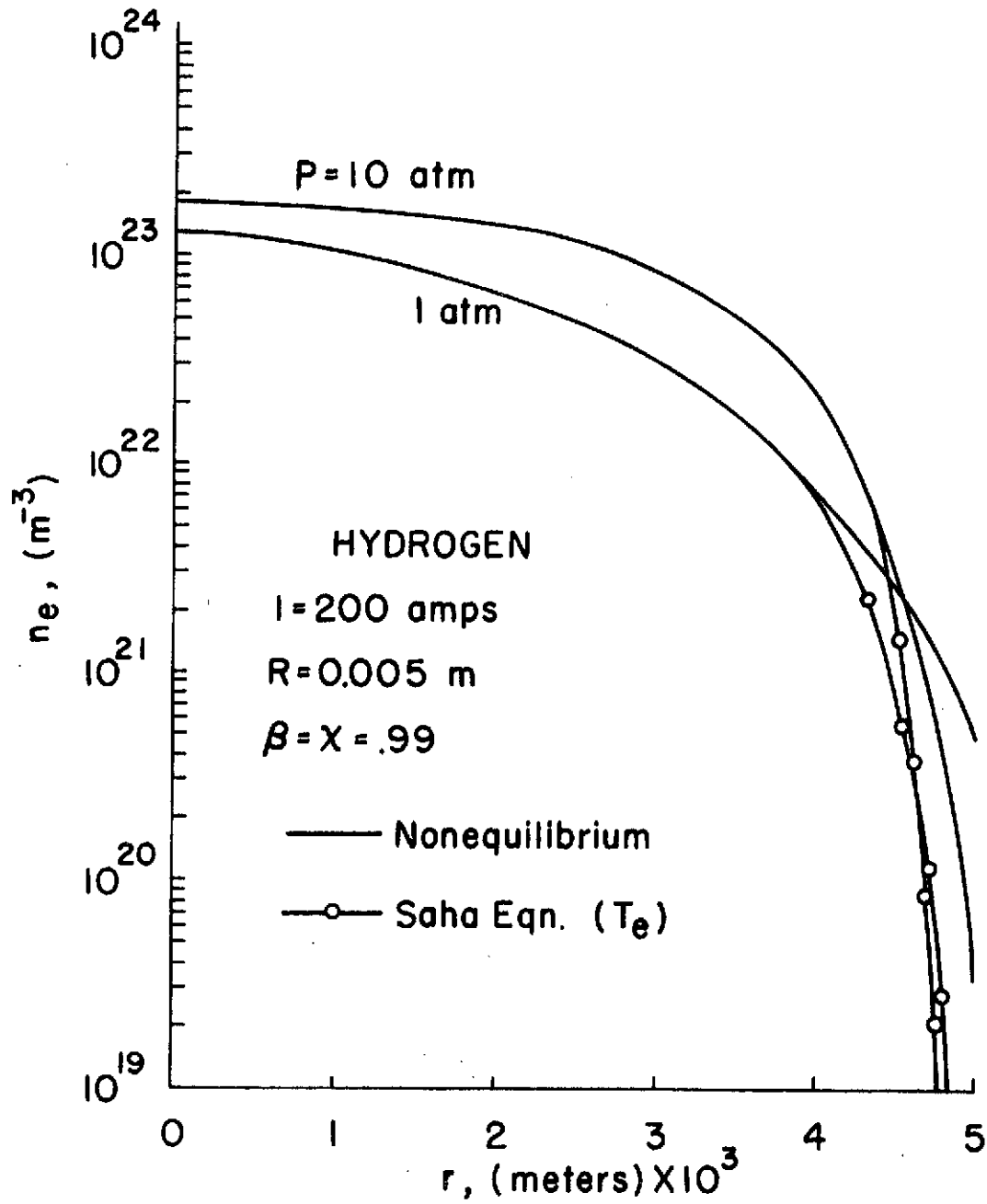
Figure 4-16.   Illustration of Pressure Dependence of Chemical
Nonequilibrium.
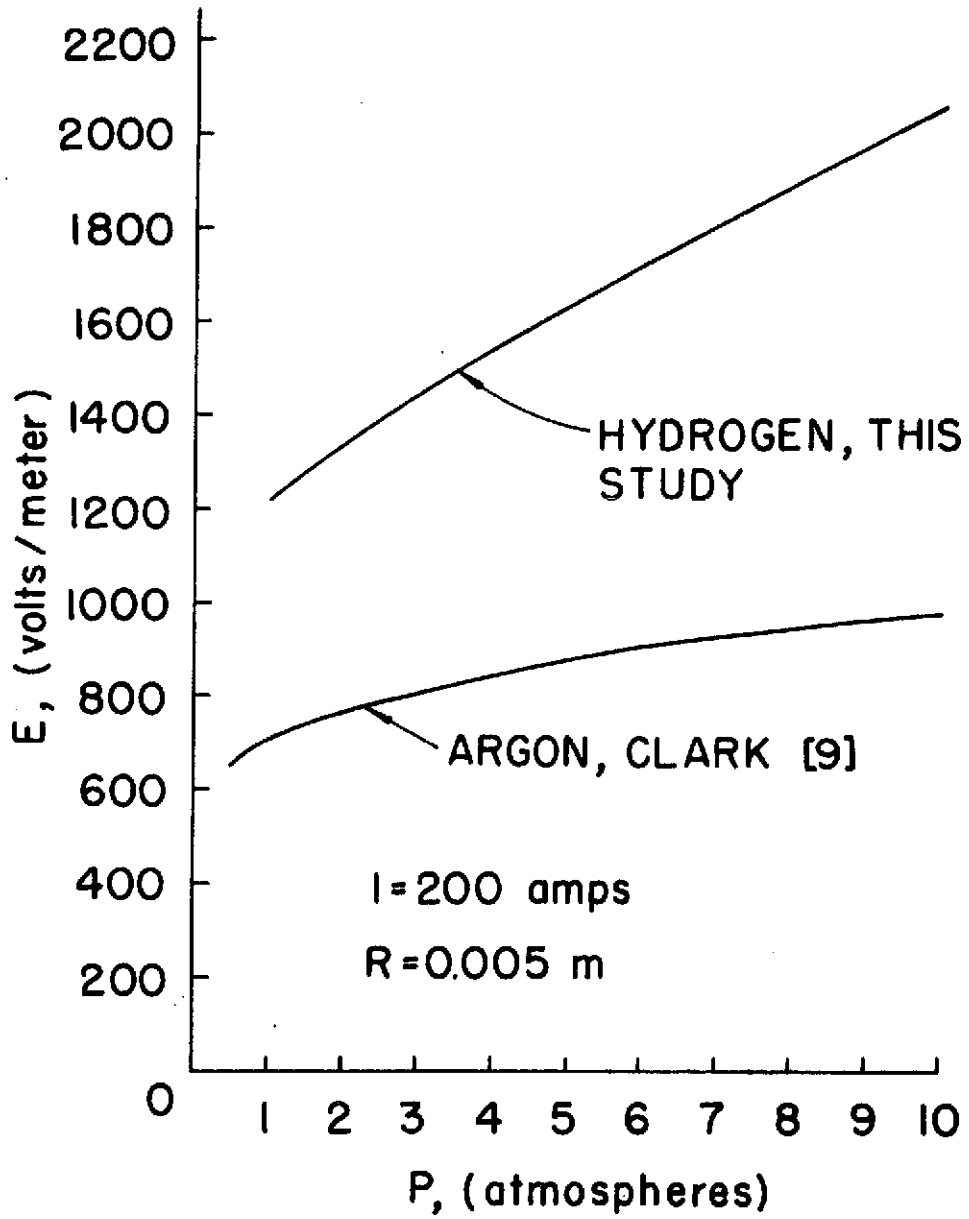
Figure 4-17. Nonequilibrium Electric Field Intensity as a
Function of Pressure for Hydrogen and Argon.

Figure 4-18 illustrates the dependence of total wall heat flux on pressure both for hydrogen and argon. Since the Ohmic dissipation and the heat output must balance in the asymptotic region, an increase in the field intensity, and hence in power input, results in increased wall heat flux for fixed arc current. A substantial portion of the increase in wall heat flux with pressure can be attributed to the increase in radiative emission, as indicated by Figure 4-19. The increased number densities associated with higher pressure increase the radiative recombination rate and hence the radiative emission.

Figures 4-20 and 4-21 depict the effect of tube radius on the temperature and electron number density profiles. The decrease in temperature and electron density with increasing radius is due to an accompanying decrease in the energy input per unit area as the radius is increased. For the 0.005 m radius profile the electron wall temperature is 1930°K, and for the radius of 0.05 m it decreases to 1014°K. Also as the tube radius is increased, the electron and heavy particle temperatures become essentially equal indicating that thermal equilibrium is established. This is due to the sharp reduction in the strength of those processes which promote thermal nonequilibrium, particularly the selective transmission of energy to the electrons by the electric field, with increasing radius.

Figure 4-18. Nonequilibrium Total Wall Heat Flux as a
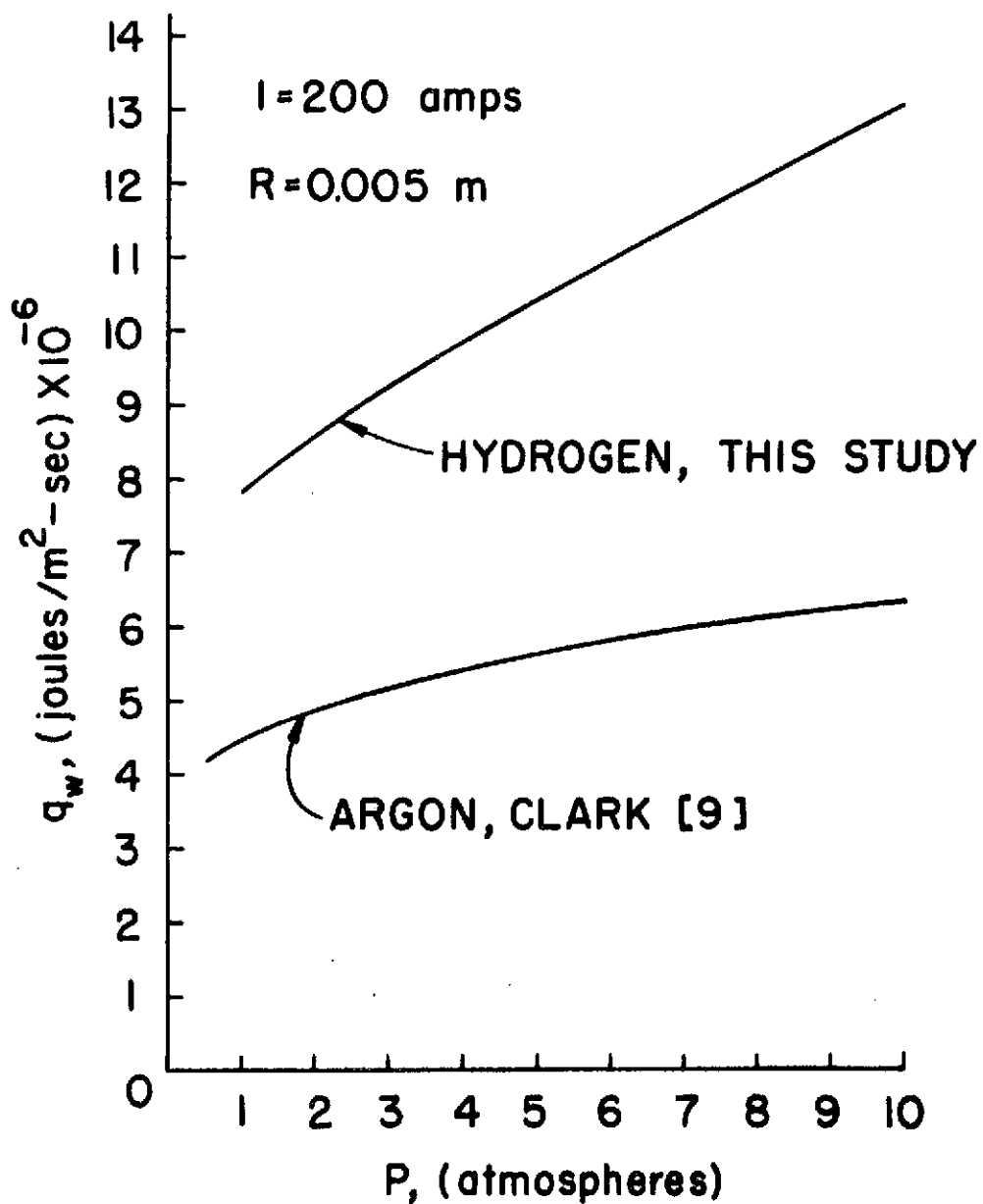Function of Pressure for Hydrogen and Argon.

104
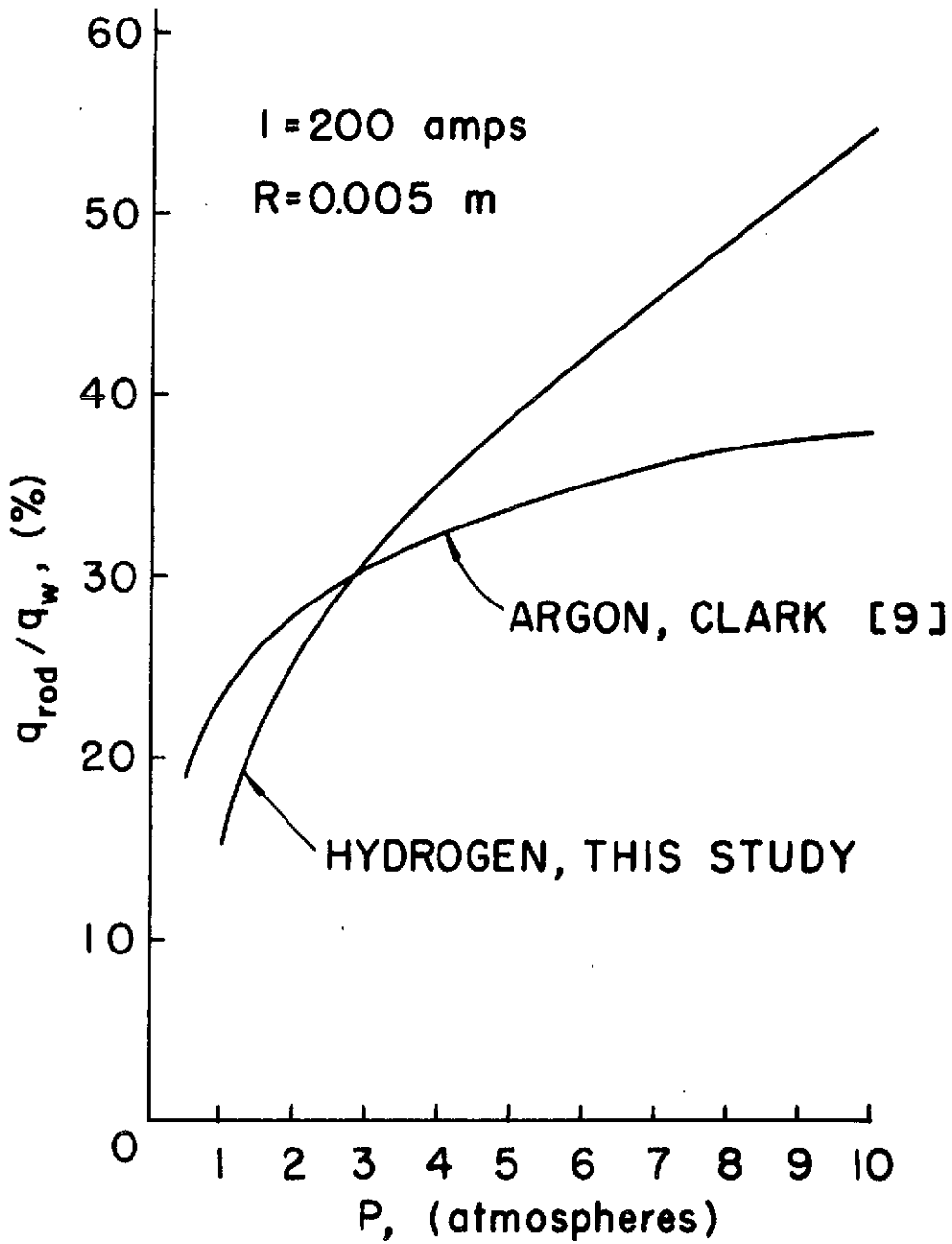
Figure 4-19. Nonequilibrium Radiative Wall Heat Flux Fraction
as a Function of Pressure for Hydrogen and Argon.
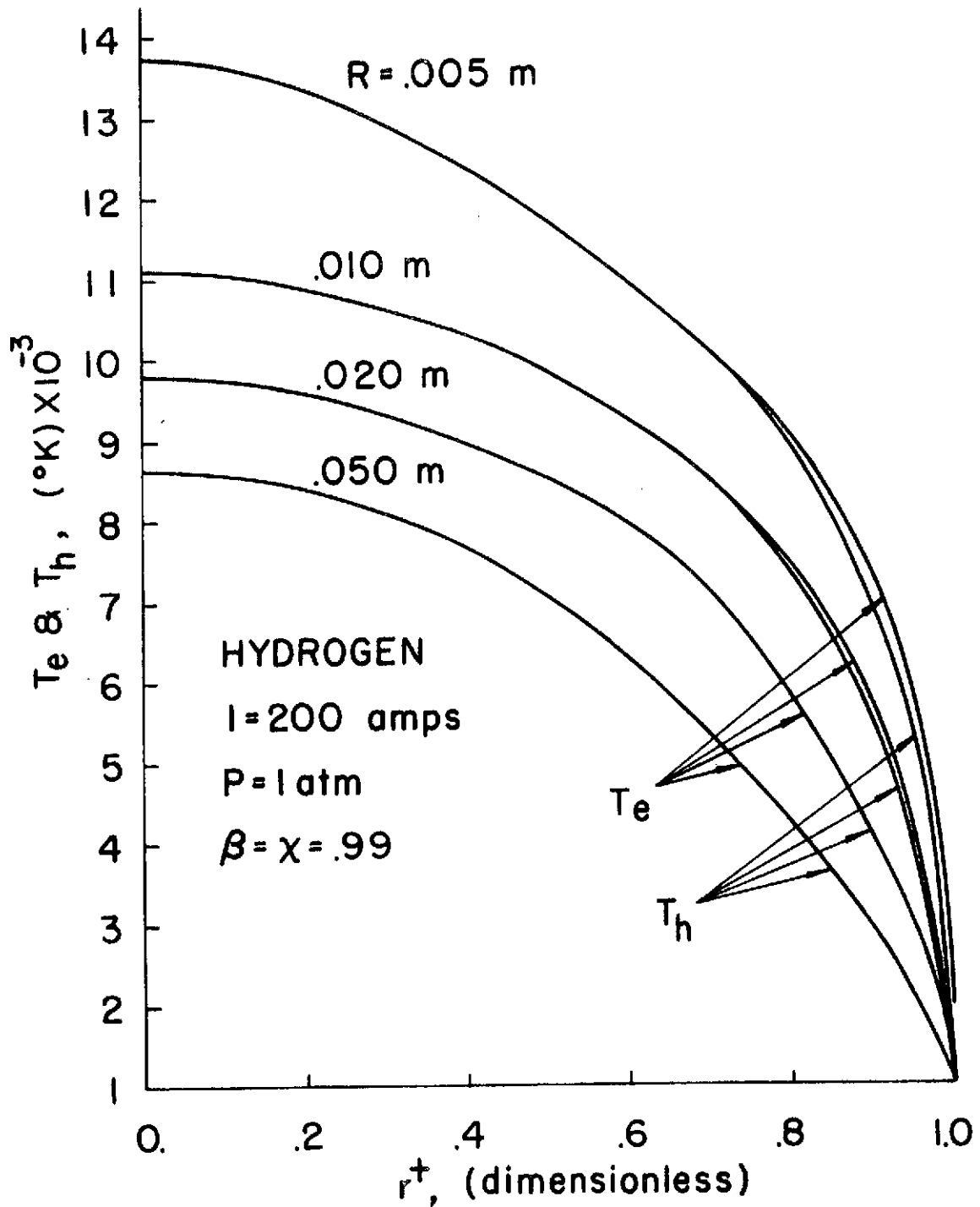
Figure 4-20.   Electron and Heavy Particle Temperature Versus
Tube Radius at I = 200 amps and P = 1 atm.
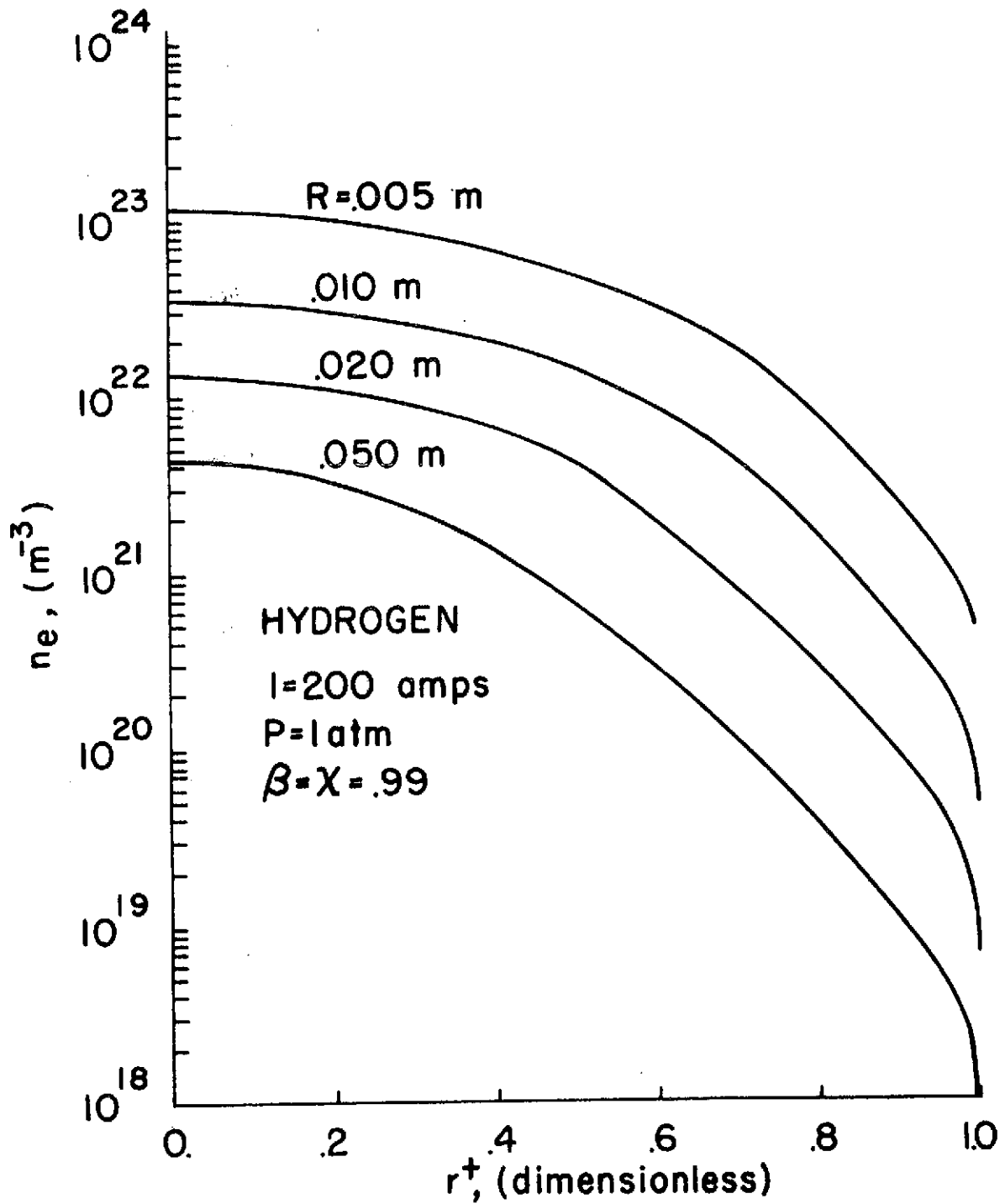
Figure 4-21.   Electron Number Density Versus Tube Radius at
                I = 200 amps and P = 1 atm.

The nature of the chemical nonequilibrium condition is shown in Figure 4-22 for radii of 0.005 and 0.05 meters. Departure from the chemical equilibrium condition occurs nearer to the centerline as the radius increases. This is due to the sharp reduction in the local ionization and recombination rates (the principal mechanisms for maintaining chemical equilibrium) that occurs with increasing radius.

The variation of the electric field intensity with tube radius is indicated in Figure 4-23. There are two major opposing processes which influence the field intensity as the tube radius is increased. With the current held fixed, the electric field is inversely proportional to the integrated conductivity of the arc cross section. As the radius increases, the higher cross-sectional area of the gaseous conductor serves to increase this integrated conductance. However, the attendant decrease in the temperature and electron density which causes the electrical conductivity to decrease, serves to lower the conductance. From Figure 4-23, it is apparent that the increasing cross-sectional area effect is dominant, causing the electric field to decrease with radius.

The total wall heat transfer per unit length of tube is plotted in Figure 4-24 and reflects the trend of the electric field intensity shown in Figure 4-23, since the total heat transfer is the product of the current and the electric field. These same trends are predicted by Clark [9] for argon.
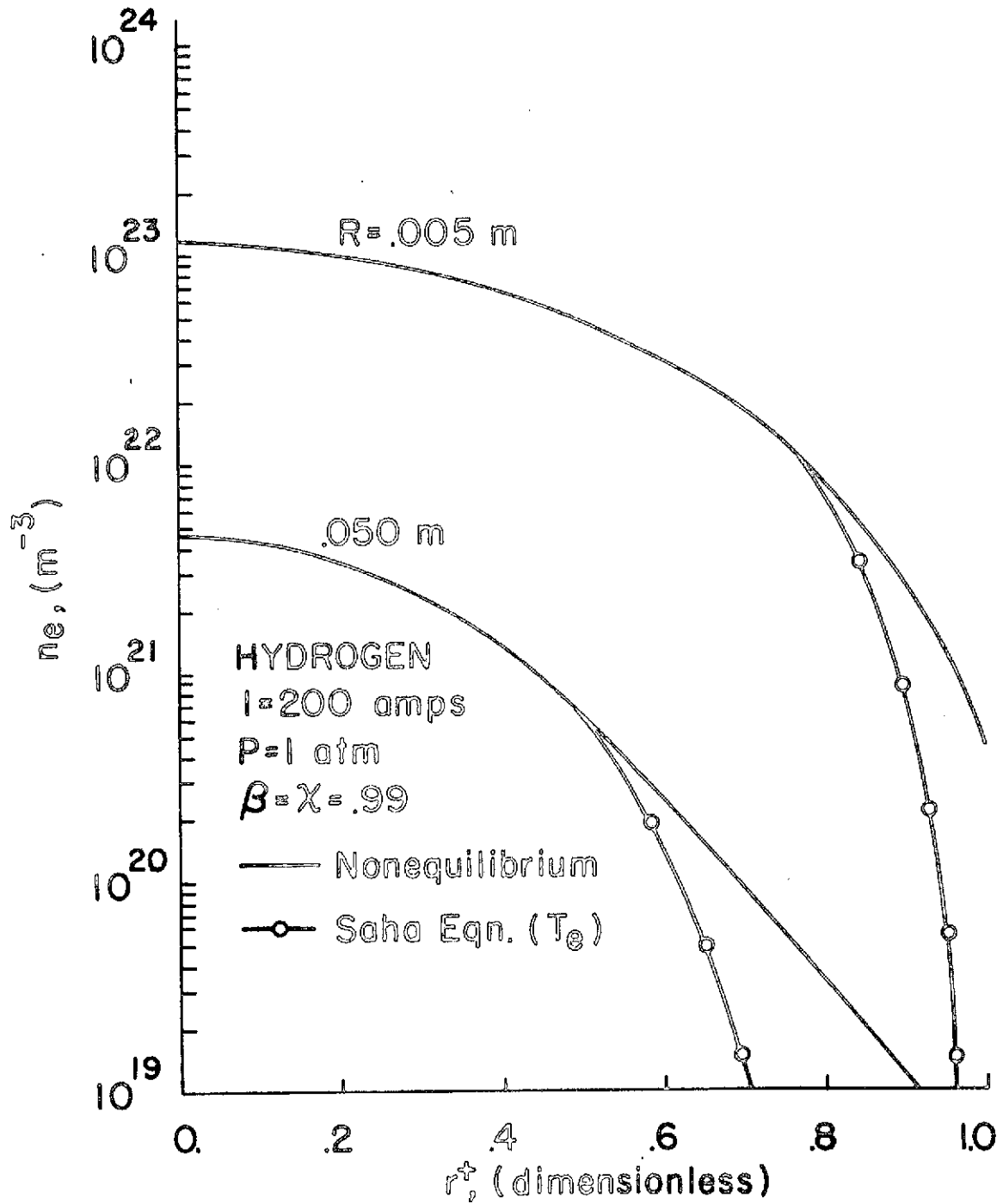
Figure 4-22.   Illustration of Tube Radius Dependence of
Chemical Nonequilibrium.
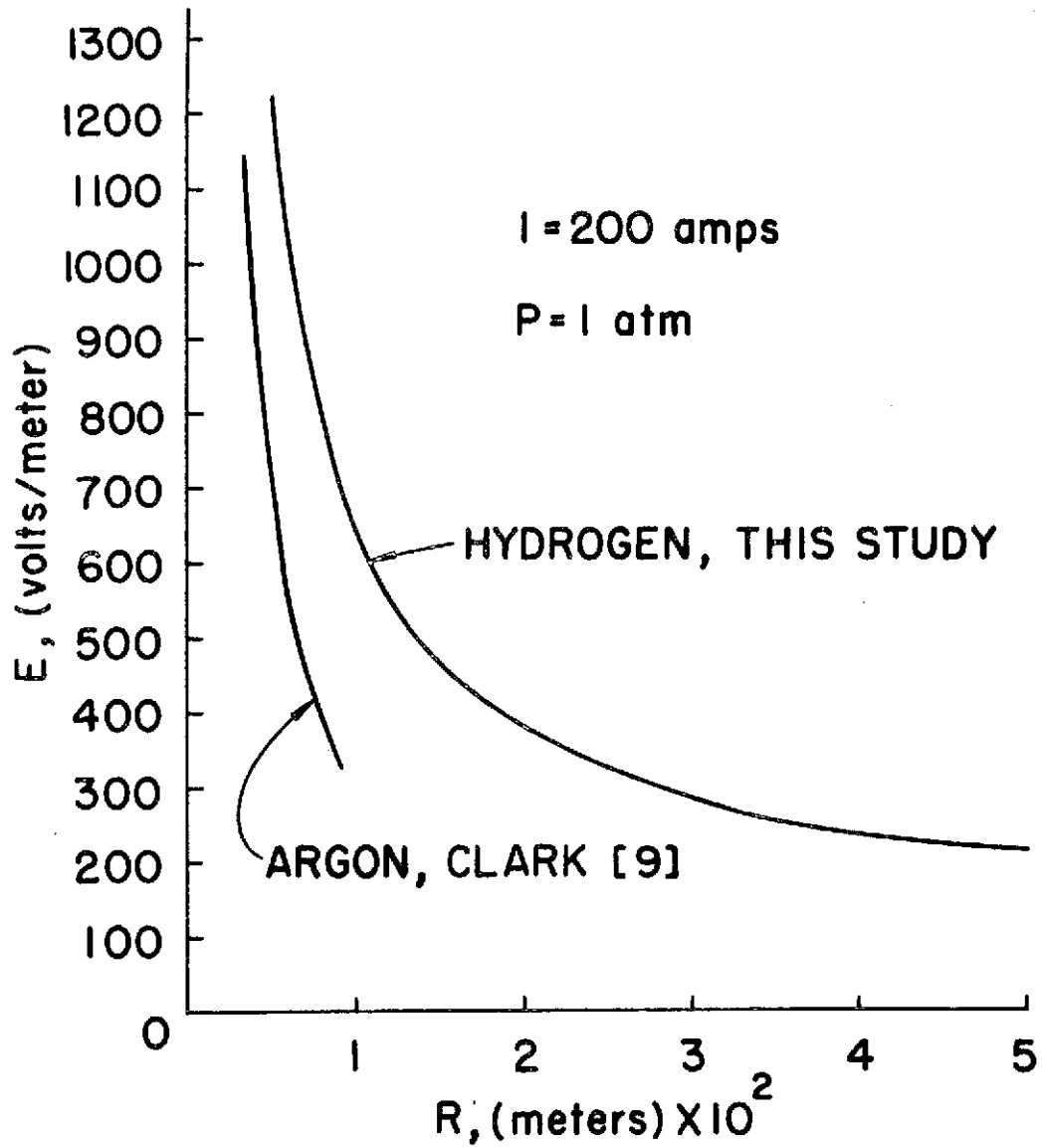
Figure 4-23. Nonequilibrium Electric Field Intensity as a Function of Tube Radius for Hydrogen and Argon.
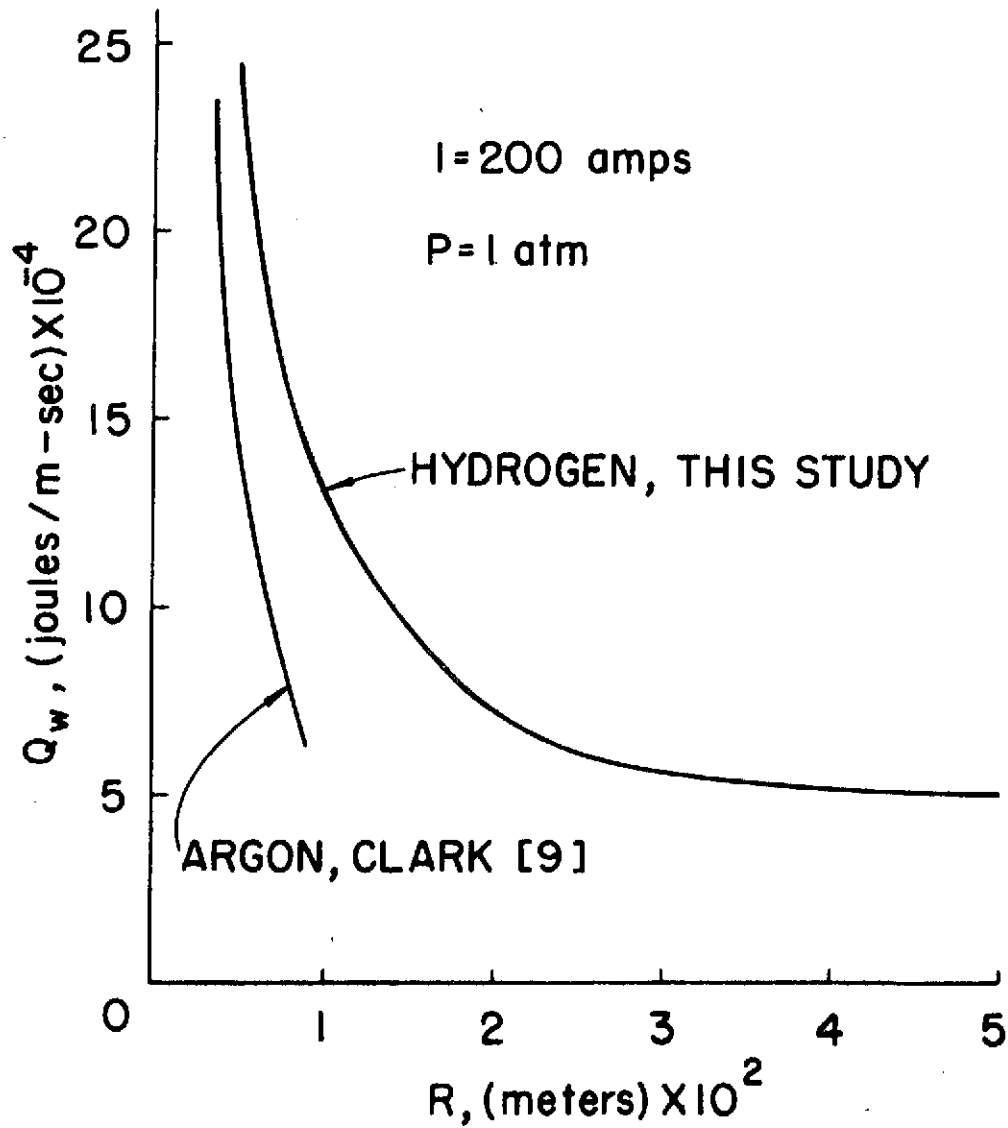
Figure 4-24. Nonequilibrium Total Wall Heat Rate per Unit Length as a Function of Tube Radius for Hydrogen and Argon.
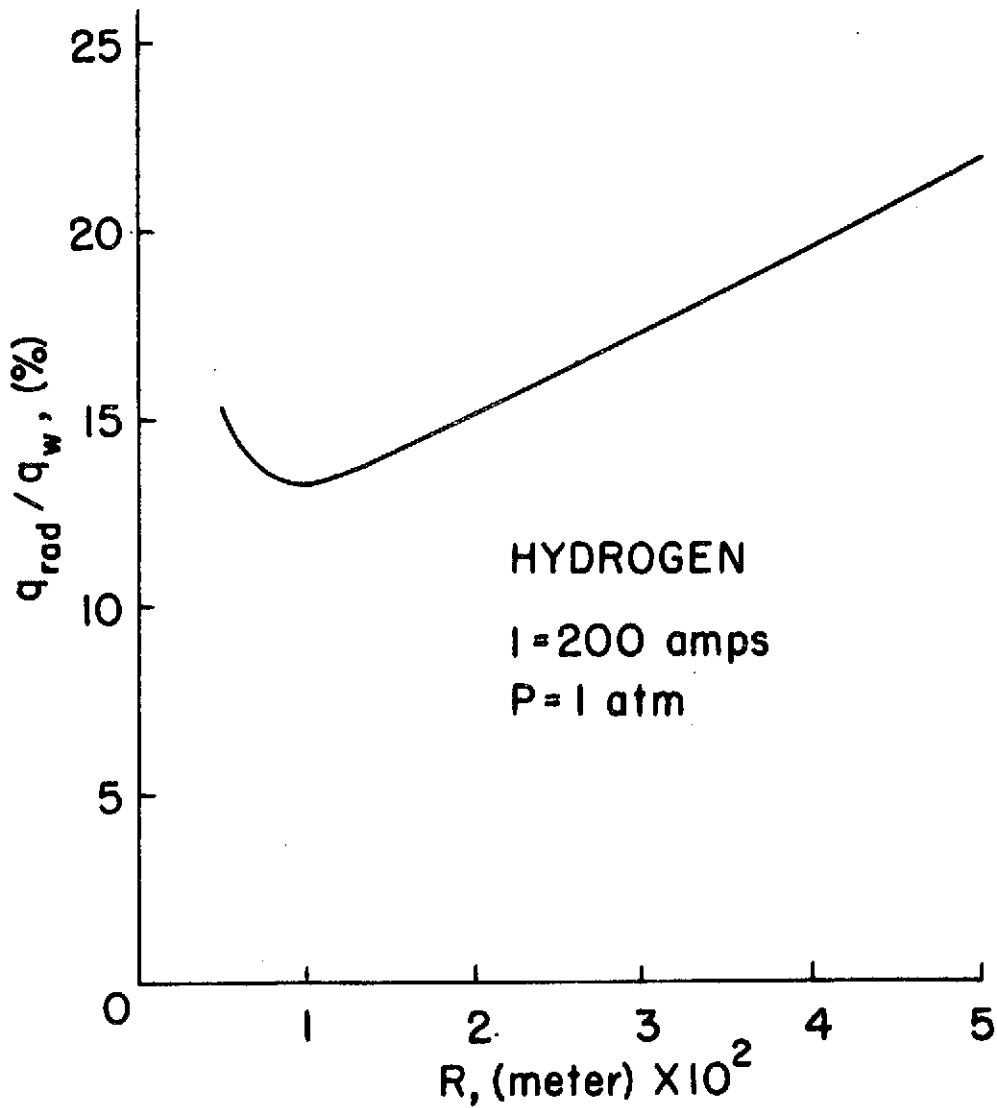
Figure 4-25.   Nonequilibrium Radiative Wall Heat Flux
Fraction as a Function of Tube Radius for
Hydrogen.

112

The percentage of radiation heat flux is plotted in
Figure 4-25, and the results reflect several opposing
phenomena. As radius increases, the electron and heavy
particle temperatures decrease, thus diminishing the radia-
tion emission per unit volume from the arc core. In contrast,
the increase in the volume of the core region and the decrease
in the total heat transfer serve to increase the percentage
of radiation flux with radius. From Figure 4-25 it is
apparent that the first phenomenon is dominant at lower radii,
but one or both of the other two dominate at larger radii.
However, neither of the magnitudes of the radiative heat flux
or radiative heat transfer per unit tube length exhibit a
minimum but decrease monotonically as the radius increases.

4.4 Uncertainty Calculations

It has been noted at various points that it is necessary
to use approximate theories and methods to obtain certain
properties required by the mathematical model. The use of
approximate theories is necessary due to the lack of accurate
data regarding transport coefficients for nonequilibrium
gases and because of the complexity of a rigorous treatment
of the radiation processes in a real gas. Therefore, it has
been necessary to utilize a mean free path theory (Appendices
A, B, C and D) to obtain the transport coefficients and an
approximate model for treating radiative emission (Section
4.2). It is therefore important to perturb these properties
in order to estimate the over-all uncertainty of the predictions.

This was done by rerunning computer solutions for which pertinent coefficients and properties were altered and comparing the results with those previously discussed.

The three-body recombination coefficient and the inverse ionization coefficient were divided by a factor of two, and a solution was obtained for $I = 200$ amps, $P = 1$ atm and $R = .005$ m. The factor of two is representative of the discrepancies between existing recombination data. Although atomic properties can be calculated rather accurately for hydrogen, they are usually determined by considering only one process at a time (e.g. radiative recombination exclusive of collisional modes of recombination). Therefore, even though the individual properties may be accurate, they are not necessarily additive.

With the ionization and three-body recombination coefficients reduced by a factor of two, the temperatures and electron densities in the core were found to be virtually unaffected, due to the presence of chemical equilibrium in this region. However, the electron temperature and density increased somewhat in the wall region. Also, the electric field and heat fluxes were essentially unchanged by this rather large perturbation. The conclusion then is that uncertainties in the ionization and three-body recombination coefficients do not introduce significant errors in the mathematical model.

As discussed in Section 4.2, the radiation model used is rather approximate, and to obtain agreement with accurate calculations in the equilibrium limit, it was necessary to multiply results by a factor of 0.4. For the uncertainty calculations it was therefore decided to use the uncorrected value of the recombination coefficient. This procedure resulted in a decrease of 800°K in the two temperatures and a 25% decrease in electron density at the centerline. The electric field and total wall heat flux increased by about 8% and the radiative heat flux increased by 65%. It is therefore obvious that an uncertainty in the radiative recombination coefficient can have a significant effect on the temperature and concentration profiles as well as the radiative flux. However, the effect on the total wall heat flux and the field intensity remains small.

The rate of energy transfer from the electron subgas to the heavy particles due to elastic collisions (S_{ec}) is another property that needs to be investigated in an uncertainty analysis. The value of S_{ec} was divided by 2 and a solution obtained for I = 100 amps, P = 1 atm and R = .005 m. This resulted in a negligible change in temperatures and electron densities in the core of the arc but increased the electron temperature in the wall region by 200 to 300°K. Electron densities near the wall increased on the order of 10%. Changes in the electric field and the total and radiative wall heat flux were negligible. Considering the fact

that an unusually large perturbation factor was used to analyze the uncertainty associated with S_{ec}, it appears that more realistic uncertainties in this property (much less than a factor of 2) have negligible effect on the accuracy of this model.

In the mean free path derivation of the transport coefficients, the calculation of the ambipolar diffusion coefficients is thought to be the most accurate (see Figure A-2). Therefore, uncertainties in the diffusion coefficients are expected to be small, and in the uncertainty analysis the coefficients were divided by a factor of 1.25 for a current of 150 amps and tube radius of .005 m. As a result of this, temperatures in the core increased by about 3% while remaining virtually unchanged in the periphery. Electron concentration increased by 14% at the centerline and decreased by about 10% in the wall region. The electric field and total wall heat flux were essentially unchanged while the radiative flux increased by about 10%. It is therefore felt that uncertainties in the ambipolar diffusion coefficient have a negligible effect on computed results.

The uncertainty associated with errors in the thermal conductivity was determined by multiplying both the electron and heavy particle thermal conductivities by a factor of 1.25, and a solution was obtained at I = 100 amps, P = 1 atm and R = .005 m. The result was a slight decrease in temperature and electron density in the core, less than a 5%

decrease in temperature near the wall, and a rather large (40%) decrease in electron density very near the wall. In terms of bulk parameters, the electric field and total wall heat flux increased by 11% and the radiative flux decreased by 20%. Uncertainties in the thermal conductivities are therefore felt to have a negligible bearing on the results of this study.

Similarly, the electrical conductivity was perturbed by a factor of 1.25, and a solution was obtained for $I = 200$ amps, $P = 1$ atm and $R = .005$ m. This resulted in moderate decreases in temperature (less than 5%) over the arc cross section. However, number densities decreased by about 14% at the centerline and 40% near the wall. The electric field and total heat transfer decreased by about 10% and the radiation flux by 25%.

From the previous considerations, it is evident that representative uncertainties in the transport coefficients and the atomic parameters have, at best, a minor influence on the thermochemical profiles and the over-all arc parameters. The quantity which is most sensitive to the uncertainties is the radiation heat flux, which may be in error by as much as 50%.

4.5 Speculations for the Molecular Hydrogen Arc

The original objective of this study was to mathematically model the molecular, rather than the atomic, hydrogen arc. To do so involves combining the model of this study with a

molecular continuity equation and representations of the
thermodynamic and transport properties which account for the
presence of the molecular species. In fact the molecular
model was derived, and a computer program was developed to
solve the governing equations of the molecular hydrogen arc
in the entrance region. A great deal of time was spent in
devising the computer program, but continued problems with
numerical instabilities precluded obtaining realistic solu-
tions. Therefore, exclusive emphasis was placed on study
of the atomic hydrogen arc.

It is possible to extrapolate the atomic hydrogen arc
behavior to that of the molecular arc by considering the
differences in the properties of the two gases. Note that,
if the entire arc is in thermochemical equilibrium, the
molecular number density in the core will be several orders
of magnitude smaller than that of the electrons or atoms.
Furthermore, close to the wall, the atom number density will
be negligible but the atom diffusion velocities will be large.
From the results of this study, thermochemical equilibrium is
known to exist in the core of the arc for all operating con-
ditions and it is reasonable to assume that this condition
would prevail for the molecular arc. For atomic hydrogen,
it was also found that the large electron number density
gradients near the wall promote a departure from chemical
equilibrium. It is expected that a similar condition would
be predicted for the molecular hydrogen arc. In fact,

relaxation time calculations reveal that characteristic electron and atom diffusion times are several orders of magnitude smaller than electron and atom recombination times. Therefore the electron and atom number densities in the wall region of the molecular arc should be many orders of magnitude larger than values characteristic of chemical equilibrium. Therefore actual molecular hydrogen number densities near the wall are expected to be somewhat lower than those values characteristic of equilibrium.

According to the calculations of Yos [21], Devoto [20] and Vanderslice [28], the thermal conductivity of a H-H_2 mixture is somewhat greater than that of atomic hydrogen for the temperatures of interest in this study. As noted in Section 4.4, an increase in thermal conductivity tends to "flatten" the temperature profile. Therefore, in the molecular arc, the higher heavy particle thermal conductivity will tend to flatten the heavy particle temperature profile near the wall.

A factor which will tend to depress the heavy particle temperature in the wall region of the molecular arc relates to the additional modes of energy storage associated with the rotational and vibrational states of the molecule. This implies that the molecular gas can store more energy at a lower temperature than atomic hydrogen.

The presence of molecular hydrogen in the wall region decreases the efficiency of elastic energy exchange between

electrons and heavy particles due to the higher mean heavy particle mass. This will act to lower the heavy particle temperature and raise the electron temperature.

As mentioned previously, it is expected that in the nonequilibrium molecular arc, the local atom number density will be somewhat higher than at equilibrium (though still lower than in the atomic hydrogen arc) near the wall. This implies an imbalance between the recombination-dissociation rates in which recombination dominates. When atomic recombination occurs to form a hydrogen molecule, the dissociation energy is transferred to another heavy particle or an electron. Therefore, atomic recombination in the wall region tends to elevate the thermal state of the gas.

Mean free path calculations for the molecular hydrogen arc indicate that the ambipolar diffusion coefficients will be somewhat lower in the wall region than for the atomic hydrogen arc. Since this tends to inhibit the flux of electrons and energy from the core to the wall region, the effect is to slightly increase electron density and temperature in the core and to diminish these quantities near the wall.

Considering all of the above factors, it is felt that those which dominate are the higher mean heavy particle mass and the greater energy storage capacity of the hydrogen molecule. Since both of these effects are influential only near the wall, it is felt that the nonequilibrium molecular

hydrogen arc will exhibit lower heavy particle temperatures and higher electron number densities and temperatures in the wall region. The more minor effect of lower ambipolar diffusion velocities near the wall may also promote a small increase in both temperature and electron density at the centerline.

Assuming the above to be true, the increased electrical conductivity in the wall region, brought about by the higher electron temperature and number density, will result in a larger integrated conductivity and, hence, lower electric field in the nonequilibrium molecular hydrogen arc as compared to the atomic hydrogen arc. Furthermore, since the total energy input to the arc, which is the product of electric field and current, must be equal to the total wall heat flux in the asymptotic region, the molecular arc should exhibit somewhat lower wall heat fluxes due to the smaller electric field. Finally, the radiative emission of the molecular arc may be slightly augmented due to small increases in the centerline electron number density and temperature and also due to molecular radiation effects in the infrared spectrum.

In summary, the nonequilibrium molecular hydrogen arc is expected to exhibit higher electron number density and temperature and lower heavy particle temperature near the wall, slightly higher electron number density and temperature in the core, somewhat smaller electric field and total wall

heat flux, and slightly larger radiative emission as compared to the nonequilibrium atomic hydrogen arc. However, as far as the bulk quantities are concerned, such as electric field and heat fluxes, it is expected that the solutions to the nonequilibrium atomic hydrogen arc provide accuracy sufficient for engineering purposes.

CHAPTER 5   SUMMARY AND CONCLUSIONS

In this chapter, the key results of the study are summarized. For ease of reference, the major results and conclusions are enumerated more or less in the same order that they appear in Chapter 4.

1. Fairly good agreement is obtained between the theoretical results of this study and the experimental temperature profiles of Wiese [27] and Steinberger [12] for cascade arcs of .0015 and .0010 m radius, respectively, and a current of 40 amps at atmospheric pressure.

2. Comparison of nonequilibrium predictions with the experimental electric field intensity and total heat flux data of Wiese [27], Morris [10] and Maecker [11] for their small radius arcs gives poor agreement at low currents with some improvement at higher currents. The reason for this disparity relates to convergence errors in the second order finite difference operator which are particularly severe at small tube radii.

3. Differences in the nonequilibrium and equilibrium [6] predictions for the hydrogen arc are readily attributable to an underprediction of the electrical

conductivity by the equilibrium model in the wall region. This results in the equilibrium model predicting high centerline temperatures and low temperatures in the wall region.

4. Use of the equilibrium theory results in a slight overprediction of the field intensity and the total wall heat flux.

5. Comparison of nonequilibrium and equilibrium radiative heat fluxes gives good agreement at higher currents, but the equilibrium results are considerably higher at lower currents.

6. The value of the electron and ion reflection coefficients has very little influence on the temperatures and electron density, except immediately adjacent to the wall. Electric field intensity and the total and radiative wall heat fluxes were unaffected by variation in these parameters. The reflection coefficients do have a strong influence on the electron heat conduction and the diffusion of kinetic and ionization energy at the wall, but the sum of these three terms accounts for less than 2% of the wall heat transfer for all parametric studies.

7. When the arc current is increased with all other operating parameters fixed, both temperature profiles and electron concentration profile increase over the

entire arc cross section. The radial location of the onset of thermal and chemical nonequilibrium increases with increasing current. The electric field exhibits an interesting phenomenon by first decreasing, passing through a minimum, and then increasing with current. The total, radiative, and heavy particle conduction wall heat fluxes increase with increasing current.

8. When the pressure is increased and all other operating parameters fixed, the centerline and wall temperatures decrease significantly, the electron concentration increases at the centerline and decreases at the wall and the radial location of the onset of thermal and chemical nonequilibrium increases. Both the electric field intensity and the total wall heat flux increase with pressure, and the radiative heat flux percentage increases from 15% to 55% as pressure increases from one to ten atmospheres. Heavy particle conduction actually decreases slightly as the pressure is increased.

9. When the tube radius is increased with all other operating parameters fixed, both temperature profiles and the electron concentration profile decrease over the entire arc cross section and the normalized radial location marking the onset of thermal and chemical nonequilibrium decreases. For tube radii greater than .02 m and I = 200 amps, P = 1 atm, thermal equilibrium is established over the entire arc cross section. The

electric field and the total and heavy particle con-
duction wall heat transfer all decrease rapidly with
increasing tube radius. Although the radiative heat
transfer percentage passes through a minimum, the
radiation heat transfer decreases rapidly as tube
radius increases.

10. Although chemical nonequilibrium is never significant
near the tube centerline, it always exists in the wall
region.

11. Thermal nonequilibrium is relatively unimportant for
the operating conditions considered in this study.
The highest electron wall temperature is 1930°K which
occurs for I = 200 amps, P = 1 atm and R = .005 m.

12. In general, comparison with the nonequilibrium calcula-
tions for argon [9] reveals the same basic trends,
with the following exceptions: thermal nonequilibrium
is a much more pronounced effect in argon and, in argon,
the diffusion of thermal and ionization energy and
electron heat conduction are not negligible contribu-
tions to the total heat flux.

13. An uncertainty analysis revealed that reasonable errors
associated with the utilization of ionization and
three-body recombination coefficients in the inelastic
collision model had an insignificant effect on the
solutions. However, it was discovered that uncertainties

in the radiative recombination coefficient, although
having negligible effect on electric field intensity
and total heat flux, could result in errors in the
radiative heat flux as high as 65%. Also, uncertain-
ties in ambipolar diffusion coefficients had an insig-
nificant effect on the predictions. Reasonable
inaccuracies in the atomic and transport properties
used in this study may result in uncertainties of the
order of 7% in centerline and wall temperatures, 25%
and 40% in centerline and wall electron concentration,
11% in the electric field intensity and total wall heat
flux and 50% in the radiation heat flux.

14. Qualitative considerations for the nonequilibrium
molecular hydrogen arc suggest that atom and electron
concentrations should be much higher and molecular
concentrations somewhat lower than those characteristic
of equilibrium in the wall region. Furthermore, in
comparison with the nonequilibrium atomic hydrogen arc,
it is felt that the molecular hydrogen arc will exhibit
lower heavy particle temperatures and higher electron
number densities and temperatures in the wall region.
Also, electron concentration and temperature are
expected to be slightly higher in the core. Finally,
it is expected that, although electric field intensity
and total wall heat flux will decrease and radiative
heat flux increase somewhat in the nonequilibrium

molecular arc, the predictions available for these quantities from the atomic hydrogen solutions provide accuracy sufficient for engineering purposes.

LIST OF REFERENCES

1. Incropera, F. P. and Viegas, J. R., "Nonequilibrium in an Arc Constrictor," AIAA Journal, Vol. 8, No. 9, September 1970, pp. 1722-1724.

2. Bahadori, M. N. and Soo, S. L., "Nonequilibrium Transport Phenomena of Partially Ionized Argon," International Journal of Heat and Mass Transfer, Vol. 9, No. 1, 1966, pp. 17-34.

3. Vincenti, W. G. and Kruger, C. H., Introduction to Physical Gas Dynamics, John Wiley and Sons, Inc., New York, 1965.

4. Watson , V., "Comparison of Detailed Numerical Solutions with Simplified Theories for the Characteristics of the Constricted-Arc Plasma Generator," Proceedings of the 1965 Heat Transfer and Fluid Mechanics Institute, Stanford University Press, California, 1965.

5. Bower, W. W., "Correlations for the Wall Parameters in the Asymptotic Region of a Laminar Constricted Arc," M. S. Thesis, Purdue University, 1969.

6. Greene, C. S., "Parametric Calculations for the Asymptotic Region of Hydrogen, Helium, Argon, Krypton, and Xenon Laminar Constricted Arcs," M. S. Thesis, Purdue University, 1972.

7. Okuno, A. F. and Park, C., "Stagnation Point Heat Transfer Rate in Nitrogen Plasma Flows: Theory and Experiment," ASME Winter Annual Meeting, Plasma Heat Transfer Session, Los Angeles, California, November 16-21, 1969.

8. Kruger, C. H., "Nonequilibrium in Confined-Arc Plasmas," Physics of Fluids, Vol. 13, No. 7, July 1970, pp. 1737-1746.

9. Clark, K. J., "Thermochemical Nonequilibrium in an Argon Constricted Arc Plasma," Ph.D. Thesis, Purdue University, 1971.

10. Morris, J. C., et al., "Evaluation of High Temperature Gas Transport Properties," NASA Cr-575, 1966.

11. Maecker, H., "Transport Properties in High Power Arcs," ARL 69-0031, 1969.

12. Steinberger, S., "Messung von Temperaturverteilungen im H_2-Kaskadenbogen bis 27,000°K," Zeitschrift für Physik, Vol. 223, 1969, pp. 1-18.

13. Holt, E. H. and Haskell, R. E., Foundations of Plasma Dynamics, The MacMillan Company, New York, 1965.

14. Delcroix, J. L., Introduction to the Theory of Ionized Gases, Interscience Publishers, Inc., New York, 1964.

15. Allen, C. W., Astrophysical Quantities, University of London, The Athlone Press, 1955.

16. Knight, D. D., "Electron Thermochemical Nonequilibrium Effects in Re-Entry Boundary Layers," AIAA Paper No. 69-82, 1969.

17. Hinnov, E. and Hirschberg, J. G., "Electron-Ion Recombination in Dense Plasmas," Physical Review, Vol. 125, No. 3, February 1962, pp. 795-801.

18. Petschek, H. and Byron, S., "Approach to Equilibrium Ionization behind Strong Shock Waves in Argon," Annals of Physics, Vol. 1, 1957, pp. 270-315.

19. Hirschfelder, J. O., Curtiss, C. F. and Bird, R. B., Molecular Theory of Gases and Liquids, John Wiley and Sons, Inc., New York, 1954.

20. Devoto, R. S., "Transport Coefficients of Partially Ionized Hydrogen," Journal of Plasma Physics, Vol. 2, Part 4, 1968, pp. 617-631.

21. Yos, J. M., "Transport Properties of Nitrogen, Hydrogen, Oxygen, and Air to 30,000°K," AVCO RAD TM-63-7, 1963.

22. Jeans, Sir J., An Introduction to the Kinetic Theory of Gases, Cambridge University Press, Cambridge, England, 1962.

23. Devoto, R. S. and Li, C. P., "Transport Coefficients of Partially Ionized Helium," Journal of Plasma Physics, Vol. 2, Part 1, 1968, pp. 17-32.

24. Bower, W. W. and Incropera, F. P., "Heat Transfer, Development Length, and Friction Factor Correlations for the Asymptotic Region of a Laminar Arc Constrictor," Wärme-und Stoffübertragung, Vol. 2, 1969, pp. 150-162.

25. Griem, H. R., Plasma Spectroscopy, McGraw-Hill Book Company, New York, 1964.

26. Richtmeyer, F. K., Kennard, E. H. and Lauritzen, T., Introduction to Modern Physics, McGraw-Hill Book Company, New York, 1955.

27. Wiese, W. L., Paquette, D. R. and Solarski, J. E., "Profiles of Stark-Broadened Balmer Lines in a Hydrogen Plasma," Physical Review, Vol. 129, Part 1, 1963, pp. 1225-1232.

28. Vanderslice, J. T., et al., "High-Temperature Transport Properties of Dissociating Hydrogen," Physics of Fluids, Vol. 5, No. 2, 1962, pp. 155-164.

29. Presnyakov, L. P., Ulantsev, A. D. and Shelepin, L. A., "Effect of Inelastic Atomic Collisions on Relaxation Processes in a Low Temperature Plasma," Optics and Spectroscopy, Vol. 24, May 1968, pp. 363-364.

APPENDIX A

AMBIPOLAR DIFFUSION IN HYDROGEN BY MEAN FREE PATH THEORY

The purpose of this appendix is to describe the theory behind calculation of transport coefficients by mean free path methods and to derive an expression for the ambipolar diffusion velocity (see assumption 13 of Section 2.1).

Consider an imaginary plane fixed with respect to the walls of a container in which gaseous, atomic hydrogen exists (see Figure A-1). It is desired to calculate the thermal flux of particles passing through this plane in the absence of gradients of temperature and concentration. The number of particles with velocity vectors lying in the direction of a cone of solid angle $d\omega$ per unit volume of gas is $n \frac{d\omega}{4\pi}$ where n is the number density of particles. If θ is the angle between the normal to the plane and the line through the center of $d\omega$, the component of velocity of the particles (with velocity vectors in $d\omega$) normal to the plane is $\bar{c} \cos\theta$ where $\bar{c}$ is the mean thermal speed of the particles. Therefore, the flux of particles through the plane with velocity vectors lying in $d\omega$ is $n \frac{d\omega}{4\pi} \bar{c} \cos\theta$. Integrating over the hemisphere gives

$$\frac{n\bar{c}}{4\pi} \int_0^{2\pi} \int_0^{\pi/2} \sin\theta \, \cos\theta \, d\theta d\phi = \frac{1}{4} n\bar{c} \qquad \text{(A-1)}$$

which is the thermal flux of particles through the plane.

$$- n + \frac{\partial n}{\partial r}\lambda, \ \bar{c} + \frac{\partial \bar{c}}{\partial r}\lambda$$

$$- n, \ \bar{c}$$

$$- n - \frac{\partial n}{\partial r}\lambda, \ \bar{c} - \frac{\partial \bar{c}}{\partial r}\lambda$$
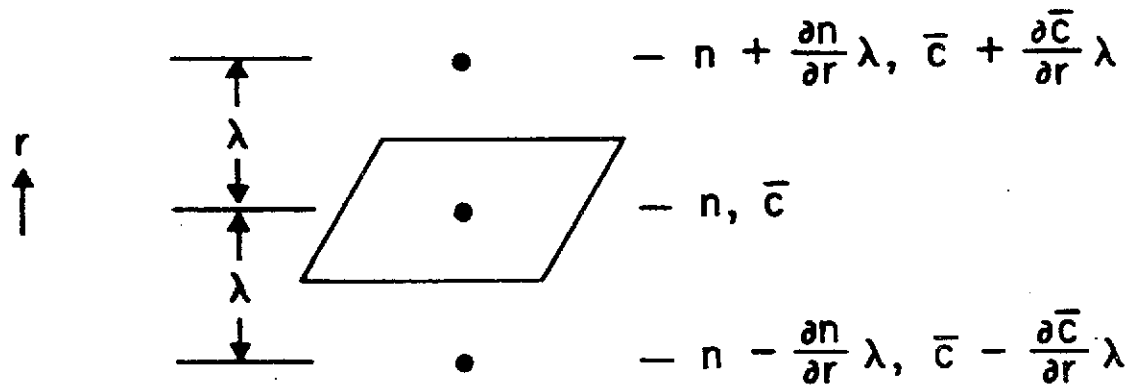
Figure A-1. Illustration of Mean Free Path Method.

In the presence of property gradients, the flux of particles through the plane is actually the value of $\frac{1}{4} n\bar{c}$ evaluated one mean free path below (or above for negative flux) the plane. This is because, on the average, each particle arriving at the plane from below does not suffer any collisions in its journey to the plane from one mean free path away. Using a Taylor series expansion to the first order, the flux of particles through the plane from below (positive flux) and above (negative flux) is then, respectively,

$$\text{positive flux} = \frac{1}{4}\left[n - \frac{\partial n}{\partial r}\lambda \right]\left[\bar{c} - \frac{\partial \bar{c}}{\partial r}\lambda \right] \qquad (A\text{-}2)$$

$$\text{negative flux} = \frac{1}{4}\left[n + \frac{\partial n}{\partial r}\lambda \right]\left[\bar{c} + \frac{\partial \bar{c}}{\partial r}\lambda \right] \qquad (A\text{-}3)$$

where λ is the mean free path length. Therefore, the net flux of particles in the positive direction is

$$\Gamma = -\frac{1}{2}\left[n\lambda \frac{\partial \bar{c}}{\partial r} + \bar{c}\lambda \frac{\partial n}{\partial r} \right]$$

The free diffusion velocity of particles in the positive direction is then given simply as

$$V^{D'} = \frac{\Gamma}{n} = -\frac{1}{2}\left[\frac{\bar{c}}{n}\lambda \frac{\partial n}{\partial r} + \lambda \frac{\partial \bar{c}}{\partial r} \right]$$

In a system of three species (electrons, ions, atoms), the above expression may be used to obtain the species diffusion velocities relative to a reference frame fixed in the container.

Utilizing the assumption that electron and ion number densities are equal (Section 2.1), the three diffusion equations are

$$V_e^{D'} = -\frac{1}{2}\left[\frac{\bar{c}_e}{n_e} \lambda_e \frac{\partial n_e}{\partial r} + \lambda_e \frac{\partial \bar{c}_e}{\partial r}\right]$$

$$V_{H^+}^{D'} = -\frac{1}{2}\left[\frac{\bar{c}_H}{n_e} \lambda_{H^+} \frac{\partial n_e}{\partial r} + \lambda_{H^+} \frac{\partial \bar{c}_H}{\partial r}\right]$$

$$V_H^{D'} = -\frac{1}{2}\left[\frac{\bar{c}_H}{n_H} \lambda_H \frac{\partial n_H}{\partial r} + \lambda_H \frac{\partial \bar{c}_H}{\partial r}\right]$$

However, the diffusion velocity of each species is influenced by the presence of the other species, an effect which is not accounted for in the above three equations. In order to remedy this situation, a fourth equation is introduced to force the mass average of the diffusion velocities to be zero:

$$\rho_e\left(V_e^{D'} + a\right) + \rho_{H^+}\left(V_{H^+}^{D'} + a\right) + \rho_H\left(V_H^{D'} + a\right) = 0 \qquad \text{(A-4)}$$

The constant a is introduced in such a manner that each of the terms in parentheses gives the correct diffusion velocity for the respective species. After simplification and use of number densities, the above expression yields

$$a = -\left(\frac{1}{n_e + n_H}\right)\left(\frac{m_e}{m_H} n_e V_e^{D'} + n_e V_{H^+}^{D'} + n_H V_H^{D'}\right)$$

The correct diffusion velocities are now written without the prime superscript and satisfy the following relationship:

$$\rho_e V_e^D + \rho_{H^+}^D V_{H^+}^D + \rho_H V_H^D = 0 \qquad (A-5)$$

Therefore, the diffusion velocities are calculated as follows:

$$V_e^D = V_e^{D'} + a; \quad V_{H^+}^D = V_{H^+}^{D'} + a; \quad V_H^D = V_H^{D'} + a$$

One of the assumptions of Section 2.1 states that the electrons and ions will diffuse, effectively, toward the wall from the centerline of the arc in pairs. In other words the electron and ion diffusion velocities are equal. Since the present derivation has not incorporated the assumption of ambipolar diffusion, the above diffusion velocities for electrons and ions are not identically equal. To incorporate the phenomena of macroscopic electric neutrality and ambipolar diffusion, the results of Holt and Haskell [13] are used. They give the following equations for the flux of electrons and ions in the presence of an electric field (from a moment of the Boltzmann equation):

$$\Gamma_e = n_e V_e^D = - D_e \nabla n_e - n_e \mu_e E \qquad (A-6)$$

$$\Gamma_{H^+} = n_e V_{H^+}^D = - D_{H^+} \nabla n_e + n_e \mu_{H^+} E \qquad (A-7)$$

where the D's are diffusion coefficients, E is the externally applied electric field, and μ denotes the charged particle mobility defined as

$$\mu_e = \frac{|e|}{m_e \nu_{eh}} \quad \text{and} \quad \mu_{H^+} = \frac{|e|}{m_H \nu_{H^+h}}$$

In the above equations, ν_{eh} is the sum of collision frequencies involving electrons and all heavy particles and ν_{H^+h} is the sum of collision frequencies involving ions and all heavy particle species. By eliminating the electric field through simultaneous solution of Equations (A-6) and (A-7), the following expression is obtained:

$$\frac{\mu_{H^+}V_e^D + \mu_e V_{H^+}^D}{\mu_{H^+} + \mu_e} = - \left(\frac{\mu_{H^+}D_e + \mu_e D_{H^+}}{\mu_{H^+} + \mu_e} \right) \frac{\nabla n_e}{n_e}$$

Holt and Haskell define the term in parentheses as the ambipolar diffusion coefficient. Hence, the left hand side of the equation is the ambipolar diffusion velocity:

$$V_{amb}^D = \frac{\mu_{H^+}V_e^D + \mu_e V_{H^+}^D}{\mu_{H^+} + \mu_e} \tag{A-8}$$

Note that the above definition of the ambipolar diffusion velocity accounts only for ordinary diffusion involving the electron (ion) number density gradient. Since the true electron and ion diffusion velocities previously defined involve other gradients as well, it is assumed that the above relationship between the ambipolar and species diffusion velocities is valid for other modes of ambipolar diffusion (i.e. thermal diffusion and pressure diffusion).

Now, the electron and ion diffusion velocities may be replaced with the ambipolar diffusion velocity and Equation (A-5) is no longer identically satisfied. However, with

the ambipolar diffusion velocity having been established, the atom diffusion velocity may now be computed to insure satisfaction of Equation (A-5). Hence,

$$\rho_e V^D_{amb} + \rho_{H^+} V^D_{amb} + \rho_H V^D_H = 0 \qquad (A-9)$$

where V^D_H is now the correct atom diffusion velocity in a gas where ambipolar diffusion of electrons and ions occurs. From Equation (A-9) it is obvious that the expression for the atom diffusion velocity is

$$V^D_H = - \frac{n_e}{n_H} V^D_{amb}$$

The expression for the electron-ion ambipolar diffusion velocity is given by

$$V^D_{amb} = A_1 \frac{\partial n_e}{\partial r} + A_2 \frac{\partial n_H}{\partial r} + A_3 \frac{\partial T_e}{\partial r} + A_4 \frac{\partial T_h}{\partial r} \qquad (A-10)$$

where

$$A_1 = \frac{1}{2}\left(\frac{1}{n_e+n_H}\right)\left(\frac{1}{\mu_{H^+}+\mu_e}\right)\left\{\left[\mu_e \frac{m_e}{m_H} n_e - \mu_{H^+}(n_e+n_H)\right]\left[\frac{\bar{c}_e \lambda_e}{n_e}\right]\right.$$

$$\left. + \left[\mu_{H^+} n_e - \mu_e n_H\right]\left[\frac{\bar{c}_H \lambda_{H^+}}{n_e}\right]\right\}$$

$$A_2 = \frac{1}{2}\frac{\bar{c}_H \lambda_H}{n_e+n_H}$$

$$A_3 = \frac{1}{2}\left(\frac{1}{n_e+n_H}\right)\left(\frac{1}{\mu_{H^+}+\mu_e}\right)\left[\mu_e \frac{m_e}{m_H} n_e - \mu_{H^+}(n_e+n_H)\right]\left[\frac{\lambda_e \bar{c}_e}{2T_e}\right]$$

$$A_4 = \frac{1}{2}\left(\frac{1}{n_e+n_H}\right)\left(\frac{1}{\mu_{H^+}+\mu_e}\right)\left\{\left[\mu_{H^+} n_e - \mu_e n_H\right]\left[\frac{\lambda_{H^+} \bar{c}_H}{2T_h}\right]\right.$$

$$\left. + \left[(\mu_{H^+} + \mu_e)n_H\right]\left[\frac{\lambda_H \bar{c}_H}{2T_h}\right]\right\}$$

The mean free paths (λ) in the above expressions are discussed in Appendix D and the mean thermal speed $(\bar{c}_i)$ of species i is calculated from

$$\bar{c}_i = \left[\frac{8kT_i}{\pi m_i}\right]^{1/2}$$

In order to compare the previous results with those obtained from equilibrium kinetic theory, the coefficients must be evaluated in the limit of thermochemical equilibrium. To facilitate this comparison the following expressions are introduced:

$$P_e = \frac{n_e}{2n_e + n_H} P = kn_e T_e = x_e P \qquad (A-11)$$

$$P_H = \frac{n_H}{2n_e + n_H} P = kn_H T_h = x_H P \qquad (A-12)$$

where P_e and P_H are the electron and atom partial pressures and x_e and x_H are the electron and atom mole fractions, respectively. Hence,

$$n_e = \frac{P}{kT_e} x_e; \quad n_H = \frac{P}{kT_h} x_H$$

Substituting the above expressions into Equation (A-10), we obtain

$$V_{amb}^D = A_1 \left(\frac{P}{kT_e}\right) \frac{\partial x_e}{\partial r} + A_2 \left(\frac{P}{kT_h}\right) \frac{\partial x_H}{\partial r}$$

$$+ \left[A_3 - A_1 \left(\frac{Px_e}{kT_e^2}\right)\right] \frac{\partial T_e}{\partial r} + \left[A_4 - A_2 \left(\frac{Px_H}{kT_h^2}\right)\right] \frac{\partial T_h}{\partial r}$$

The last two terms (in brackets) are associated with the thermal diffusion coefficient and for the sake of comparison with results generated from the rigorous kinetic theory [20], they will be dropped and only ordinary diffusion considered. Substituting once more from Equations (A-11) and (A-12) and algebraically manipulating, we obtain

$$V_{amb}^D = A_1 \frac{n_e}{x_e} \frac{\partial x_e}{\partial r} + A_2 \frac{n_H}{x_H} \frac{\partial x_H}{\partial r}$$

$$= A_1 \frac{n_e}{x_e} \frac{\partial x_e}{\partial r} - 2A_2 \frac{n_H}{x_H} \frac{\partial x_e}{\partial r}$$

$$= \left[A_1 \frac{n_e(2n_e + n_H)}{n_e} - 2A_2 \frac{n_H(2n_e + n_H)}{n_H} \right] \frac{\partial x_e}{\partial r}$$

$$= - \frac{(2n_e + n_H)^2}{n_e(n_e + n_H)} \left[- \frac{n_e(n_e + n_H)}{(2n_e + n_H)} (A_1 - 2A_2) \right] \frac{\partial x_e}{\partial r} \qquad (A-13)$$

Note that in the second step $\frac{\partial x_H}{\partial r} = - 2 \frac{\partial x_e}{\partial r}$.

In the equilibrium limit for equal electron and heavy particle temperatures and electron number densities calculated from the Saha equation, the term in brackets in Equation (A-13) becomes the equilibrium ambipolar diffusion coefficient (D_{amb}) [23].

Figure A-2 is a comparison between results obtained from rigorous kinetic theory [20] and from the mean free path calculations of this study evaluated in the equilibrium limit. Although agreement between the two theories is good over the entire range of temperature, a multiplicative factor of 1.2 was introduced to force excellent agreement of the mean free path and rigorous kinetic theory results.
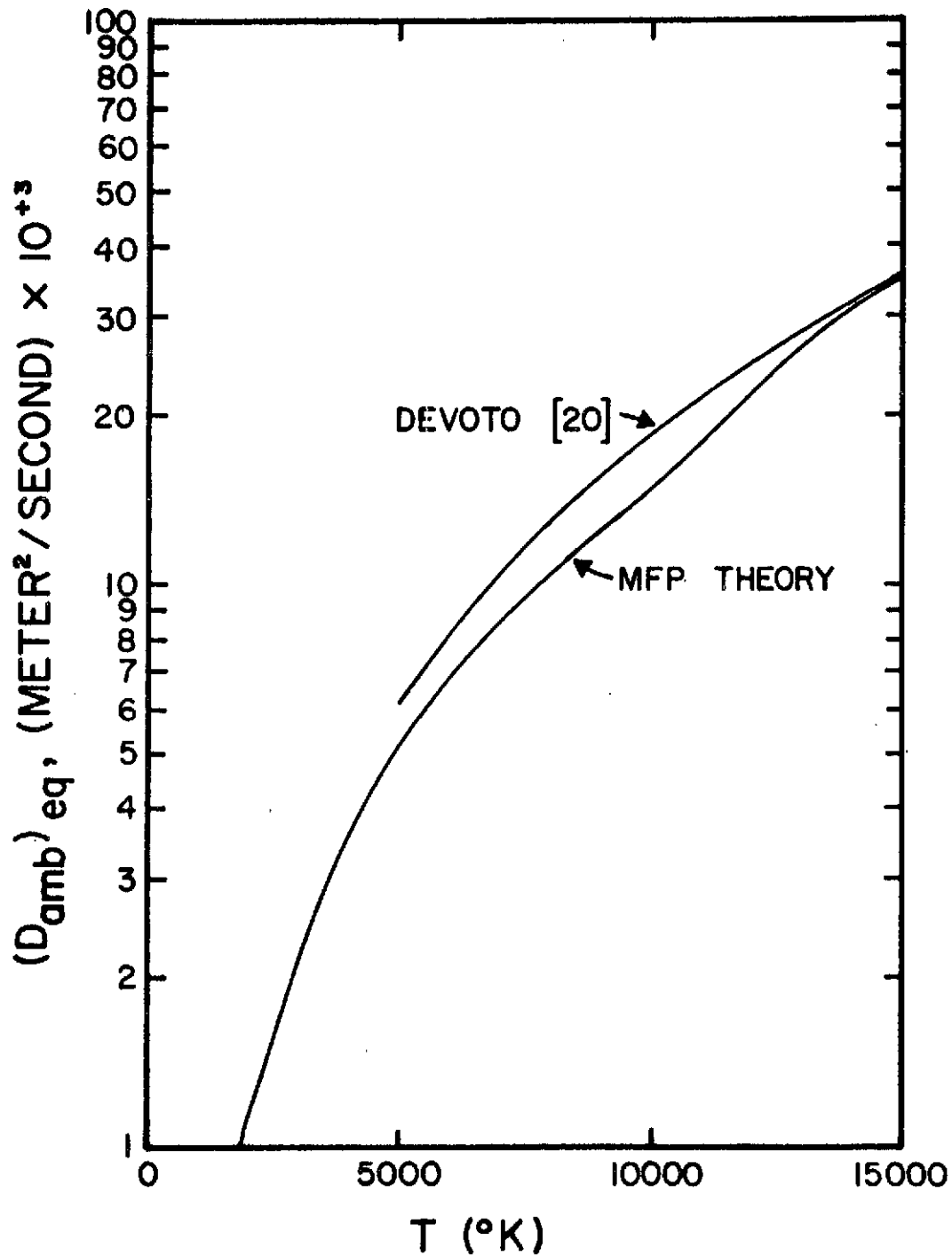
Figure A-2. Comparison of Equilibrium Ambipolar Diffusion
Coefficient from Mean Free Path Calculation
and Rigorous Kinetic Theory.

APPENDIX B

HEAT FLUX AND SHEAR STRESS IN HYDROGEN

BY MEAN FREE PATH THEORY

In this appendix, mean-free-path expressions are derived for the electron and heavy particle heat fluxes and the total shear stress.

The flux of particles through an imaginary, infinitesimal plane (see Figure A-1) in the positive and negative directions, is derived in Appendix A, and the results given by Equations (A-2) and (A-3). Assume that some property, ϕ, is associated with the particles passing through the plane and that its value is a function of the radial coordinate. The positive and negative fluxes of that property (kinetic energy, momentum, etc.) through the plane can then be written from Equations (A-2) and (A-3) as

$$\text{positive flux of } \phi = \frac{1}{4}\left[n - \frac{\partial n}{\partial r}\lambda\right]\left[\bar{c} - \frac{\partial \bar{c}}{\partial r}\lambda\right]\left[\phi - \frac{\partial \phi}{\partial r}\lambda\right]$$

$$\text{negative flux of } \phi = \frac{1}{4}\left[n + \frac{\partial n}{\partial r}\lambda\right]\left[\bar{c} + \frac{\partial \bar{c}}{\partial r}\lambda\right]\left[\phi + \frac{\partial \phi}{\partial r}\lambda\right]$$

The net flux of the property, ϕ, in the positive radial direction is then obtained by subtracting the negative flux from the positive flux

$$\text{net flux} = -\frac{1}{2}\bar{c}\phi\lambda\,\frac{\partial n}{\partial r} - \frac{1}{2}n\phi\lambda\,\frac{\partial \bar{c}}{\partial r} - \frac{1}{2}n\bar{c}\lambda\,\frac{\partial \phi}{\partial r} \qquad (B\text{-}1)$$

where all higher order terms in λ have been excluded, n is the particle number density and $\bar{c}$ is the mean kinetic speed of the particles.

To obtain the heat flux contribution of a given species in the gas, let ϕ be the mean kinetic energy of that species. For electrons and other non-molecular components, the mean kinetic energy per particle is $\frac{3}{2}$ kT. Making this substitution for ϕ and substituting the expression for $\bar{c} = \left(\frac{8kT}{\pi m}\right)^{1/2}$ in the derivative of $\bar{c}$ with respect to r in Equation (B-1) gives the following for the radial heat flux of species i

$$q_{r_i} = -\frac{9}{8}\lambda_i n_i \bar{c}_i k\,\frac{\partial T_i}{\partial r} - \frac{3}{4}\lambda_i \bar{c}_i kT_i\,\frac{\partial n_i}{\partial r}$$

where the first and second terms relate to Fourier conduction and thermal diffusion, respectively. In the electron energy equation, the electron heat flux is obtained from the above equation simply by replacing the i subscript with the subscript e. In the heavy particle energy equation, the heavy particle heat flux is obtained by summing the above expression over the ions and atoms (i = H^+ and i = H).

In order to obtain the Fourier conduction for hydrogen in the equilibrium limit, the electron and heavy particle temperatures are equated, the electron number density is related to the temperature and atom number density through the Saha equation and the Fourier terms of the individual

143

heat fluxes are summed. Therefore, the equilibrium Fourier conductivity of hydrogen from mean free path theory is obtained from the expression

$$(q_r)_{eq} = - \left[\frac{9}{8} k(\lambda_e n_e \bar{c}_e + \lambda_{H^+} n_e \bar{c}_H + \lambda_H n_H \bar{c}_H)\right] \frac{\partial T}{\partial r}$$

where n_e is given by the Saha equation and the term in square brackets is the equilibrium thermal conductivity.

Figure B-1 provides plots of the above result (labeled "mfp theory") and that obtained from the rigorous kinetic theory calculation for atomic hydrogen thermal conductivity [20]. Note that if a weighting factor of 3 is multiplied by the mean free path expression, very good agreement is obtained with the rigorous calculations in the equilibrium limit. For this reason, a weighting factor is introduced into the nonequilibrium heat flux expressions used in the computer programs of this work.

To obtain the contribution of a given gaseous species to the total axial shear stress acting on the radial plane, let ϕ in Equation (B-1) be the average axial momentum of a species i particle, $\phi = m_i U$, where U is the mass average axial velocity. Since shear stress only involves velocity gradients, the first two terms of Equation (B-1) are dropped giving

$$- \tau_{rz_i} = - \left[\frac{1}{2} n_i \bar{c}_i \lambda_i m_i\right] \frac{\partial U}{\partial r}$$

where $- \tau_{rz_i}$ is the shear stress (or the viscous flux of axial momentum in the radial direction) and the negative
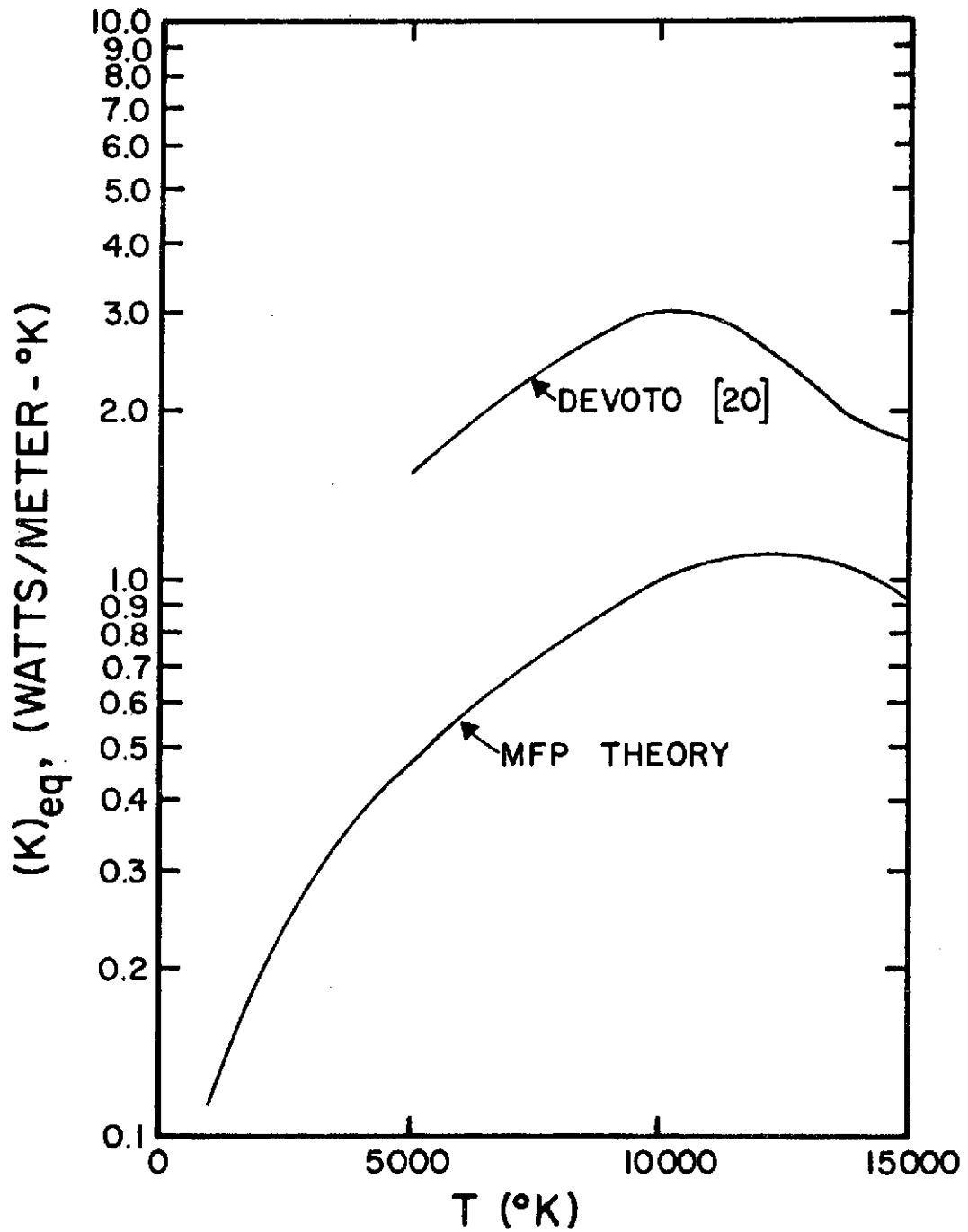
Figure B-1. Comparison of Equilibrium Thermal Conductivity
from Mean Free Path Calculation and Rigorous
Kinetic Theory.

sign is introduced on the left side of the equation to comply with the usual sign convention. Therefore, the term in parentheses is the contribution of the ith species to the total gas viscosity, which is obtained by summing over all species. Therefore

$$\mu = \frac{1}{2}\left(m_e n_e \bar{c}_e \lambda_e + m_H n_e \bar{c}_H \lambda_{H^+} + m_H n_H \bar{c}_H \lambda_H\right)$$

where μ is the total gas viscosity. In order to obtain the equilibrium viscosity, the above expression must be evaluated for equal electron and heavy particle temperatures and the electron number density must be calculated from the Saha equation.

Figure B-2 is a plot of the equilibrium limit of the mean free path calculation of atomic hydrogen viscosity compared with results of a rigorous kinetic theory calculation [20]. Note that in the case of viscosity, a weighting factor of about 1.8 would bring the mean free path calculations into relatively good agreement with the rigorous results. Therefore, a weighting factor of 1.8 is introduced into the nonequilibrium shear stress used in the computer programs of this work.

Expressions for the mean free paths used to calculate thermal conductivity and viscosity for each gaseous species are given at the end of Appendix D. Note that, for these two transport phenomena, the value of ℓ is 2 for the collision frequencies which appear in the mean free path definitions.
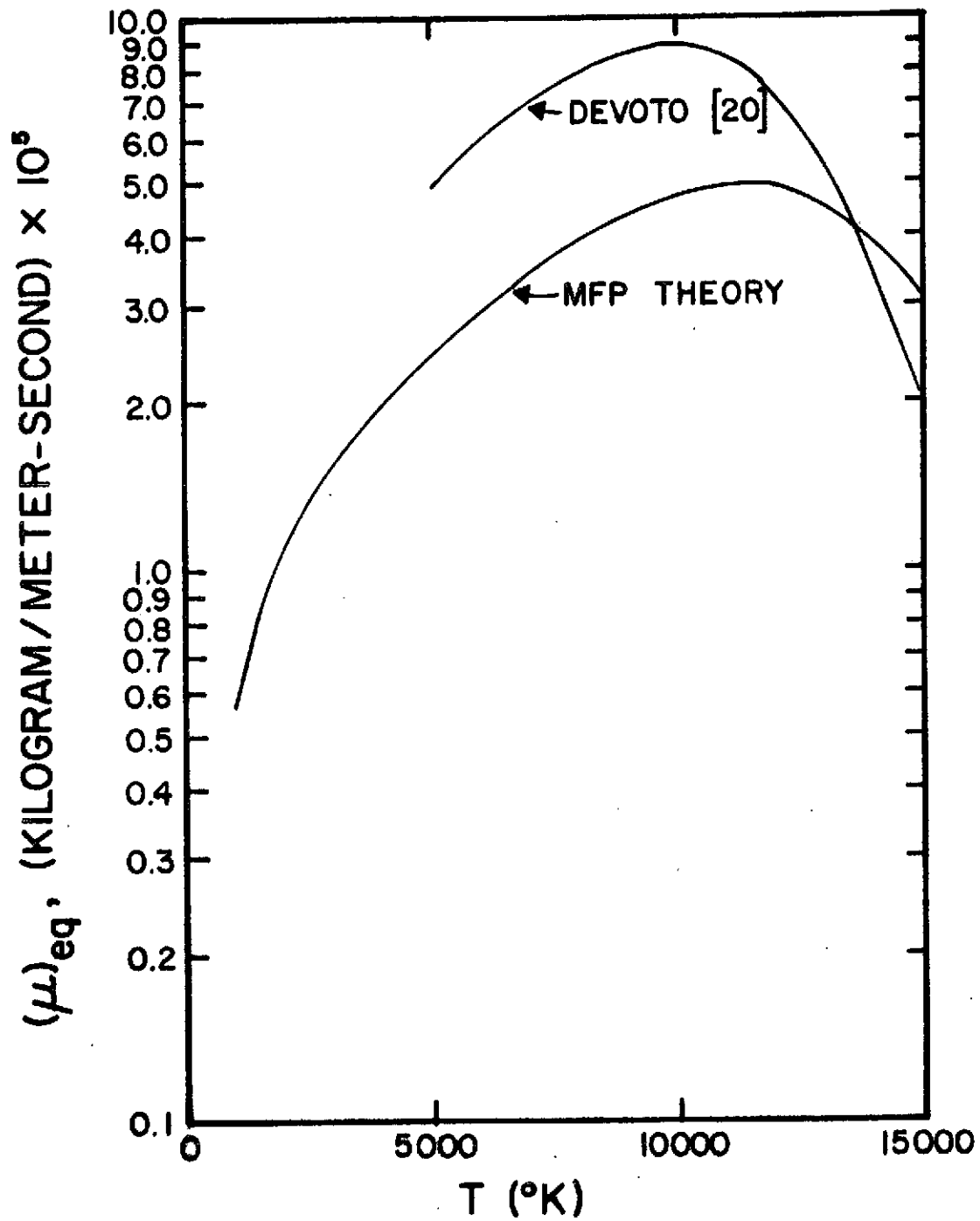
Figure B-2. Comparison of Equilibrium Viscosity from Mean Free Path Calculation and Rigorous Kinetic Theory.

APPENDIX C

ELECTRICAL CONDUCTIVITY

To obtain a nonequilibrium expression for the electrical conductivity, it is assumed that the electric field is constant and uniform in the axial direction of the cascade arc. The force that the electric field exerts on a test electron in the axial direction is assumed to be balanced by the average rate of electron momentum loss in the axial direction (Newton's Second Law) due to elastic collisions with heavy particles. In other words, although each individual electron is continually being accelerated by the electric field, the effect of elastic collisions with heavy particles is to prevent the electron subgas from accelerating on a macroscopic scale. A reference frame translating with the mass average gas velocity in the axial direction is used and the heavy particles are assumed to be stationary relative to the energetic electrons.

Since a heavy particle remains essentially stationary while an electron collides with it, the electron momentum loss in its original direction of motion is, on the average, $m_e \vec{c}_e (1-\cos\chi)$, where χ is the angle at which the electron is deflected away from its original path.

The density of electrons with velocities in the vector range $\vec{c}_e$, $d\vec{c}_e$ is given in Appendix D by Equation (D-1). The flux of such electrons incident upon a stationary heavy particle species per unit volume is obtained by multiplying the above referenced expression by c_e and n_h (heavy particle number density) to obtain

$$n_h n_e f(c_e) d\vec{c}_e c_e$$

The rate at which these electrons pass through impact parameter ring segments of area b db dϕ centered about each heavy particle (see Appendix D) is

$$n_h n_e f(c_e) c_e \ b \ db \ d\phi \ d\vec{c}_e$$

$$= n_h n_e f(c_e) c_e \sigma(\chi, \ c_e) \sin(\chi) d\chi \ d\phi \ d\vec{c}_e \qquad \text{(C-1)}$$

where $\sigma(\chi, \ c_e)$ is the differential scattering cross section. The momentum loss rate per electron (with velocity in $\vec{c}_e$, $d\vec{c}_e$) is obtained by dividing the above equation by n_e, multiplying by the momentum loss per collision, $m_e \vec{c}_e (1-\cos\chi)$, and integrating over the angles χ and ϕ. This gives

$$n_h f(c_e) c_e d\vec{c}_e \int_0^{2\pi} \int_0^\pi \sigma(\chi, \ c_e) \sin(\chi) [m_e \vec{c}_e (1-\cos\chi)] d\chi d\phi$$

$$= n_h f(c_e) c_e m_e \vec{c}_e Q_{eh}^1 (c_e) d\vec{c}_e$$

where $Q_{eh}^1 (c_e)$ is the electron-heavy particle total cross section for diffusion. Integrating over all velocity ranges gives the total momentum loss rate of an electron to the

heavy particle species

$$m_e n_h \int f(c_e) c_e \vec{c}_e \; Q_{eh}^1(c_e) d\vec{c}_e$$

The momentum loss rate in the axial direction is then

$$m_e n_h \int f(c_e) c_e \; c_{e_z} \; Q_{eh}^1(c_e) \; d\vec{c}_e$$

The above expression is simplified by replacing c_{e_z}, the axial component of electron velocity, by the average axial component of electron velocity, which is simply the electron drift velocity, U_d. Therefore, U_d can be removed from the integral which results in

$$m_e n_h U_d \int f(c_e) c_e \; Q_{eh}^1(c_e) \; d\vec{c}_e$$

If now the vector differential $d\vec{c}_e$ is expanded into the scalar differential in spherical coordinates, integration is carried out over the angular spherical coordinates, and the substitution $\gamma^2 = \dfrac{m_e c_e^2}{2kT_e}$ is made (see Appendix D), the following expression is obtained:

$$m_e n_h U_d \left[8 \left(\frac{kT_e}{2\pi m_e} \right)^{1/2} \int_0^\infty e^{-\gamma^2} \; \gamma^3 \; Q_{eh}^1(c_e) d\gamma \right]$$

$$= 8 \, m_e \, n_h \, U_d \, \Omega_{eh}^{(1,0)} \, (T_e)$$

where $\Omega_{eh}^{(1,0)}(T_e)$ is the gas kinetic collision integral for electron-heavy particle collisions. As mentioned in Appendix D, the collision integral $\Omega_{eh}^{(1,1)}(T_e)$ is more commonly available and its use will introduce a factor of 0.5 in the above

expression. Therefore, the momentum loss rate per electron now becomes

$$4 \, m_e \, n_h \, U_d \, \Omega_{eh}^{(1,1)} (T_e) = m_e \, U_d \, \nu_{eh}^{1}$$

where ν_{eh}^{1} is the electron-heavy particle collision frequency for diffusion.

It was mentioned previously that the electron momentum loss rate is balanced by the force exerted by the electric field on the electron. This is expressed mathematically as

$$eE_z = m_e \, U_d \, \nu_{eh}^{1}$$

Therefore,

$$U_d = \frac{eE_z}{m_e \, \nu_{eh}^{1}}$$

$$= \frac{eE_z}{m_e (\nu_{eH^+}^{1} + \nu_{eH}^{1})}$$

where e is the electronic charge and E_z is the axial electric field component. Note that the specific heavy particle species (ions and atoms) have been introduced in the expression.

The current density, J, can be defined as

$$J = n_e \, e \, U_d = \sigma_e \, E_z$$

Therefore,

$$U_d = \frac{\sigma_e E_z}{e \, n_e}$$

Now that there are two formulas for U_d, an explicit expression can be obtained for the electrical conductivity

$$\sigma_e = \frac{n_e \, e^2}{m_e(\nu^1_{eH^+} + \nu^1_{eH})} \tag{C-2}$$

This is the same expression that Holt and Haskell [13] obtain by taking moments of the Boltzmann equation.

By equating the electron and heavy particle temperatures and evaluating the electron number density from the Saha equation, Equation (C-2) can be expressed in the equilibrium limit and compared with accurate kinetic theory calculations of electrical conductivity. Figure C-1 shows the equilibrium limit of Equation (C-2) compared with Devoto's [20] calculations of electrical conductivity. Agreement between the two curves is good over the entire range and, consequently, no correction factors are needed to adjust Equation (C-2). The collision frequencies appearing in this equation are discussed at length in Appendix D.
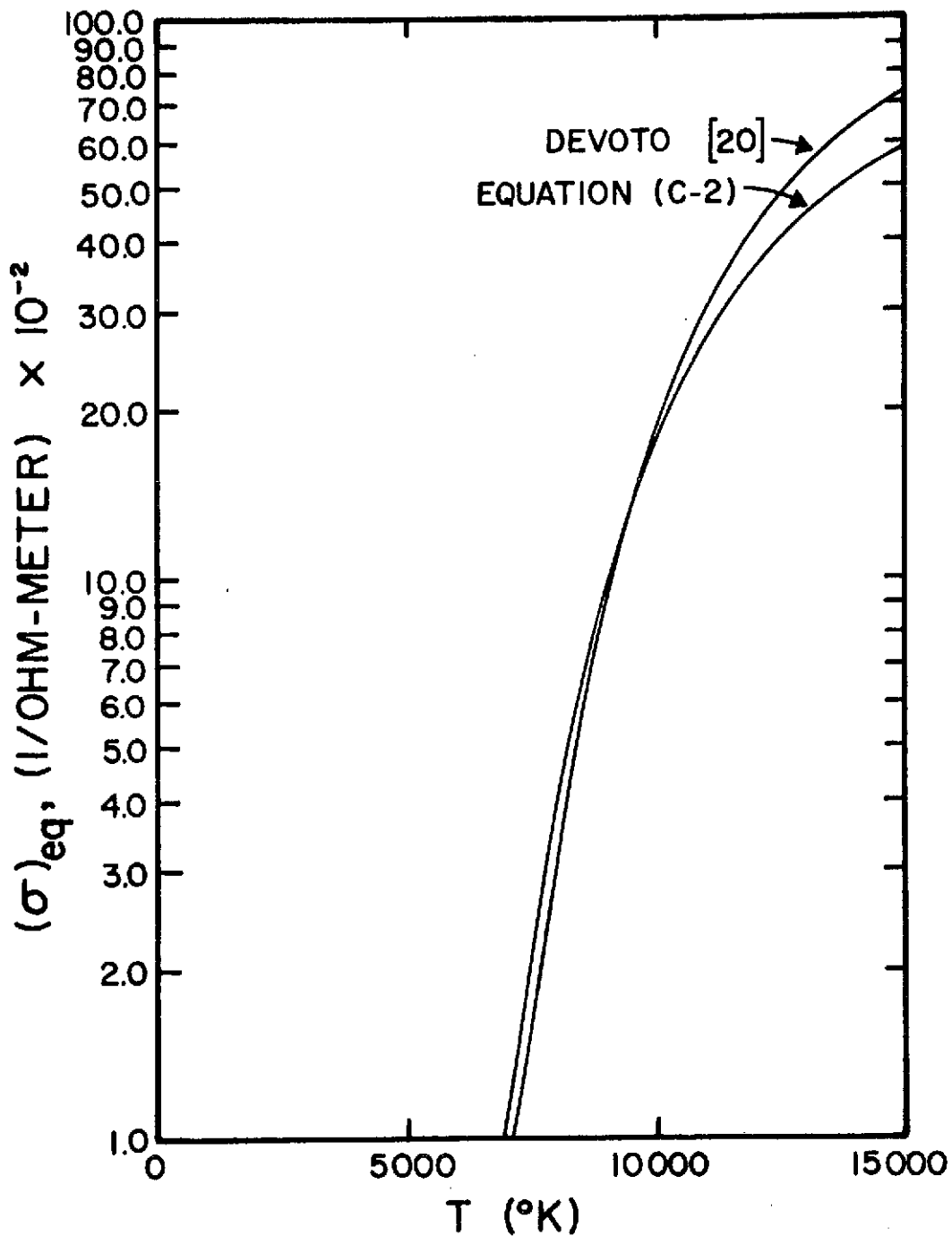
152

Figure C-1. Comparison of Equilibrium Electrical Conductivity from Equation (C-2) and Rigorous Kinetic Theory.

APPENDIX D

MEAN FREE PATH DERIVATION

The mean free path length is an important property in the calculation of transport coefficients by the mean free path theory. Once the appropriate collision frequencies are known it is a simple matter to obtain the mean free path length of a given particle, as it is simply the ratio of the thermal speed of the particle to the sum of the collision frequencies. Therefore, expressions for collision frequency will first be derived.

The Maxwellian velocity distribution function is defined such that the density of particles of some species A with velocity vectors that lie in the interval $(c_{A_x}, c_{A_x} + dc_{A_x})$, $\ldots$, $(c_{A_z}, c_{A_z} + dc_{A_z})$ or $\vec{c}_A$, $d\vec{c}_A$, is given by

$$n_A f(c_A) d\vec{c}_A \qquad \text{(D-1)}$$

Consider now a single particle of another species B, having a different velocity vector interval. The vector interval of a B particle is $\vec{c}_B$, $d\vec{c}_B$ and the magnitude of the velocity difference of A and B particles is $|\vec{c}_B - \vec{c}_A| \equiv |\vec{g}_{AB}|$. Therefore, the flux of A particles approaching a single B particle per unit time and area, where $|\vec{g}_{AB}|$ is the magnitude of the velocity of A particles

relative to the B particle, is

$$n_A f(c_A) d\vec{c}_A |\vec{g}_{AB}|$$

The total flux of A particles approaching all B particles per unit time then becomes

$$n_A f(c_A) d\vec{c}_A |\vec{g}_{AB}| n_B f(c_B) d\vec{c}_B$$

Imagine now an annular ring (impact parameter ring) segment of radius b, width db and arc $d\phi$ centered about each B particle. The number of A particles with center of mass passing through this impact parameter ring segment of area $bdbd\phi$ for all of the B particles per unit volume and time is

$$n_A f(c_A) d\vec{c}_A |\vec{g}_{AB}| n_B f(c_B) d\vec{c}_B \ b \ db \ d\phi$$

However, the quantity bdb is equal, by definition, to $\sigma(|\vec{g}_{AB}|, \chi) \sin\chi d\chi$ where χ is the deflection angle of the A particle.trajectory relative to the B particle and $\sigma(|\vec{g}_{AB}|, \chi)$ (the differential elastic cross section) is the probability of an A particle of relative velocity $|\vec{g}_{AB}|$ being deflected through the angle χ. Therefore, the number of A particles being deflected into the interval $(\chi, \chi + d\chi)$, $(\phi, \phi + d\phi)$ by B particles per unit time and volume is

$$n_A n_B f(c_A) f(c_B) |\vec{g}_{AB}| \sigma(|\vec{g}_{AB}|, \chi) \sin\chi d\chi d\phi d\vec{c}_A d\vec{c}_B$$

The rate at which one A particle "collides" with B particles per unit volume resulting in a deflection $\chi,\chi+d\chi$ and passing through the azimuthal increment $\phi,\phi+d\phi$ is then

$$n_B f(c_A) f(c_B) |\vec{g}_{AB}| \sigma(|\vec{g}_{AB}|,\chi) \sin\chi \, d\chi \, d\phi \, d\vec{c}_A \, d\vec{c}_B$$

If a collision were defined as an interaction between an A and B particle which resulted in any nonzero deflection χ, then the collision rate would be obtained by integrating the above expression. Since χ is zero, theoretically, only for a distance of approach, b, which is infinite, integration of this expression might give an infinite result.

For the purpose of transport property calculations, it is desired to include a weighting factor in the above expression so that the more important collisions are weighted more heavily than the rest. It will turn out that the transport coefficients are inversely proportional to the collision frequency. Therefore, those collisions which tend to promote the transport process should be given the smallest weighting factor and vice versa. In the case of diffusion, small angular deflections promote the process most effectively and so a weighting factor of $(1-\cos\chi)$ is appropriate. For thermal conduction and momentum transfer (viscosity), small and large deflections (as opposed to 90° deflections) are most effective and a weighting factor of $(1-\cos^2\chi)$ is appropriate. Other weighting factors could have been selected but from rigorous kinetic theory, the above are known to be

correct. The normalization factors for these weighting factors are

$$NF_1 = \frac{\int_0^\pi d\chi}{\int_0^\pi (1-\cos\chi)\,d\chi} = 1$$

$$NF_2 = \frac{\int_0^\pi d\chi}{\int_0^\pi (1-\cos^2\chi)\,d\chi} = 2$$

It is the convention to designate the parameter ℓ as having the value of 1 or 2 to denote the diffusion process or the thermal conduction and momentum transfer process, respectively. Therefore, utilizing the normalization factors, the weighting factor for diffusion becomes $\ell(1-\cos^\ell\chi)$, $\ell = 1$, and that for conduction and viscosity is $\ell(1-\cos^\ell\chi)$, $\ell = 2$.

The collision rate between one A particle and all B particles (with velocity increments $\vec{c}_A$, $d\vec{c}_A$ and $\vec{c}_B$, $d\vec{c}_B$ respectively) for all angles χ and ϕ becomes

$$n_B f(c_A) f(c_B) |\vec{g}_{AB}| d\vec{c}_A d\vec{c}_B \int_0^{2\pi}\int_0^\pi \sigma(|\vec{g}_{AB}|,\chi)\,\ell(1-\cos^\ell\chi)\sin\chi\,d\chi\,d\phi$$

where $\ell = 1$ for diffusion and $\ell = 2$ for thermal conductivity and viscosity. By definition, though,

$$\int_0^{2\pi}\int_0^\pi \sigma(|\vec{g}_{AB}|,\chi)(1-\cos^\ell\chi)\sin\chi\,d\chi\,d\phi = Q_{AB}^\ell(|\vec{g}_{AB}|)$$

which is termed the total cross section.

Finally, integrating over both A and B particle velocity distributions yields the total collision frequency of an A particle with the B particles.

$$\nu_{AB}^{\ell} = n_B \iint f(c_A) f(c_B) |\vec{g}_{AB}| \ell Q_{AB}^{\ell} (|\vec{g}_{AB}|) d\vec{c}_A d\vec{c}_B \qquad (D-2)$$

There are two special cases of the above equation which are important.

I. A is an electron (e) and B is a heavy particle (h)

Equation (D-2) for this case becomes

$$\nu_{eh}^{\ell} = n_h \iint f(c_e) f(c_h) |\vec{g}_{eh}| \ell Q_{eh}^{\ell} (g_{eh}) d\vec{c}_e d\vec{c}_h$$

Since the electron thermal speed is much larger than that of the heavy particles, the above equation can be simplified to

$$\nu_{eh}^{\ell} = n_h \int f(c_h) d\vec{c}_h \int f(c_e) c_e \ell Q_{eh}^{\ell} (c_e) d\vec{c}_e$$

According to Vincenti and Kruger [3] the vector differentials ($d\vec{c}_h$ and $d\vec{c}_e$) can be transformed into scalar differentials in three dimensional spherical coordinates which yield

$$\nu_{eh}^{\ell} = n_h \int_0^{2\pi} \int_0^{\pi} \int_0^{\infty} f(c_h) c_h^2 dc_h \sin\theta d\theta d\phi$$

$$\int_0^{2\pi} \int_0^{\pi} \int_0^{\infty} f(c_e) \ell Q_{eh}^{\ell} (c_e) c_e^3 dc_e \sin\theta d\theta d\phi$$

By substituting the Maxwellian distributions and carrying out integrations wherever possible, the following result is obtained.

$$\nu_{eh}^{\ell} = 4\pi n_h \ell \left[\frac{m_e}{2\pi k T_e} \right]^{3/2} \int_0^{\infty} e^{-\frac{m_e c_e^2}{2kT_e}} Q_{eh}^{\ell} (c_e) c_e^3 dc_e$$

Finally, by making the substitution

$$\gamma^2 = \frac{m_e c_e^2}{2kT_e}$$

the above equation assumes the form

$$\nu_{eh}^{\ell} = 8n_h \ell \left(\frac{kT_e}{2\pi m_e}\right)^{1/2} \int_0^{\infty} e^{-\gamma^2} Q_{eh}^{\ell}(c_e) \gamma^3 d\gamma \qquad (D-3)$$

II. A and B are particles of nearly equal mass

In Chapter 2 of their book, Vincenti and Kruger [3] prove that if $\vec{G}_{CM}$ is the velocity of the center of mass of the two particles (A and B), then

$$d\vec{c}_A d\vec{c}_B = d\vec{G}_{CM} d\vec{g}_{AB}$$

and

$$\frac{1}{2} m_A c_A^2 + \frac{1}{2} m_B c_B^2 = \frac{1}{2} (m_A + m_B) G_{CM}^2 + \frac{1}{2} \mu g_{AB}^2$$

where

$$\mu = \frac{m_A m_B}{m_A + m_B}$$

and

$$\vec{G}_{CM} = \frac{1}{m_A + m_B} (m_A \vec{c}_A + m_B \vec{c}_B)$$

Assuming the temperature of A and B particles to be equal, substituting the above relations into Equation (D-2), and carrying out all possible integrations, the following expression is obtained for the collision frequency of an A particle with a B particle

$$\nu_{AB}^{\ell} = n_B \ell \left(\frac{\mu}{2\pi kT}\right)^{3/2} 4\pi \int_0^{\infty} e^{-\frac{\mu g_{AB}^2}{2kT}} g_{AB}^3 Q_{AB}^{\ell}(g_{AB}) dg_{AB}$$

Upon making the substitution

$$\gamma^2 = \frac{\mu g_{AB}^2}{2kT}$$

the above equation reduces to

$$\nu_{AB}^{\ell} = 8n_B \ell \left(\frac{kT}{2\pi\mu}\right)^{1/2} \int_0^{\infty} e^{-\gamma^2} \gamma^3 Q_{AB}^{\ell}(g_{AB}) d\gamma \qquad (D-4)$$

Hirschfelder, et al. [19], give the following definition
of the kinetic theory collision integral

$$\Omega^{\ell,s}(T) = \left(\frac{kT}{2\pi\mu}\right)^{1/2} \int_0^{\infty} e^{-\gamma^2} \gamma^{2s+3} Q^{\ell}(g) d\gamma \qquad (D-5)$$

Utilizing the above definition for the collision integral
in the two expressions just obtained for the e-h and A-B
collision frequencies gives

$$\nu_{eh}^{\ell} = 8n_h \ell \Omega_{eh}^{\ell,0}(T_e)$$

$$\nu_{AB}^{\ell} = 8n_B \ell \Omega_{AB}^{\ell,0}(T)$$

where $\ell = 1$ indicates diffusion and $\ell = 2$ indicates conduc-
tion and viscosity.

The significance of the last substitution is that the
collision (or omega) integrals are important properties for
the gas kineticist; hence, they are readily available (as
functions of temperature only) in the literature. However,
collision integrals are usually only tabulated for the case
when $\ell = s$. This involves the introduction of the factor
γ^{2s} in Equations (D-3) and (D-4). From calculations of

$\Omega_{eh}^{(1,0)}$, $\Omega_{eh}^{(1,1)}$, $\Omega_{eh}^{(2,0)}$, $\Omega_{eh}^{(2,2)}$ (which are readily available in analytical form) it is evident that the introduction of the factor γ^{2s} has the effect of increasing the collision frequency by a factor of 2 for $s = 1$ and by a factor of 4 for $s = 2$. Therefore, the collision frequencies must be divided by a compensating factor of 2^s, and the final form of the collision frequencies for the two special cases is (note that $\ell/2^s = \frac{1}{2}$ for $\ell = s = 1$, 2)

$$\nu_{eh}^{\ell} = 4n_h \; \Omega_{eh}^{\ell,s}(T_e) \qquad \ell = s = 1, 2$$

$$\nu_{AB}^{\ell} = 4n_B \; \Omega_{AB}^{\ell,s}(T) \qquad \ell = s = 1, 2$$

In this study, the collision integrals for the electron-atom, ion-atom and atom-atom elastic collisions were obtained from the work of Devoto [20] and Yos [21] and the collision integrals for charged particle collisions (electron-electron, electron-ion, ion-ion) were obtained analytically through use of Rutherford's formula for the differential scattering cross section in a coulomb field.

Finally, it remains to define the mean free paths for the species of the gas. As mentioned earlier, this is simply the ratio of the mean thermal speed of the particle ($\bar{c}_i$) to the sum of the appropriate collision frequencies. Therefore

$$\lambda_e^\ell = \frac{\bar{c}_e}{\nu_{ee}^\ell + \nu_{eH^+}^\ell + \nu_{eH}^\ell}$$

$$\lambda_{H^+}^\ell = \frac{\bar{c}_{H^+}}{\nu_{H^+H^+}^\ell + \nu_{H^+H}^\ell}$$

$$\lambda_H^\ell = \frac{\bar{c}_H}{\nu_{HH^+}^\ell + \nu_{HH}^\ell}$$

where

$$\bar{c}_i = \left(\frac{8kT_i}{\pi m_i}\right)^{1/2}$$

The superscript ℓ on the mean free path definitions indicates that the mean free path of a certain species for diffusion is not necessarily the same as for thermal conduction and viscosity. Also, the mean free paths of ions and atoms do not account for collisions of these heavy particles with electrons. The reason for this is that when a heavy particle collides with an electron, the heavy particle is virtually uninfluenced by that collision. This is further substantiated by the "persistence of velocity" theory described by Jeans [22].

APPENDIX E

ELECTRON-ATOM BREMSSTRAHLUNG

The purpose of this appendix is to derive an expression
for the rate of electron energy loss due to the acceleration
of electrons in the potential field of a neutral atom. This
loss of energy due to acceleration of charged electrons will
herein be referred to as electron-atom Bremsstrahlung. The
derivation of electron-ion Bremsstrahlung is given by Clark
[9].

Larmor's formula for the rate of radiative emission
from an accelerating charged particle is [26]

$$\frac{dP_r}{dt} = \frac{2}{3}\left(\frac{e^2 a^2}{c^3}\right) \qquad \text{(E-1)}$$

To obtain the energy radiated during a single interaction
between an electron and an atom, Equation (E-1) can be
evaluated as an average during the collision and then multi-
plied by the time of significant interaction. This time of
interaction is the distance traveled by the electron during
significant interaction divided by its speed. The interac-
tion distance is somewhat arbitrarily estimated to be twice
the atomic (or molecular) diameter and the interaction time
is therefore expressed as $\frac{2d_{atom}}{c_e}$, where c_e is the electron
speed. The energy radiated in a single collision is then

$$\frac{dP_r}{dt} \Delta t = \frac{2}{3}\left(\frac{e^2 a^2}{c^3}\right) \frac{2d_{atom}}{c_e}$$

The average acceleration of the electron during colli-sion is given by the vector difference in electron velocity before and after collision divided by the interaction time. Since the atom is much heavier and slower it can be con-sidered stationary relative to the electron; hence the electron speeds before and after collision are approximately equal. This implies that the absolute value of the velocity vector difference is given from the following diagram as
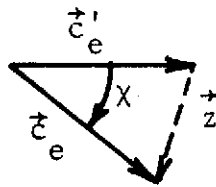
$$|\vec{z}| = 2\sin\left(\frac{\chi}{2}\right)c_e = |\vec{c}_e{}' - \vec{c}_e|$$

where $|\vec{c}_e{}'| = |\vec{c}_e|$

and χ is the angle by which the electron is deflected after collision with the atom. Finally, the acceleration is given by the following formula:

$$a^2 = \frac{2c_e^2(1-\cos\chi)}{\Delta t^2}$$

and
$$\frac{dP_r}{dt} \Delta t \approx \frac{2}{3}\frac{e^2}{c^3}\frac{c_e^3}{d_{atom}}(1-\cos\chi).$$

The flux of electrons with velocities in the incremental range $\vec{c}_e$, $d\vec{c}_e$ is

$$c_e n_e f(c_e) d\vec{c}_e$$

The rate at which these electrons pass through impact parameter ring segments of area $b\,db\,d\phi$ centered about each heavy particle is given by Equation (C-1):

$$n_e n_h f(c_e) c_e \sigma(\chi, c_e) \sin(\chi)\, d\chi\, d\phi\, d\vec{c}_e \qquad \text{(C-1)}$$

The rate of energy loss due to collisions between electrons with velocities in $\vec{c}_e$, $d\vec{c}_e$ and resulting in a deflection between χ and $\chi + d\chi$ is therefore,

$$n_e n_h f(c_e) c_e \sigma(\chi, c_e) \sin(\chi)\, d\chi\, d\phi\, d\vec{c}_e \; \frac{2}{3} \frac{e^2}{c^3} \frac{c_e^3}{d_{atom}} (1-\cos\chi)$$

Finally, the total energy loss rate due to collisions of all electrons deflected through all angles is

$$\frac{2}{3} \frac{e^2}{c^3 d_{atom}} n_e n_h \int f(c_e) c_e^4 \left[\int_0^{2\pi} \int_0^{\pi} \sigma(\chi, c_e) \sin\chi (1-\cos\chi)\, d\chi\, d\phi \right] d\vec{c}_e$$

The quantity in brackets is usually defined as the total elastic diffusion cross section (Q_{eh}^D) and is a function of c_e. Substituting the total cross section and expanding the differential vector velocity into its scalar spherical coordinate form yields the following expression for electron atom Bremsstrahlung

$$P_r = \frac{2}{3} \frac{e^2}{c^3 d_{atom}} n_e n_h \int_0^{2\pi} \int_0^{\pi} \int_0^{\infty} f(c_e) c_e^4 Q_{eh}^D(c_e) c_e^2 dc_e \sin\theta\, d\theta\, d\phi$$

$$= \frac{2}{3} \frac{e^2}{c^3 d_{atom}} n_e n_h 4\pi \int_0^{\infty} f(c_e) c_e^6 Q_{eh}^D(c_e)\, dc_e$$

Substituting the expression for the Maxwellian distribution and setting $\gamma^2 = \dfrac{m_e c_e^2}{2kT_e}$, P_r becomes:

$$P_r = \frac{2}{3} \frac{e^2}{c^3 d_{atom}} n_e n_h \frac{4}{\pi^{1/2}} \left[\frac{2kT_e}{m_e}\right]^2 \int_0^\infty Q_{eh}^D \gamma^6 e^{-\gamma^2} d\gamma$$

Since the integral is not significantly affected by varying the exponent of γ by one (see Appendix D), the exponent is reduced to 5 in order to satisfy Equation (D-5) for $\ell = s = 1$, which is the gas kinetic collision integral for diffusion. The final form of the expression for electron atom Bremsstrahlung emission is then,

$$P_r = \frac{128}{3} \left(\frac{e^2}{c^3 d_{atom}}\right) n_e n_h \left(\frac{kT_e}{2m_e}\right)^{3/2} \Omega_{eh}^{(1,1)}$$

$$= \frac{32}{3} \left(\frac{e^2}{c^3 d_{atom}}\right) n_e \left(\frac{kT_e}{2m_e}\right)^{3/2} \nu_{eh}^1$$

where ν_{eh}^1 is the collision frequency defined in Appendix D.

VITA

Robert Kenmer Scott ███████████████████
███████████████ He was raised in that city and attended
public schools in both Denver and Englewood.

Upon completion of high school, he entered the University of Colorado, School of Engineering in September, 1964. He was awarded the degree, Bachelor of Science in Mechanical Engineering in June, 1968.

Mr. Scott then moved to West Lafayette, Indiana and enrolled as a graduate student in the Department of Mechanical Engineering at Purdue University and obtained a Master of Science degree in January, 1970. After this he continued on at Purdue University to pursue the Ph.D. degree.

In June, 1966, Mr. Scott married Miss Kay Moore in Denver, Colorado. They now have two children: Brian Lee, age 5 and Tania Lynn age 2 1/2.